Do Glaciers Enhance Organic Carbon Burial?: An Isotopic Approach Linking Continental Weathering, Iron-(oxhydr)oxides and Climate Change.

SCOTT MICHAEL HAWLEY

Do Glaciers Enhance Organic Carbon Burial?: An Isotopic Approach Linking Continental Weathering, Iron-(oxhydr)oxides and Climate Change.

Scott Hawley

Do Glaciers Enhance Organic Carbon Burial? : An Isotopic Approach Linking Continental Weathering, Iron-(oxhydr)oxides and Climate Change.

Scott Hawley

This thesis explores continental weathering patterns in glacial and non-glacial river catchments in Iceland and Greenland. Specific attention is placed on characterizing the relative iron (oxyhydr)oxide export rates of glacial and non-glacial catchments to the ocean. Total element concentration and iron stable isotope measurements indicate that chemical weathering differences do exist between glacial and non-glacial catchments. The differences appear primarily related to variations in soil formation and organic matter availability between the environments. Physical, rather than chemical, differences between glacial and non-glacial catchments however dominate the relative differences in (oxyhyr)oxide export rates. Glacial and non-glacial river sediments from otherwise analogous terrains contain about the same quantity of iron (oxyhyr)oxide on a weight normalized basis. This equates to glacial rivers exporting far more iron (oxyhyr)oxides on a discharge weighted basis, because glacial rivers contain far higher suspended sediment concentrations that non-glacial rivers. Existing research shows that organic carbon accumulation and burial in marine environments scale directly with iron (oxyhydr)oxide accumulation. This means that shifts in continental weathering over glacial-interglacial cycles drive further changes in marine carbon burial creating a global climate feedback loop.

Do Glaciers Enhance Organic Carbon Burial?: An Isotopic Approach Linking Continental Weathering, Iron-(oxhydr)oxides and Climate Change.

Scott Michael Hawley

A thesis presented for the degree of Doctor of Philosophy

Department of Earth Sciences, Durham University

2017

Table of Contents

List of Figures

List of Tables

Acknowledgements and Statement of Copyright

I would like to thank my supervisors Kevin Burton, Helen Williams and Philip Pogge von Strandmann for all the support they provided in the lab, field and office. This thesis has been a constantly evolving work-in-progress and their guidance has been essential in keeping me on track and ensuring the project was always headed in the correct direction.

I would also like to thank my extended advisorial MetTrans team. Sigurdur Gislason, Eydis Eiriksdottir and Becca Neely provided valuable assistance in the field and were able to organize an excellent conference while also managing to keep the volcanic eruption under control. The rest of the MetTrans network provide much needed support and training opportunities, and I am glad the opportunity to work with-in the network.

My lab work at Durham would not have been possible without the hard work of Geoff Nowell, Chris Ottley and Joe Peterkin. Geoff's refusal to compromise on the quality of the lab during the laboratory refurbishment was especially important in ensuring I was able to make the measurements I needed with-in the right time-scale in-spite of what seemed liked the best efforts of the people carrying out the refurbishments. Marc Alban-Millet, Baptiste Debret and Edward Inglis also provided essential training and assistance on the mass-spec as well as back-up when the machine needed to be forced into submission. Dave Selby, James Baldini, Bob Hilton, and Sophie Opfergelt also provided useful feedback on project as it progressed. Sophie's collaboration on the soil work proved to be a key piece needed to draw this research together.

Finally, I would like to thank the wider geochemistry at Durham, my office friends, and my wife for their support.

Chapter 1-

Marine Sedimentation and Organic Carbon Burial: Linking Continental Weathering and the Organic Carbon Cycle

Abstract

River deltas and estuaries are key environments of organic carbon preservation and coastal sedimentation. This may or may not be coincidental. Some theories propose organic matter preservation has nothing to do with inorganic sediments (i.e. geopolymerization) while other theories suggest organic matter preservation is intrinsically linked to inorganic sedimentation (i.e. mineral surface protection). If there is a causal mechanism linking organic carbon preservation and sedimentation rates in nearshore marine environments, then terrestrial weathering drives a climate feedback mechanism. Over glacial-interglacial cycles total sediment accumulation in coastal environments changes significantly due to the interplay of climate change and terrestrial erosion. If these changes alter organic carbon preservation they will also modulate Earth's climate. This chapter summarizes the dominant theories currently proposed to explain organic carbon preservation in coastal sediments as they relate to sediment accumulation. Based on the existing data we propose that two parameters - total sedimentation export rates and iron (oxyhydr)oxide deposition rates - can be used in combination to provide a reliable indication of how climatically driven weathering changes will alter marine organic carbon accumulation.

1.1 Terrestrial Weathering and Carbon.

Silicate mineral weathering is a significant inorganic carbon sink (Berner and Kothvala 2001; Misra and Freolich 2012). As a result, changes in continental weathering rates throughout Earth's history have been intrinsically linked to long-term climate variability (Berner and Kothvala 2001). The time-scales involved with silicate weathering however have led many to discount the viability of continental weathering to account for rapid climate changes such as glacial-interglacial cycles (Caisis et al., 2013). More than 25 years ago John Martin proposed that continental weathering was in fact relevant over glacial-interglacial climate cycle by shifting the focus from inorganic to organic carbon. Martin proposed changes in continental weathering patterns modulate organic carbon preservation in the Southern Ocean as part of idea which became known as the Iron Hypothesis or 'iron fertilization' (Martin 1990). The idea has subsequently been extensively studied, and the theory that primary production in the Southern Ocean is dependent on continental

weathering has been largely confirmed (e.g. Coale et al., 2004; Brietbarth et al., 2011). Recently Ocean Drilling Program site 1090 (Gersonde et al., 1999) was specifically sampled to further investigate iron fertilization in the Southern Ocean (e.g. Jaccard et al., 2013; Marino et al., 2013; Martinez-Garcia et al., 2014), and data from this core clearly indicates that iron deposition, primary production, organic carbon preservation and global atmospheric carbon dioxide (CO_2) changes are correlated in the Southern Ocean.

The corollary relationships between climate, iron deposition, primary production and carbon preservation at ODP site 1090 are illustrated on Figure 1.1 by highlighting the peaks in alkenone concentrations from Marino et al., (2013). Alkenone concentrations are interpreted as a proxy for primary production. The Alkenone peak also correspond to troughs in sediment organic carbon content, peaks in sediment inorganic carbon content, peaks in iron accumulation rates and troughs in atmospheric CO_2 concentrations. It is impossible from the core data alone to determine which, if any, of these relationships trends reflect directly dependencies. Any of variables could be strongly correlated because they are both dependent on some other parameter in the system rather than eachother. There is however ample outside evidence to help distinguish the relationships between these parameters.

The relationship between atmospheric CO_2 concentrations and iron accumulation is almost certainly a direct dependency related to continental weathering (Coale et al., 2004). The direct dependency between climate changes and continental weathering also explains why sediment inorganic carbon concentrations follow the same pattern; inorganic carbon originates from marine biogenic sediment production which on a bulk normalized basis is inversely related to lithogenic sediment deposition. The correlation between iron accumulation and primary production is also almost certainly a result of direct dependency (Brietbarth et al., 2004). Iron is the limiting nutrient in the Southern Ocean and primary production does increase following iron fertilization (Brietbarth et al., 2010). There is significant reason to suspect the correlation between continental weathering and organic carbon preservation is also characterized by direct dependency. Inorganic sediments, specifically iron (oxyhydr)oxide bearing minerals, enhance organic carbon preservation in marine sediments (Canfield 1994; Hedges and Kiel 1995; Lalonde et al., 2012). Therefore, increasing the proportion of terrestrial material relative to marine biogenic carbonates in marine sediments will increase sediment organic carbon concentrations. These dependent relationships explain 100% of the data. In other words, nothing in the data from ODP site 1090 implies primary production and/or carbon burial in the Southern Ocean have any direct relationship with atmospheric CO_2 concentrations. This raises the question of if primary production is truly related to the larger climate signal commonly associated with iron fertilization.

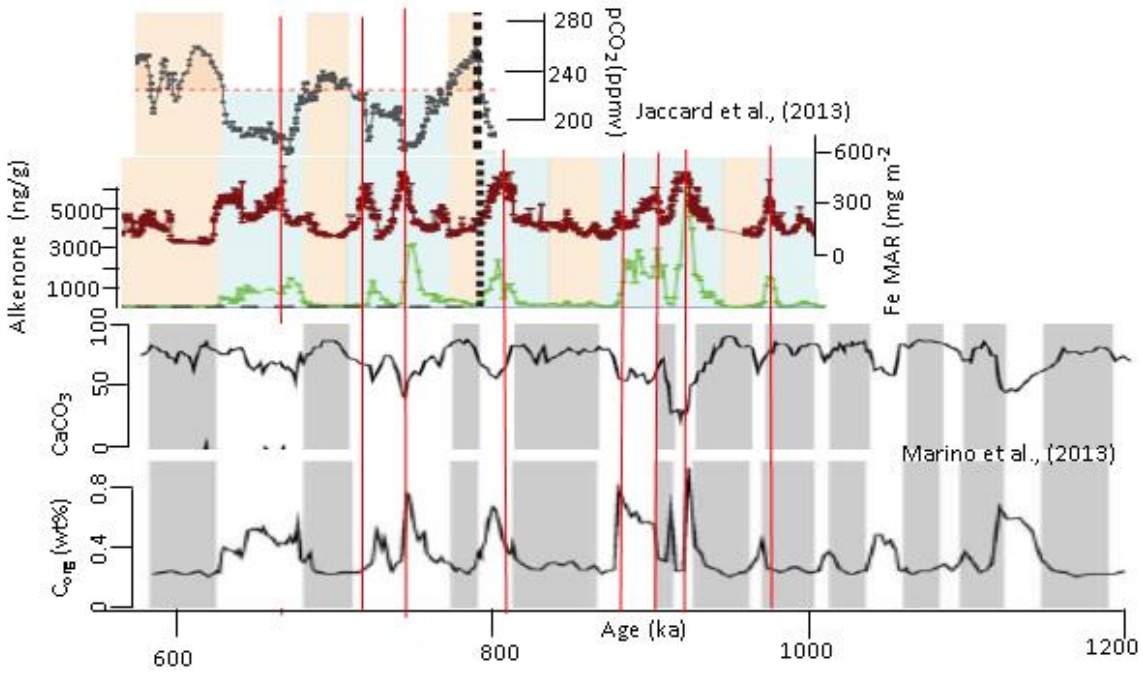

Figure 1.1. Core Data from ODP Site 1090 modified from Marino et al., (2013) and Jaccard et al., (2013). Alkenone concentrations are interpreted as reflecting absolute primary productivity rates with peaks in alkenone concentrations highlighted by the red lines. The peaks in primary production correspond to peaks in iron accumulation, peaks in sediment organic carbon concentrations, troughs in sediment inorganic carbon concentrations, and troughs in atmospheric CO_2 concentrations.

There is significant reason to believe that organic matter production and organic matter preservation are independent parameters in most other marine environments. Numerous review studies on marine OM preservation have concluded primary production is not a dominant control of OM preservation and have not been able to account for marine OM preservation patterns by changing primary production rates between environments (see reviews by Hedge and Kiel 1995; Burdige 2005; Burdige 2007; Blair and Aller 2013). The three direct attempts to link primary production in the Southern Ocean to carbon sequestration have been equally ambivalent (see review by Buessler and Boyd 2003). During 13-day and 21-day iron enrichment experiments in the Southern Ocean increases in primary production were found to have no impact of carbon export to the sediment (Buessler and Boyd 2003). A longer 28-day study found particulate carbon export rates in the Southern Ocean (below 50 and 100m) increase slightly following an iron fertilization in the region (Buessler et al., 2004). However, microbial remineralization during sediment maturation would be expected to reduce the impact of carbon export on carbon preservation, and the absolute magnitude of the identified export change was small relative to the background natural system. There are regions of the ocean characterized by high primary production and high OM accumulation rates but the co-existance of the two patterns doesn't mean they are

related. The remainder of this chapter establishes the grounds for linking organic carbon preservation directly to continental weathering without invoking primary productivity.

1.2 Linking Organic Carbon Accumulation and Total Sediment Accumulation

The preservation of organic matter (OM) in nearshore marine environments is a climatically significant carbon sink accounting for the sequestration of 250 Tg C yr^{-1} (Burdige 2007; Caisis et al., 2014). This is 6% of the rate at which anthropogenic activity is increasing carbon concentrations in the atmosphere (4 Pg C yr^{-1}, Caisis 2014), and is 25 times greater than the carbon exchange rate needed to drive the atmosphere from the Last Glacial Maximum to pre-industrial conditions (9.4 Tg C yr^{-1}, Martin 1990). Therefore, even relatively small changes in global marine organic carbon preservation have the potential to significantly influence Earth's climate over geologic timescales. However, organic carbon burial in marine sediments is an inefficient process, and there is limited scientific consensus of the factor or factors controlling the process (Burdige et al., 2007).

Sediment oxygenation state is the most widely proposed control of OM preservation, but the actual relationship between sediment oxygenation is complex due to the interplay of physical geography and sediment exposure (Canfield 1994; Blair and Aller 2013). Of the other parameters which correlate with organic carbon preservation in marine sediments, total sedimentation accumulation rate appears to be the most consistent (Hedges and Kiel 1995). The relationship between organic carbon and total sediment accumulation rate, as well as the interplay of environmental redox and organic carbon preservation is highlighted on Figure 1.2 which is a compilation of data from studies of a range of marine environments. Across open marine and coastal environments there is a strong and significantly significant positive correlation between total sediment and organic carbon accumulation rates (shown by the dashed line).

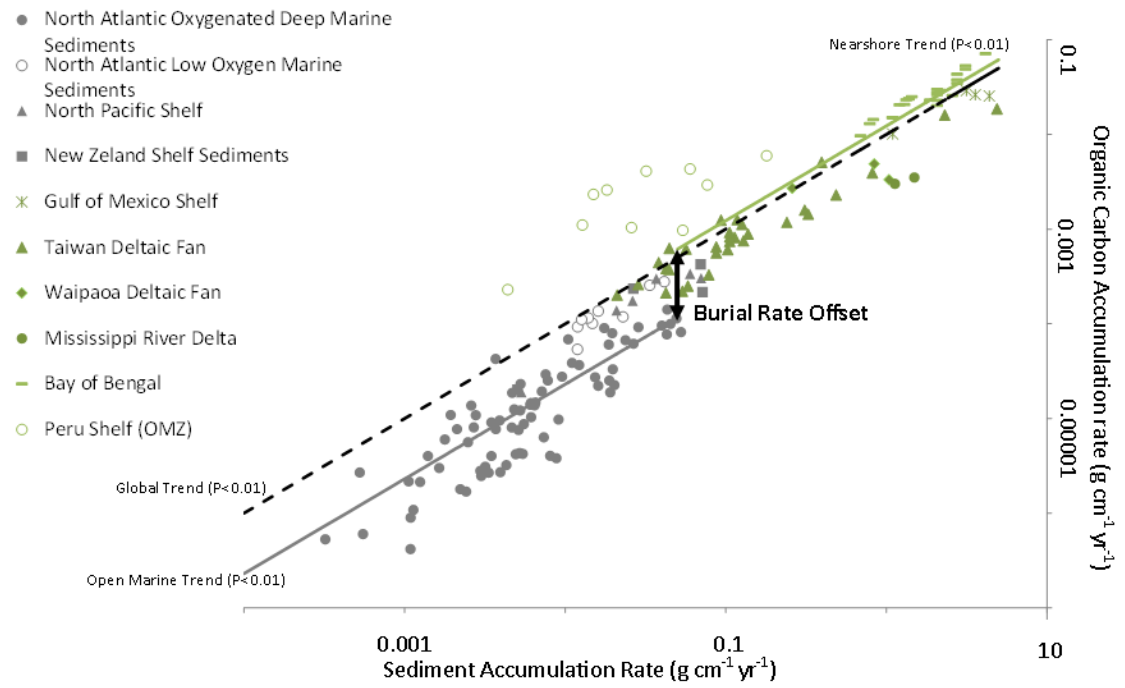

Figure 1.2: Sediment and organic carbon accumulation. Organic carbon accumulation in marine environments adheres to strong linear relationship with total sediment accumulation. Open ocean locations tend to fall below this line while estuarine locations tend to fall above the line consistent different environments having different relative carbon burial efficiencies. The data in the figure is from Talwani et al., (1976); Lyendyk et al., (1978); Barker et al., (1990); Barron et al., (1991); Eadie et al., (1994); Saunders et al., (1998); Barker et al., (1999); Raymo et al., (1999); Flemmings et al., (2006); Kao et al., (2006); Aller et al., (2008); Brackley et al., (2010); Dale et al., (2015) and Peketi et al., (2015).

Two patterns standout against the global (dashed) trend line. If the data is separated into open marine and coastal samples the two environments are offset on the graph. Coastal sediments accumulate more OM at a given sedimentation rate than open marine sediments (illustrated by the solid lines). Additionally, in both coastal and open marine environments sediment overlain by anoxic and/or low oxygen bottom waters has a greater OM burial rate than its well oxygenated equivalence.

Nearly all the theories surrounding the mechanism(s) which sets the relationship between total sediment and organic carbon accumulation can be classified into one of three models. The first model assumes organic matter recalcitrance controls the carbon preservation efficiency of sediments e.g. Westrich and Berner (1984). The second model assumes environmental redox, as modulated by geographic and environmental conditions, controls the carbon preservation efficiency of sediments e.g. Canfield (1994). The final model assumes inorganic/continental sediment inputs are the key to OM preservation e.g Mayer (1994). When it comes to addressing how changing sedimentation rates will alter

organic matter preservation rates these models come to very different conclusions. It is therefore important to understand the relative merits of each of these theories and how well each is supported by existing data.

1.3 Organic Carbon Preservation and Organic Carbon Recalcitrance

From a pure biologic standpoint, OM preservation should be controlled by the recalcitrance of the organic compounds present in the environment. In the laboratory, organic compounds vary significantly in terms of their susceptibility towards microbial remineralization, and a logical conclusion is that the same should apply to environmental samples. On this basis one might expect that OM preservation rates are strongly dependent on the type of organic compounds which are delivered into the sediment at any location. There is some evidence that OM composition influences OM burial, but overall OM composition appears to be no more than a minor control of organic carbon accumulation (see review by Burdige 2007).

Most of the specific research on the relationship between OM composition and OM preservation has focused on the difference between open marine and coastal marine environments. Terrestrial organic matter (TOM) is considered more recalcitrant than marine organic matter (MOM), and coastal settings receive significantly more TOM than open marine environments (Burdige 2005). As previously shown on Figure 1.2, coastal sediments are more efficient at preserving OM than marine sediments creating a logical bridge between OM preservation and OM recalcitrance. However, data shows the relationship between TOM inputs and marine OM accumulation rates are globally inconsistent (Blair and Aller 2013). Carbon isotope work has also shown that in many marine environments TOM is preferentially degraded while MOM is preserved (Burdige 2007). There are a few specific settings, namely Taiwan, which receive large quantities of fossil organic carbon and in these settings recalcitrant organic compounds do appear to be preferentially preserved during marine sediment maturation (Hilton et al., 2010). However, sedimentation style also appears to play a big role in the OM preservation dynamics of these fossil organic carbon rich systems (Blair and Aller 2013).

Geopolymerization is the dominant theory proposed to rebut all the objections to organic recalcitrance being a minor control over OM preservation. Geopolymerization proposes that simple organic compounds interact and combine during physical sediment transport creating more complex organic coagulates. The coagulates are proposed to be significantly more recalcitrant towards remineralization than their individual components which enhances the preservation of apparently labile organic compounds. Complex organic coagulates do exist in marine sediment (Ransom et al., 1997), and geopolymerization is a direct extension of humification which has been potentially shown to occur in soils (Zech et al., 1997). The

biggest issue with geopolymerization is that there is essentially no direct evidence that it is an important process in marine sediments (see review by Burdige 2007). Moreover, the importance of humification (on which geopolymerization is based) on OM stabilization in soils is being increasingly questioned. Inorganic mineral stabilization appears to be far more important in terms of stabilizing labile OM in soils than humification (Mikkuta et al., 2006; Schrumpf et al., 2014).

The suggestions that inorganic mineral stabilization is important for preserving OM in soils highlights that fact that OM recalcitrance can arise from factors other than organic composition. The physio-chemical accessibility of OM to microbes is affected by more than just the organic structure of a compound, and in natural environments these other factors need to be considered.

1.4 Redox Controlled Sediment Maturation

From a theoretical perspective, redox conditions exert at least as much control on natural OM remineralization rates as OM recalcitrance (Westrich and Berner 1984). There is ample evidence that highly reducing marine environments are more efficient at preserving OM than well oxygenated marine environments (Burdige 2007), but the detailed relationship between environmental redox state and OM preservation is complex (Blair and Aller 2013). In many cases the length of time sediment is exposed to oxygen is dependent on both redox state and total sedimentation rate of an environment (Hedges and Kiel 1995). This means that sedimentation dynamics need to be considered alongside absolute environmental redox conditions when investigating sediment redox dynamics. This raises the question of to what degree the relationship between total sediment and OM accumulation rates is a function of integrated redox dynamics.

The traditional way to estimate the interplay of sedimentation rates and redox controlled OM preservation rates is to compare the ‘organic carbon preservation efficiencies’ of locations with different absolute oxygen saturations and sedimentation rates. If sedimentation is enhancing OM preservation by a redox mechanism then increasing sedimentation environmental sedimentation rates and decreasing environmental oxygen saturation should have similar impacts of organic carbon preservation efficiencies. To estimate the organic carbon preservation efficiency of any sediment it is first necessary to determine either: 1) the total amount of OM which has already been degraded (denoted G for historic reasons) which from here-on-in will be referred to as the G-based approach or; 2) the organic carbon content of the sediment before it started to be buried (C_i) which from here on we will refer to as the C_i-based approach.

The mathematically basis for each of these approaches is fundamentally different which significantly complicates how figures must be interpreted if G-based and C_i-based data is shown side-by-side. The important aspect of all G-based organic carbon preservation data is that sedimentation rates and OM preservation rates are dependent variables related by the function: $y = \frac{x}{x+G'}$ where G'=G/sediment organic carbon concentration (Canfield 1994). When it comes to C_i-based data sedimentation rates and OM preservation rates are independent variable. Ideally the data sets needed to be plotted differently, such that each reflects the relationship between independent variables, but recent reviews have chosen to published figures mixing data from the two approaches (e.g. Burdige 2005; Burdige 2007; Blair and Aller 2013). Figure 1.3 modified from Blair and Aller (2013) is one such mixed figure, and we have superimposed patterns need to accurately interpret the figure ontop of the original data.

Sedimentation rates and OM preservation rates are dependent variables when calculated based on G values because the method assumes that total organic matter degradation (G) is independent of sedimentation rates but that total OM deposition is dependent on sedimentation rates. The calculated OM preservation rates are a function of OM deposition and therefore dependent on the measured sedimentation rates. The C_i-based approach makes no attempt to directly quantify total organic matter degradation but rather only looks are the relative difference bulk normalized sediment OM concentrations (C_{org}) and an idealized initial bulk normalized sediment OM concentration (C_i). In other words, all the G-data needs to be normalized for sedimentation rates in order to compare the data with C_i-based data. This requires looking at a G-data as a function of G' values where G' is the ratio of (G) to the bulk normalize OM concentration of the residual sediment (C_{org}) (See Figure 1.3). Overall if sedimentation promotes OM preservation through a redox mechanism: i) in the G-based data increases in sedimentation should be affiliated with a clear shift towards lower G' values as lower G' values indicate higher sediment normalized OM preservation rates; and ii) in the C_i-based data increases in sedimentation rates should drive significant positive increases in organic carbon preservation rates. The data does not appear to follow this trend. All the coloured data is C_i based data. The lack of a correlation between OM preservation efficiencies and sedimentation rates is in the C_i data also indicates increased sedimentation does not increase OM preservation via a redox mechanism. Clearly environmental redox state effects relative or sediment normalized OM preservation rates, but sediment normalized preservation rates do not appear to be a function of sedimentation rates.

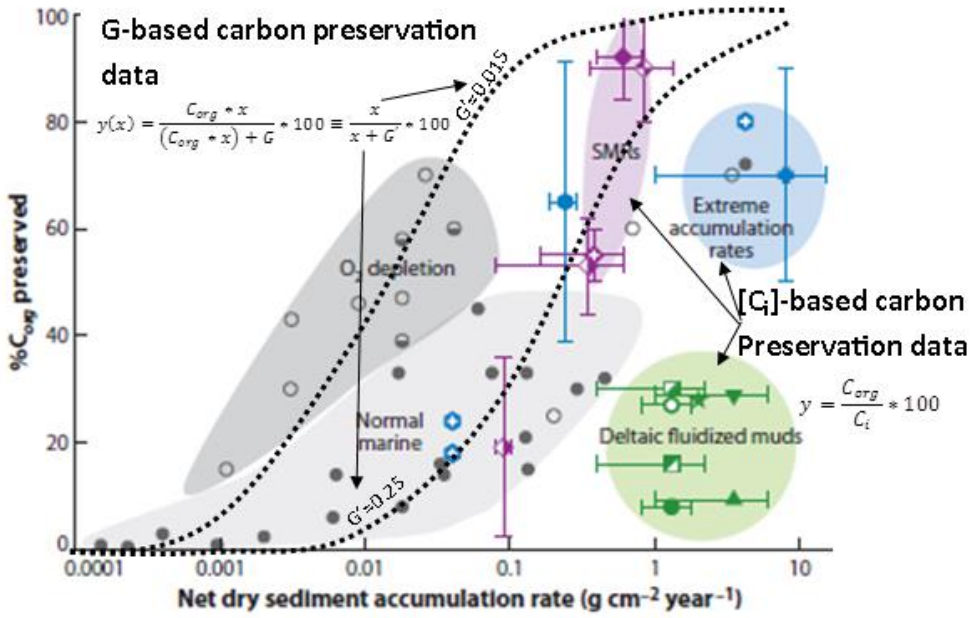

Figure 1.3 Modified from Blair and Aller (2013). All the coloured data points were determined using a method which assumes organic matter deposition is a function of total sediment deposition ($\%C_{org}preserved = \frac{C_{org}}{C_i} * 100$). The three distinct groupings suggest environmental redox controlled OM burial is not a simple function of sedimentation rates. The black and white data points were determined based on measurements of total OM remineralization (G): $\%C_{org}preserved = \frac{C_{org} * x}{(C_{org} * x) + G} * 100 \equiv \frac{x}{x + G'} * 100$. This data appear to be best explained by constant G' values within normal marine and O_2 depleted environments indicating sediment OM accumulation scales directly with sediment accumulation rates.

Blair and Aller (2013) came to a similar conclusion and proposed that this is because the relationship between sedimentation rates and sediment burial is highly geographically dependent. Resuspension, bioturbation and/or lateral deposition significantly affect the relationship between sedimentation and sediment burial especially at high sedimentation rates. At low sedimentation rates oxygen diffusion, rather than sedimentation, dictates the redox burial history of marine sediments (Canfield 1994). Sedimentation rates are therefore a much less straightforward control of sediment redox history than linear burial models e.g. Canfield (1994) might suggest. As a result the relationship between sediment accumulation rates and OM accumulation rates can't be written off a product of redox preservation. This leads into the idea that sediments might directly promote OM preservation with redox conditions acting a secondary process i.e. Hedges and Kiel (1995).

1.5 Inorganic Mineral Protection and the Rusty Carbon Sink.

Mayer (1994) was the first study to present a clear argument that inorganic minerals directly protect organic matter from remineralization in marine sediments. Mayer (1994)'s original 'surface adsorption protection' theory has subsequently undergone several iterations but it is now broadly accepted that physio-chemical interactions between inorganic minerals and OM promote OM preservation (Kiel et al., 1994; Hedges and Kiel 1995; Kennedy et al., 2002; Kennedy and Wagner 2011). Accepting mineral-OM interactions as a primary control of OM preservation makes it relatively straightforward to account for why OM and total sediment accumulation rates are so strongly correlated in marine sediments (Figure 1.2). Minerals protect-OM therefore mineral and OM accumulation rates are intrinsically linked. This raises the possibility of using total sedimentation rates alone to relate changes in continental weathering to changes in marine OM accumulation. Several of the subsequent chapters will consider this possibility. However, recent research indicates a more accurate approach is available which is much more able to account for the differences in OM burial rates between aquatic environments. This better approach involves tracing iron (oxyhydr)oxide deposition rather than total sediment deposition.

There is still no universal scientific consensus on the exact mechanism which promotes OM stabilization by inorganic minerals (Greathouse et al., 2014). What is clear, however, is that iron (oxyhydr)oxide concentrations provide an accurate measure of mineral-OM stabilization interactions. For logistical reasons iron (oxyhydr)oxides are not measured directly but are estimated using selective chemical extractions (see review by Raiswell and Canfield 2012). Figure 1.4 summarizes published data relating extractable iron concentrations to total organic carbon concentrations in terrestrial soils and aquatic sediments. While different environments are characterized by different slopes relating total organic carbon and extractable iron the two variables are significantly correlated across all the environments. (It should be noted that comparing reducing and oxidizing environments in this manner is potentially misleading. Pyritization reactions selectively reduce (oxyhydr)oxides (Berner 1970) such that iron sulphide concentrations need to be added to extractablve iron concentrations to accurately compare iron-OM dynamics between reducing and oxidizing environments). The prevalence of this correlation across the range of marine and terrestrial sedimentary environments makes iron (oxyhydr)oxide concentrations a uniquely powerful indicator of organic carbon burial. In a review of soil OM preservation research Schrumpf et al., (2013) concluded that "the association with [(oxyhydr(oxide)] minerals is the most important factor in stabilization (sic) of OC in soils, irrespective of vegetation, soil type and land use." Lalonde et al., (2012) named this pool of iron-bound organic carbon in marine sediment the 'The Rusty Carbon Sink'. In many ways the Rusty

Carbon Sink provides a new name for a process that has been extensively studied for some time under a variety of names.

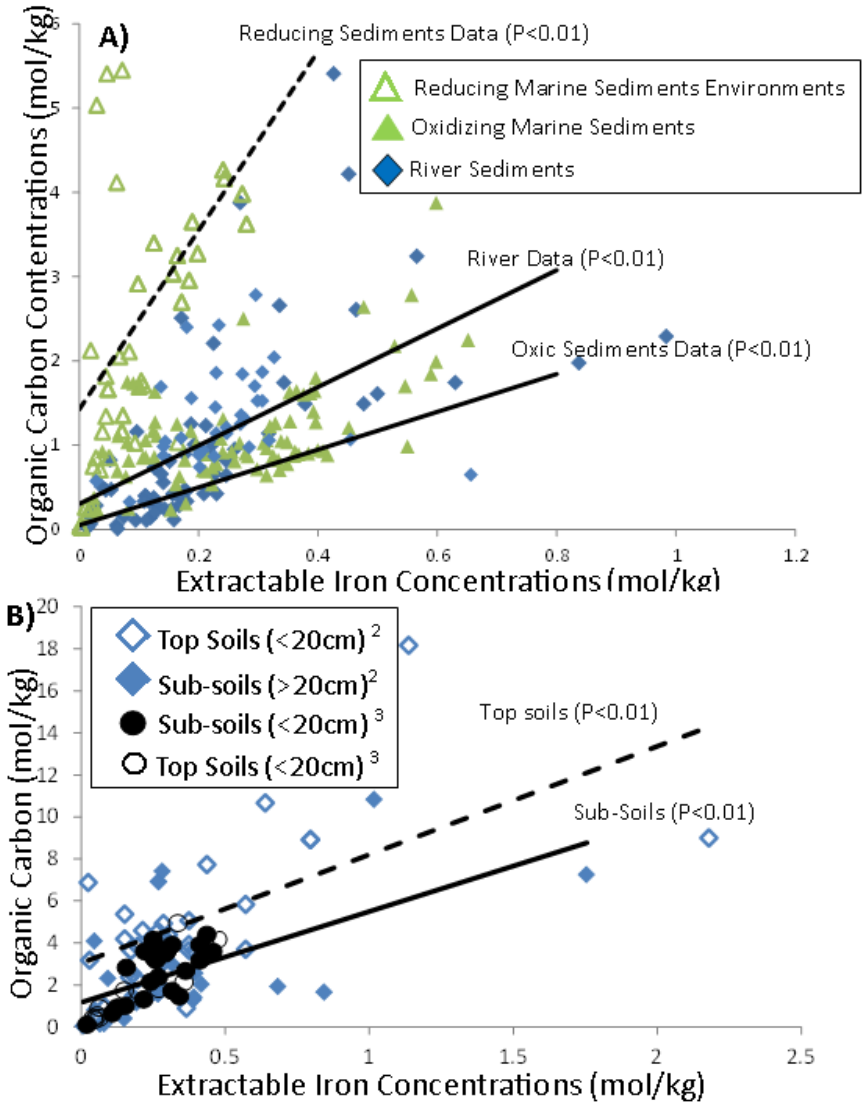

Figure 1.4. Organic Carbon Preservation and Chemically Reactive Iron. A) Aquatic sediment data from Berner (1970); Poulton and Raiswell et al., (2005); Lalonde et al., (2012); Sabadini-Santos et al., (2014); and Sheng et al., (2015). Chemical reactive iron was defined as HCl extractable iron by Berner (1970) and as dithionate extractable iron by the remaining studies. There is a significant correlation between extractable iron concentrations and organic carbon concentrations within the riverine, oxic marine and reducing marine datasets. B) Modified from (2) Mikkuta and Guggenberg (2002) with additional data from (3) Kiem and Kögnel-Knabner (2002) Mikkuta et al., (2006); Xu-hui et al.,(2007); von Lutzlow et al.,(2008); and Thompson et al., (2011). All the extractable iron data is based on dithionate extractions. Organic carbon concentration and extractable iron are significantly correlated across the top and sub-soil samples.

The mixed iron-OM complex covered by the Rust Carbon Sink can be generally referred to as iron-organic colloids (IOCs). These IOCs have been recognized under a number of

different names: physically-chemically associated humic-iron river colloids (Sholkovitz et al., 1977), organo-ferric complexes (Boudot et al., 1989), Fe-C colloids (Ingri et al., 2006), OC-Fe macromolecular structures (Lalonde et al., 2012), and/or strong iron-OC complexes (Barber et al., 2014). The exact structure of IOCs is a matter of debate (Greathouse et al., 2014) but iron stability (Lyven et al., 2003; Ingri et al., 2006; Andersson et al., 2006; Boye et al., 2010; Lalonde et al., 2012; Vasyukova 2012), theoretical bonding (Ilenia 2013), and sediment incubation studies (Barber et al., 2014) all suggest that IOCs contain ferro-organic bonds. Consequently, the carbon within IOCs is bonded in a way which makes it energetically much more difficult to access than carbon within free and/or adsorbed OM. The net effect is that organic carbon bound in IOC should be highly recalcitrant towards microbial remineralization explaining the near universal correlation between sediment (oxyhydr)oxide and organic carbon concentrations.

Preferential IOC preservation is completely consistent with the known patterns in marine sediment and OM accumulation. Continental material, especially very fine grained continental material, is the largest source of iron (oxyhydr)oxides to marine sediment (Hedges and Kiel 1995, Canfield and Raiswell 2012). As a result (oxyhydr)oxide deposition in marine sediment broadly scales with total sedimentation rate in a linear manner, but the slope of the linear relationship depends on the (oxyhydr)oxide concentration of sedimentary material. Biogenic silca and carbonate will not contain (oxyhydr)oxides and therefore sediments derived mainly from marine biologic activity will be relatively poor in (oxyhydr)oxide. Coastal environments receive a greater ratio of continental material to marine biogenic material than open marine environments (Burdige 2005) such that coastal sediment will have a greater bulk normalized iron (oxyhydr)oxide concentration than open marine sediment. Iron redox cycling also promotes (oxyhydr)oxide formation and deposition (Severmann et al., 2006; Rediel et al., 2014) such that sediments in low-oxygen environments will have higher iron (oxyhydr)oxide concentrations than their well-oxygenation equivalences. (Oxyhydr)oxide precipitation in the upwelling zone can further supercharge bulk normalized sediment iron (oxyhydr)oxide concentrations in areas of upwelling (Hedges and Kiel 1994). This means that at a given total sediment deposition rate there should be an increase in iron (oxyhydr)oxide accumulation along the trend: open marine<low O_2 marine<coastal marine <low O_2 coastal<low O_2 upwelling zone. This pattern fits well with known patterns of organic matter accumulation (Hedge and Kiel 1994).

The main argument against the Rusty Carbon Sink is the notion that iron (oxyhydr)oxides will enhance OM remineralization through dissimilatory iron reduction (DIR). By enhancing DIR (oxyhydr)oxides must therefore be unable to promote OM preservation. In reality, this is non-sequitur argument. Bio-physical dynamics control DIR, not (oxyhydr)oxides deposition,

such that altering (oxyhydr)oxides depositional rates in a manner consistent with natural depositional process will have limited influence on DIR.

The relationship between DIR and (oxyhydr)oxide deposition is encapsulated in the difference Severmann et al., (2006) found between adjacent basins off the coast of California. One of the basins preserves little in the way of organic carbon and was found to have significant rates of DIR. The other basin was far more efficient in terms of organic carbon preservation and far less efficient in terms of DIR. The two basins are at a similar depth and receive effectively the same sediment load and sediment composition. The big difference between the two basins is that the one with low OM preservation is heavily bioturbated while the other basin has little benthic activity. Bioturbation facilitates iron re-suspension and efficient DIR cycling. It is this resuspension process, not sediment deposition, which creates the OM degradation offsets between the basins (Severmann et al., 2006). The same pattern has been found in shallow coastal sediments where sediment bioturbation allows iron atoms to cycle several hundred times during burial process promoting efficient DIR (Canfield et al., 1993). Importantly to drive the OM remineralization rates of an environment characterized by limited DIR to one characteristized by active DIR, there would need to be a two order of magnitude increase in total (oxyhydr)oxide inputs without a simultaneous change in total sediment inputs. Such a change is fundamentally different in scale from the (oxyhydr)oxide changes proposed for continental weathering changes and underscores the physical disconnect between preferential IOC preservation as a mechanism for preferential carbon preservation and DIR as a mechanism for carbon remineralization.

1.6 Climate Change Marine Sediment Accumulation Changes.

Linking marine organic carbon accumulation to changes in total sediment and (oxyhydr)oxide accumulation rates requires re-visiting the feedback between continental weathering and Earth's climate over glacial-interglacial cycles. Glaciers significantly enhance physical sediment denudation from terrestrial catchments (Anderson et al., 1997). At the peak of the Last Glacial Maximum (LGM) the global sediment discharge rate from glacially weathered terrains was at least 3 times the current glacial sediment flux rate (Raiswell et al., 2008). This trebling of glacial sediment discharge equates to a 20-40% increase in global marine coastal deposition over the present conditions (Styviski et al., 2005). Marine sediments are estimated to account for the preservation of 250 Tg Cyr^{-1} (Burdige 2007; Caisis et al., 2013) therefore a 20-40% increase in marine OM burial equates to a 50-100 Tg C yr^{-1} increase in carbon sequestration. This in not a trivial difference when extrapolated over geologic timescales

This thesis aims to more accurately characterize the climatic importance glacial-interglacial continental weathering changes by using (oxyhydr)oxide accumulation to trace changes in OM burial. Flux normalized chemical weathering rates of glacial and non-glacial catchments are similar (Anderson et al., 1997), therefore much of the glacial sediment being deposited in the ocean might be poor in secondary minerals including (oxyhydr)oxides. This could greatly reduce the magnitude to glacial-interglacial weathering changes on the carbon cycle. The chapters which follow represent the first concrete attempt to firmly link these marine sediment discharge changes directly to changes in marine organic accumulations. Such a link is of scientific interest not only because it would constitute a novel climate feedback mechanism but also because of the potential magnitude of the processes being discussed.

The next four chapters will present data:

1) Linking terrestrial weathering differences glacial and non-glacial terrains to changes in mineral formation rates;
2) Development of a novel approach to measuring iron (oxyhydr)oxide concentrations in aquatic sediments;

3) Utilizing this novel approach to quantify the climatic implication of glacial-interglacial weathering changes in Iceland; and

4) Quantifying the climatic impact of glacial-interglacial weathering changes in Greenland.

1.7 References.

Aller C A, Blair N E, Brunskill G J (2008). Early diagenetic cycling, incineration, and burial of sedimentary organic carbon in the central Gulf of Papua (Papua New Guinea). Journ. Geophys. Res. **113**: F01S09

Anderson S.P., Drever J.I., Humphrey N.F. (1997) Chemical weathering in glacial environments. *Geology* **25**: 399-402.

Andersson K, Dahlqvist R., Turner D., Stople B., Larsson T., Ingri J., Andersson P. (2006) Collodial rare earth element in a boreal river: Changing sources and distributions during the spring tide. *Geochim. Cosmochim Act*. **70**: 3261-3274.

Barber A, Lalonde K., Mucci, A., Gelinas Y. (2014) The role of iron in the diagenesis of organic carbon and notrigen in sediments: A long-term incubation experiment. *Marine Chem*. **162**: 1-9

Barker, P. F., Kennett, J. P., et al., (1990). Proc. ODP, Sci. Results, 113: College Station, TX (Ocean Drilling Program).

Barker, P.F., Camerlenghi, A., Acton, G.D., et al., (1999). *Proc. ODP, Init. Repts.,* 178 [Online]. Available from World Wide Web: <http://www-odp.tamu.edu/publications/178_IR/178TOC.HTM>.

Barron, J., Larsen, B., et al., (1991). Proc. ODP, Sci. Results, 119: College Station, TX (Ocean Drilling Program).

Berner R.A. (1970) Sedimentary Pyrite Formation. *American Journal of Science* **268**: 1-23.

Berner R.A. (1982) Burial of organic carbon and pyrite sulphur in the modern ocean: its geochemical and environmental significance. *Amer. Journ. Sci*. **282**: 451-473.

Berner R.A, Kothavala Z. (2001) GEOCARB III: A Revised Model of Atmospheric CO2 Over Phanerozoic Time. *Americ. Jounr. Scienc*. **301**: 182-204.

Berner R.A. (2003) The long-term carbon cycle, fossil fuels and atmospheric composition. *Nature*. **426**: 323-326.

Blair N.E. and Aller R.C. (2013) The fate of terrestrial organic carbon in the marine environment. *Annu. Rev. Marine Sci*. **4**: 401-423.

Boudot J.-P., Bel Hadj Brahim A., Steiman R., Seigle-Murandi F. (1989) Biodegradation of synthetic organo-metallic complexes of iron and aluminium with selected metal to carbon ratios. *Soil Biol. Biochem*. **21**(7):961-966.

Boye M., Nishioka J., Croot P., Laan P., Timmermans K.R., Strass V.H., Takeda S., de Barr H.J.W. (2010) Significant portion of dissolved organic Fe complexes in fact is Fe colloids. *Mar. Chem.* **122**: 20-27.

Brackley H.L., Blair N.E., Trustman N.A., Carter L, Leithold E.L. Canuel E.A., Johnston J.H., Tate K.R. (2010) Dispersal and transformation of organic carbon across an episodic high sediment discharge continental margin, Waipaoa Sedimentary System, New Zealand. Marine Geology. **270**: 202-212

Buesseler K.O. and Boyd P.W. (2003) Will Ocean Fertilization Work? *Science*. **300**: 67-68.

Buesseler K.O., Andrews J.E., Pike S.M., Charette M.A. (2004) The Effects of Iron Fertilization on Carbon Sequestration in the Southern Ocean. *Science*. **304:** 414-417.

Burdige D.J. (2005) Burial of terrestrial organic matter in marine sediments: A re-assessment. *Global Biogeochem. Cycles*. **19**: GB4011.

Burdige D.J. (2007) Preservation of organic matter in marine sediments: controls, mechanisms, and an imbalance in sediment organic carbon budgets? *Chem. Rev.* **107**: 467-485.

Canfield D.E., Thamdrup B, Hansem J.W. (1993) The anaerobic degradation of organic matter in Danish coastal sediments: Iron reduction, manganese reduction and sulfate reduction. *Gechem Cosmochem Act*, **57**:3867-3883.

Canfield D.E. (1994) Factors influencing organic carbon preservation in marine sediments. *Chem. Geo.* **114**: 315-329.

Ciasis P. and Sabine C. (2013). *Carbon and Other Biogeochemical Cycles.* In: Climate Change 2013: The Physcial Sciences Basis. Contribution of Working Group 1 to the Fifth Assessment Report of the Intergovernmental Panel on Climate Change. Cambridge University Press, United Kingdom.

Dale A.W., Sommer S., Lomnitz U., Montes I., Treude T., Liebetrau V., Gier J., Hensen C., Dengeler M., Stolpovsky K., Bryant L.D., Wallmann K. (2015) Organic carbon production, mineralisation and preservation on the Peruvian margin. *Biogeosciences*. **12**: 1537-1559.

Dean W.E. and Arthur M.A. (1989) Iron-sulfur-carbon relationships in organic-carbon-rich sequences I: Cretaceous western interior seaway. *Am Journ. Sci*. **289**: 708-743.

Greathouse J.A., Johnson K.L., Greenwell H.C. Interactions of natural organic matter with layered minerals: recent developmentsw in computational methods at the nanoscale (2014) *Minerals*. **4**:519-540

Hedges J.I. and Keil R.G. (1995) Sedimentary organic matter preservation: an assessment and speculative synthesis. *Mar. Chem*. **49**: 81-115.

Hilton R.G., Galy A, Hovius N, Horng M-J, Chen H. (2010) The isotopic composition of particulate organic carbon in mountain rivers of Taiwan. *Geochem Cosmochem Act*, **74**: 3164-3181.

Ingri J., Malinovsky D., Rodushkin I., Baxter D.C., Widerlund A., Andersson P., Gustafsson O., Forsling W., Ohlander B. (2006) Iron isotope fractionation in river colloidal matter. *Earth Plan Sci Lett*. **245**: 792-798.

Ilina S.M., Poitasson F., Lapitskiy S.A., Alekhin Y.V., Viers J., Pokrovshy O.S. (2013) Extreme iron isotope fractionation between colloids and particles of boreal and temperate organic-rich waters. *Geoch. Cosmo. Act.* **101**: 96-111.

Jaccard S.L., Hayes, C.T., Martinez-Gargia A, Hodell D.A., Anderson R.F., Sigman D.M., Haug G. H. (2013). Two Modes of Change in Southern Ocean Productivity Over the Past Million Years. *Science* **339**: 1419-1423.

Kao S-J, Shiah F-K, wangs C-H, Li K-K (2006) Efficient trapping of organic carbon in sediments on the continental margin with high fluvial sediment input off southwestern Taiwan. *Continental Shelf Research*. **26**(20): 2520-2537.

Kaiser K. and Guggenberget G. (2000) The role of DOM sorption to mineral surfaces in the preservation of organic matter in soils. *Organic Geochem.* **31**:711-725

Keil R.G., Montlucon D.B., Prahl F.G., Hedges J.I. (1994) Sorptive preservation of labile organic matter in marine sediments. *Nature*. **370**: 549-552.

Kennedy M.J., Pevear D.R., Hill R.J. (2002) Mineral surface control of organic carbon in black shale. *Science*. **295**: 657-660.

Kennedy M.J., Wagner T. (2011). Clay mineral continental amplifier for marine carbon sequestration in a greenhouse ocean. *PNAS*. **108**(24): 9776-9781.

Kiem R., Kognel-Knbaner I. (2002) Refractory organic carbon in particle-size fractions of arable soils II: organic carbon in relation to mineral surface area and iron oxides fractions <6 µm. *Organic Geochem*. **33**: 1699-1713.

Kogel-Knabner I., Guggenberger G, Kleber M., Kandeler E., Kalbitz K, Scheu S., Eusterhues K, Leinweber P. (2008) Organo-mineral associations in temperate soils: integrating biology, mineralogy and organic matter chemistry. *J. Plant Nutr. Soil Sci*. **171**: 61-82.

Lalonde K., Mucci A., Ouellet A., Gelinas Y. (2012) Preservation of organic matter in sediments promoted by iron. *Nature.* **483**: 198-200.

von Lutzow M., Kogel-Knabner I., Ludwig B., Matzner E., Flessa H., Ekschmitt K., Guggenberger G., Marschner B., Kalbitz K. (2008) Stabilization mechanisms of organic matter in four temperate soils: development and application of a conceptual model. *J. Plant Nutr. Soil Sci*. **171**: 111-124.

Luyendyk, B.P., Cann, J.R., et al. (1978). Intial Reports of the Deep Sea Drilling Project, v. 49: Washington (US Government Printing Office)

Lyven B., Hassellov M., Turner D.R., Halraldsson C., Andersson K. (2003) Competition between iron- and carbon-based colloidal carriers for trace metals in a freshwater assessed using flow filed-flow fractionation coupled to ICPMS. *Geochem Cosmo Act*. **67**(20):3791-3802.

Marino M, Maiorano P., Lirer F. Pelosi N. (2009). Response of calcareous nannofossil assemblages to paleoenvironmental changes through the mid-Pleistocene revolution at Site 1090. *Palaeogeog. Palaeoclim. Palaeoeco*. **208**: 333-349.

Martin J.H. (1990) Glacial-interglacial CO2 change: the iron hypothesis. *Paleoceanogr.* **5**(1):1-13.

Martinez-Garcia A., Sigman D.M., Ren H., Anderson R.F., Straub M., Hodell D.A., Jaccard S.L. Eglinton T.I. Haug G.H. (2014) Iron fertilization of the subantarctic ocean during the last ice age. *Science*. **334**: 1347-1350.

Mayer L.M. (1994) Surface area control of organic carbon accumulation in continental shelf sediements. *Geoch. Cosmoch. Act.* **58**(4):1271-1284.

Mikutta R., Kleber M., Torn M.S., Jahn R. (2006) Stabilization of soil organic matter: association with minerals or chemical recalcitrance? *Biogeochem*. **77**: 25-56.

Misra S. and Froelich P.N. (2012) Lithium Isotope History of Cenozoic Seawater: Changes in Silicate Weathering and Reverse Weathering. *Science.* **335**:818-822.

Morse J.W. and Berner R.A. (1995) What determines sedimentary C/S ratios? *Geochim. Cosmoch. Act.* **59**(6): 1073-1077.

Peketi A., Mazumdar A., Joao H.M., Patil D.J., Usapkar A. Dewangan P. (2015) Coupled C-S-Fe geochemistry in a rapidly accumulation marine sediment system: Diagenetic and depositional implications. *Geochem. Geophys, Geosyst*. **16**: 2865-2883.

Ransom B., Bennett R.H., Baerwald R, Shea K. (1997) TEM study of organic matter of continental margins: occurrence and the “monolayer” hypothesis. *Marine Geology*. **138**: 1-9.

Raiswell R. and Berner R.A. (1985) Pyrite formation in euxinic and semi-euxinic sediments. *Am. Journ. Sci*. **285**: 710-724.

Raiswell R., Tranter M., Benning L.G. Siegert M., De’ath R., Huybrechts P., Payne T. (2006) Contributions from glacially derived sediment to the global iron (oxyhydr)oxide cycle: implication for iron delivery to the oceans. *Geoch. Cosmo. Act.* **70**: 2764-2780.

Raiswell R. and Canfield D.E. (2012) The iron biogeochemical cycle past and present. Geochemical Perspectives, European Association of Geochemistry, 1(1)

Raymo, M.E., Jansen, E., Blum, P., and Herbert, T.D. (Eds.), 1999. *Proc. ODP, Sci. Results,* 162: College Station, TX (Ocean Drilling Program).

Sabadini-Santos E., Senez T.M., Silve, T.S., Moreira M.R., Mendoca-Filho J.G., Santelli R.E. Crapez M.A.C. (2014) Organic matter and pyritization relationship in recent sediments from a tropical and eutrophic bay. *Marine Pollution Bullet*. **89**: 220-228.

Schrumpf M., Kaiser K., Guggenberger G., Persson T., Kogel-Knabner I., Schulze E.-D. (2013) Storage and stability of prganic carbon in soils as related to depth, occlusion within aggregates and attachment to minerals. *Biogeosci*. **10**: 1675-1691.

Severmann S., Johnson C.M., Beard B.L., McManus J. (2006) The effect of early diagenesis on the Fe isotope compositions of porewaters and authigenic minerals in continental margin sediments. *Geoch. Cosmo. Act.* **70**: 2006-2022.

Sheng, Y., Sun Q., Shi W., Bottrell S., Mortimer R. (2015). Geochemistry of reduced inorganic sulfur, reactive iron, and orgnanic carbon in fluvial and marine surface sediment in the Laizhou Bay region, China. *Environ. Earth Sci*. **74**: 1151-1160.

Sholkovitz E.R. and Copland D. (1981) The coagulation, solubility and adsorption properties of Fe, Mn, Cu, Ni, Cd, Co and humic acids in a river water. *Geochem Cosmochem Act*. **45**: 181-189.

Suanders, A.D, Larsen, H.C., and Wise, S.W., Jr. (Eds.), 1998. Proc. ODP, Sic. Results, 152:College Station, TX (Ocean Drilling Program)

Syvitski J.P.M., Vorosmarty C.J., Kettner A.J. Green P. (2005) Impact of humans of the flux of terrestrial sediment to the global coastal ocean. *Science*. **308**: 376-380.

Talwani, M., Udintsev, G., et al., 1976. Initial Reports of the Deep Sea Drilling Project, Volume 38, Washington (U.S. Government Printing Office), 1256

Thompson A., Rancourt D.G., Chadwick O.A., Chorver J. (2011) Iron soild-phase differentiatone along a redox gradient in basaltic soils. *Geochem Cosmochem. Act.* **75**: 119-133.

Vasyukova E., Pokrovsky O.S., Viers J., Dupre B. (2012) New operational method of testing colloid complexation with metals in natural waters. *Appl. Geochem.* **27**: 1226-1237.

Westrich J.T., Berner R.A. (1984). The role of sedimentary organic matter in bacterial sufate reduction: The G model tested. *Limnol. Oceanogr.* **29**(2): 236-249.

Xu-hui Z., Lian-qing L., Gen-xing P. (2007) Topsoil organic carbon mineralization and CO2 evolution of three paddy soils from South China and the temperature dependence. *Journ. Environ. Sciences.* **19**: 319-326.

Zech W., Senesi N., Guggenberger G., Kaiser K., Lehmann J., Miano T.M., Miltner A., Schroth G. (1997) Factors controlling humifcation and mineralization of soil organic matter in the tropics. *Geoderma*, **79**: 117-161.

Chapter 2-
The Relationship between Weathering and (Oxyhydr)oxide Formation in Glacial and Non-glacial Catchments in Iceland.

Abstract

Glaciers enhance terrestrial erosion and sediment export to the ocean. Glaciers can also impact mineral specific weathering rates relative to analogous non-glacial terrains. In tandem these processes affect continent sediment export to the oceans over glacial-interglacial cycles. This study summarizes field data from glacial and non-glacial Icelandic river catchments to quantify the impact of weathering regime on iron and aluminium (oxyhydr)oxide mineral formation and flux rates. Aluminium and iron (oxyhydr)oxides are strong indicators of organic carbon preservation in soils and marine sediments. Tracing changes in (oxyhydr)oxide formation and deposition therefore provides a means of evaluating potential changes in organic carbon sequestration rates over glacial-interglacial cycles. Overall, there are several measurable chemical differences between the studied glacial and non-glacial catchments which reflect the key role of soil formation on terrestrial weathering. One of the noted chemical difference is that weathering in non-glacial catchments is characterized by higher apparent rates of iron and aluminium (oxyhydr)oxide formation relative to glacial catchments. However, the offset in (oxyhydr)oxide formation does not appear to be transferred into river sediment compositions, and physical weathering appears to be the dominant control of river sediment composition and export. Glacial rivers export far more total sediment to nearshore marine environments than analogous non-glacial rivers suggesting glacial weathering enhances carbon burial by increasing nearshore marine (oxyhydr)oxide accumulation.

2.1 Introduction

Iron and Al (oxyhydr)oxide (Fe/Al_{OOH}) concentrations are approximated based on selective chemical extractions techniques. The pool of dithionate-citrate-bicarbonate (DCB) reducible minerals, referred to as 'highly reactive Fe/Al' (Fe_{HR}/Al_{HR}), is one of the most commonly used methods for estimating for both Fe_{OOH} and Al_{OOH} (Raiswell and Canfield 2012). There are strong correlations between the concentrations of Fe_{HR} and organic carbon in marine sediments and Fe_{HR}/Al_{HR} and organic matter in soils (Schrumpf et al., 2013). These correlations are thought to reflect the physiochemical protection of organic matter by Fe_{OOH} and Al_{OOH} (see review by Schrumpf et al., 2013); a process which has been dubbed the 'Rusty Carbon Sink' (Lalonde et al., 2012, Barber et al., 2014).

The Rust Carbon Sink is not the first hypothesis to propose Fe_{OOH} can have a major impact on Earth's climate cycle. The Iron Hypothesis (Martin, 1990) is the well-studied idea that Fe_{OOH} accumulation in the Southern Ocean controls primary productivity in the region. While much of the research into the Iron Hypothesis has focused on atmospheric dust (e.g. Coale et al., 2004; Martinez-Garcia et al., 2014), Martin (1990) proposed the intensity of glacial weathering on Antarctica was itsef a major control of iron export to the ocean. Glacial weathering has specifically been shown to allow for both the formation and large scale export of iron (oxyhydr)oxides to coastal marine environments (Raiswell et al., 2008; Hawkins et al., 2014, Eirkisdottir et al 2015). This raises the question of if glacial weathering promotes organic carbon burial, in addition to primary production, as a result of enhanced marine Fe_{OOH} discharge?

This study re-examines published physical and chemical weathering data from glacial and non-glacial catchments in Iceland. River waters, sediment and soils are compared to derive generalized patterns of continental weathering in glacial and non-glacial catchments. Novel PHREEQC inverse models are also used to approximate the Fe_{OOH} and Al_{OOH} formation rates based on comprehensive river monitoring datasets. The geologic and geographic nature of Iceland limits the impact of bedrock variability and emphasizes the impact of continental weathering on sediment composition. This allows a more accurate determination of the potential impact of chemical offsets between glacial and non-glacial weathering on (oxyhydr)oxide formation.

2.2 Icelandic Geology, Hydrology and Sample Locations

Iceland has four characteristics which favour its use as a type locality for linking glacial and non-glacial weathering differences to differences in Fe/Al_{OOH} dynamics. Iceland's geologic and geographic history has combined to create river catchments, which are can be chemically differentiated based on their extents of soil formation (Gislason et al., 1996). Iceland's human geography ensures that the catchments are not significantly altered by anthropogenic activity. Icelandic rivers have been intensively sampled providing a large historic chemical database which can be utilized to investigate chemical weathering. Finally, existing thermodynamic scientific studies have defined clear expectations of how chemical weathering should progress in Iceland.

Bed rock rheology and chemical composition significantly impact continental weathering rates (Syvitski and Milliman 2007). Therefore, geologically similar and well-characterized catchments are useful when comparing glacial and non-glacial weathering rates. Iceland is a geologically young and active island, formed primarily (>80%) of basaltic

lavas, with a mixed mid-ocean ridge/ocean island melt source composition. The remainder of the island is composed of more acidic/rhyolitic lavas (Jakobsson 1972). Iceland was completely covered by a single glacial icesheet ~9 ka ago, which collapsed during the Early Holocene stabilizing to near modern conditions about 6 ka ago (Gislason 1996; Norðdhal and Petersson et al., 2005). Since the collapse of the icesheet vegetation and soil formation processes have created significant chemical differences between glacial and non-glacial catchments, reflected in the distribution of Iceland's major soil/sediment types distributed across the island (Figure 2.1). Soil formation has been attributed to as the principle cause of a number of chemical differences between the glacial and non-glacial catchments (Gislason et al., 1996; Pogge von Strandmann et al., 2006, 2012; Opfergelt et al., 2013; Opfergelt et al., 2014).

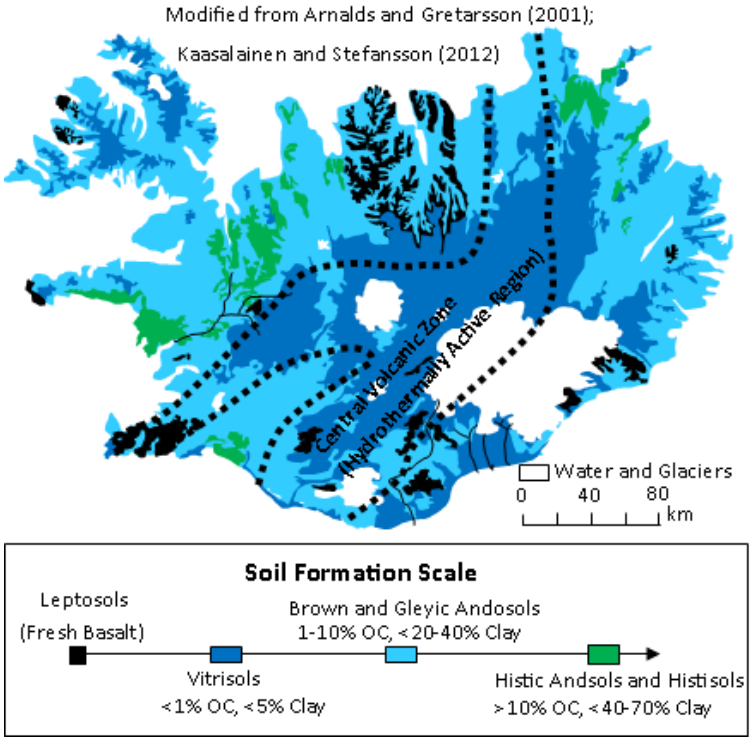

Figure 2.1. Icelandic soil coverage map as modified from Arnalds and Gretasson (2001). The Central Volcanic zone defines the general limits of significant hydrothermal groundwater formation as mapped by Kaasalainen and Stefansson (2012).

A number of previous studies have sampled Icelandic soils, sediments, rivers and groundwaters in the context of continental weathering and this study will draw extensity on data from: Gislason and Stefansson (1993), Gislason et al., (1996), Stefansson et al., (2001), Arnorsson et al., (2002), Pogge von Strandmann et al., (2006), Vigier et al., (2006), Vigier et al., (2009), Oskarsson et al., (2012), Pogge von Strandmann et al., (2012), Eiriksdottir et al., (2008), Louvat et al., (2008) and Opfergelt et al., (2014). This previously published work provides what is likely the most complete and extensive data-set on the

interplay of weathering regimes and chemical weathering ever collected on a single geologic terrain. Because the chemistry of river waters and sediment can show a high degree of temporal and special variability, large sample sets are required to make statistically robust conclusions about the chemical weathering process.

2.3 Methods

2.3.1 Field sample collection:

River water and sediment samples from Iceland were collected during September 2003, August 2005 reported in Pogge von Strandmann et al., (2006) and then again by the same methods in August 2012 and August 2013 at locations shown on Figure 2.2. River samples were collected from near the water surface in the centre of the flow with access facilitated by road bridges. For filtered and suspended sediment samples, 15L of water was collected and filtered shortly after sampling through 0.2µm cellulose-acetate Millipore filters, using a pressurized PFA unit. To prevent sample cross contamination the units were flushed with milli-Q water and at least 2 L of sample which were discarded prior to sample collection. Elemental iron and aluminium concentrations within this filtered water will be referred to as 'filtered' iron/aluminium rather than the more commonly used 'dissolved' moniker. The filters were sealed in petri-dishes for immediate storage and transport to controlled lab conditions where the sediment was physically removed with a tephlon spatuala and transferred into glass vials. Total suspended sediment (TSS) concentrations were measured separately by filtering a known volume of water through a pre-weighted 0.2µm filter. These filters were also sealed in petri-dishes for transport to the laboratory where they were dried and re-weighed. Total anion samples, utilizing containers cleaned without acids to avoid NO_3^{2-} or Cl^- contamination, were also collected. Temperature, pH, alkalinity and conductivity were measured in the field, and where possible a river bed sediments (RBS) sample was also taken.

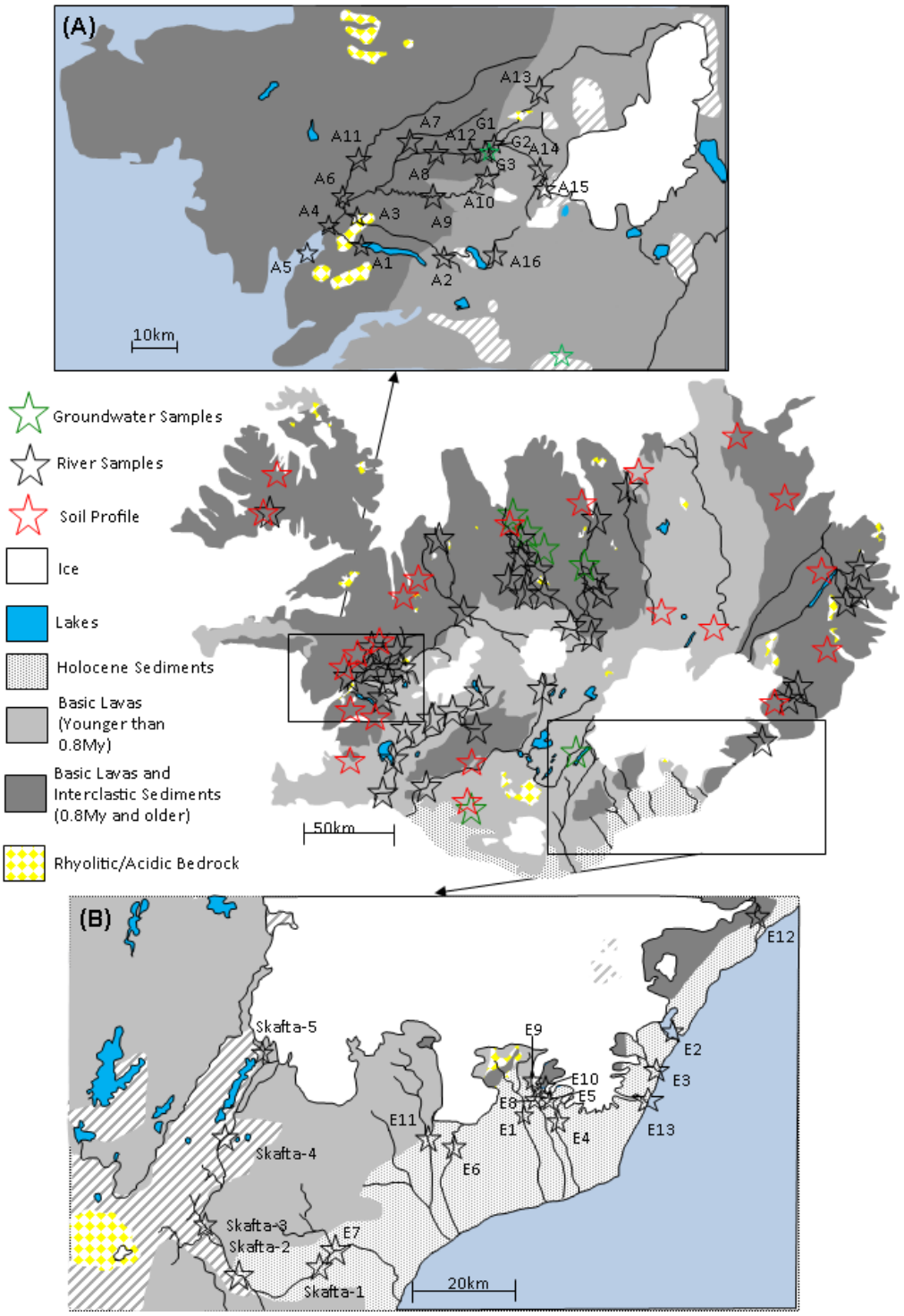

Figure 2.2. Bedrock Map and River Catchments. The middle figure shows the locations of samples from Gislason et al., (1996), Arnorsson et al., (2002), Oskarsson et al., (2012), and Opfergelt (2014) on a modified version of the Icelandic bedrock map from the Natural History Museum of Iceland. (A) Shows sample locations in the Borgarfjörður region and (B) shows the sample locations in the Vatnajökull region.

We will consistently compare our data with Gislason and Arnorsson (1993), Gislason et al., (1996) and Arnorsson et al., (2002) who sampled at locations shown on Figure 2.2.

The only significant difference between the methods used in these studies and our methods is that these previous studies utilized a 0.1µm cut-off size for filtering their water. Waters filtered at the 0.2µm and 0.1µm level are predicted to be closely comparable in terms of Fe, based on studies of the relationship between particle size and Fe speciation (e.g. Lyven et al., 2003, Andersson et al., 2006).

2.3.1 Major and Trace Element Analysis:

Samples from the 2003 and 2005 field seasons were analysed by Pogge von Strandmann et al., (2006) with methods reported therein. Anions and cations from the 2012 and 2013 samples were analysed using a Dionex D-500X ion exchange chromatograph at Durham University. Iron and aluminium concentrations were measured by a Thermo-Fisher X-Series inductively coupled plasma mass spectrometry (ICP-MS) at Durham University, calibrated against multi-element synthetic standards prepared from high purity single element standards. A collision cell was used to reduce oxide formation and improve accuracy. The natural water certified reference material SLRS-5 was used confirm the accuracy of the measurements. External reproducibility for all measurements was better than ±5%.

The total carbon concentrations of a selected range of suspended sediment samples were measured during stable carbon and nitrogen analysis on an isotope ratio-mass spectrometer at Durham University. The total carbon concentrations of river bedload sediments were not directly measured but loss-on-ignition values collected during XRD analysis by Pogge von Strandmann et al., (2006) are used to reflect maximum potential carbon concentrations in these samples.

2.4. Theory and Model Calculations

PHREEQC v. 3.0.6 (Parkhurst and Appelo 1999) parameterized with the Bureau de Recherches Geologiques et Minieres database (Blanc et al., 2011) was used to build an inverse dissolution/precipitation weathering model. The model calculates primary mineral specific dissolution rates and secondary mineral precipitation rates. This is done by numerically determining the balance of primary mineral dissolution and secondary mineral dissolution needed to recreate the measured river water chemistry of a sample from an initial idealized rainwater solution. In effect this modelling approach provides a way of utilizing the overall chemical patterns of the rivers to investigate chemical weathering rather than depending on one or two element comparisons.

The measured chemical composition (alkalinity, pH Al, Ca, Cl, Fe, K, Mg, NO_3, Na, Si, SO_4) of the river samples was used to define a solution for every filtered water sample.

The Cl concentrations of each sample were then used to define an idealized initial rainwater solution for each sample according to the method developed by Gislason et al., (1996). The idealized Cl derived rainwater solutions are not however perfectly charge balanced so a 5% elemental uncertainty was included in the model calculations to account for the charge imbalances. The 5% threshold was set by assuming the charge imbalances reflected analytic uncertainty. All chemical pathways which reproduce the river solutions from the dissolution of primary bedrock phases and precipitating the secondary phases starting from the idealized rainwater solutions were calculated. These pathways were then averaged, yielding a single set of mineral precipitation and dissolution values characteristic of the weathering signature of each sample.

The primary mineralogy of both the primary basaltic bedrock (excluding basaltic glass) and secondary clay and (oxyhydr)oxide phases are well constrained and have been defined based on Jackobsson (1972), Gislason and Arnorsson (1993), Stefansson (2001), and Opfergelt et al., (2013) as reported in Table 2.1. The inverse models depend on stoichiometric calculation, rather than thermodynamic data, preventing the inclusion of amorphous phases namely, basaltic glass and allophone, which have no set formula. The stoichiometric nature of the model also makes it impossible to differentiate minerals with the same chemical formula. Ferrihydrite and boehmite were excluded from the models on this basis as these minerals have the same chemical formulas (as defined in the PHREEQC database) as goethite and gibbsite, respectively. PHREEQC requires all elements used for charge balance during inverse model calculations to be included in model input phases requiring the addition of CO_2, O_2, Cl_2, NH_3 and SO_2 into the model parametrization.

Table 2.1 Summary of minerals included in PHREEQC inverse-models.

Charge Balance	Primary Mineral Phase (Dissolved Only)		Secondary Mineral Phases (Precipitate Only)	
CO_2	Forsterite: Mg_2SiO_4	Hedenbergite: $CaFe(SiO_3)_3$	Imogolite: $Al_2SiO_3(OH)_4$	Goethite: FeOOH
O_2	Fayalite: Fe_2SiO_4	Ilmentite: $FeTiO_3$	Heulandite: $Ca_{1.07}Al_{2.14}Si_{6.86}O_{18}$:6.17$H_2O$	Boehemite: AlOOH
Cl_2	Ferrosilite: $FeSiO_3$	Albite: $NaAlSi_3O_8$	Montmorillonite(A): $Ca_{0.17}Mg_{0.34}Al_{1.66}Si_4O_{10}(OH)_2$	
NH_3	Enstatite: $MgSiO_3$	Anorthite: $CaAl_2Si_2O_8$	Montmorillonite (B): $Na_{0.34}Mg_{0.34}Al_{1.66}Si_4O_{10}(OH)_3$	
SO_2	Diopside: $CaMg(SiO_3)_2$	Sandine: $KAlSi_3O_8$	Kaolinite: $Al_2Si_2O_5(OH)_4$	

The biggest potential problem with utilizing inverse-chemical weathering models is that the results are dependent on knowing the exact chemical formulas of all the mineral

phases. Ideally every potential mineral phase needs to be precisely and accurately defined however this is not possible in the context of Icelandic weathering. Specifically, additional consideration needs to be given for the behaviour of basaltic glass and allophane.

Basaltic glass is the first component of Icelandic basaltic to be chemical weathered in most low temperature environments (Stefansson et al., 2001). The thermodynamics of glass dissolution in Iceland have been studied but the process has only been defined as a function of a theoretical pure SiAl(OH) form i.e. Gislason and Oelkers (2003), Eiriksdottir et al., (2015). As our model is dependent on mineral stoichiometry, the inclusion a theoretical glass formula, which does not contain Fe, Ca, Mg, etc., would strongly bias the model predicted impact of glass dissolution. Glass dissolution is a well quantified source of Fe_{OOH} formation (Gislason and Arnorsson 1993). The exclusion of basaltic glass in the model is equivalent to the assumption that Fe and Al will behave in the same way during glass weathering. That is glass weathering is assumed to not lead to preferential Fe_{OOH} vs Al_{OOH} formation. A different stoichiometric problem prevents the inclusion of allophane, one of the most common secondary minerals in Icelandic soils (Oskarsson et al., 2012), in the models.

Secondary alumina-silica formation in Iceland has been described as involving the formation of ‘amorphous sponge-like balls of kaolinite, allophane and imogolite’ which are in quasi-equilibrium with gibbsite (Stefansson and Gislason 2001). The precise composition of these alumina-silicate agglomerates appears to vary with changing conditions (Stefansson and Gislason 2001), making it impossible to define a fixed chemical formula for the species. Kaolinite and Imogolite are the endmembers of the kaolinite-allophane-imogolite series so they were included in the model and allowed to vary relative to one another. The overall uncertainty of the Al/Si ratio of the amorphous alumina-silicates however does limit the certainty which can be ascribed to the Al_{OOH} formation rate estimates.

In other localities, the inclusion of iron in certain clay minerals would also introduce uncertainty in terms of the model-predicted Fe/Al_{OOH} formation rates. In Iceland, this does not appear to be a significant problem. While Fe-smectites have been identified in mature Icelandic soils (Stefansson and Gislason 2001), very little iron appears to be directly incorporated into Icelandic clay minerals. Data supporting this assertion will be outlined in subsequent sections, but, in short, the most altered Icelandic soil samples from Opfergelt et al., (2014) are 82.5 and 98 wt. % clay and organic matter, and the iron within these samples is 91% and 95% DCB-extractable, respectively. Consequently, no more than about 5% of iron cycling during chemical weathering is affiliated with the formation of iron bearing clays.

2.5 Results

All data is presented in figures containing a mixture of new and published data which are cited accordingly. The solid phase concentration data is reported normalized to titanium. Titanium is considered to be immobile during basaltic weathering and behaves conservatively in basaltic soils (Nesbitt and Wilson 1992) favouring its use to normalize against organic matter dilution and/or mobile element leaching.

2.5.1 Icelandic Bedrock

Pristine Icelandic basaltic lavas from Jakobsson (1972), Arnorsson et al., (2002), Eiriksdottir et al., (2008), Louvat (2008) and Schuessler et al., (2009) are characterized by relatively constant Ti normalized elemental ratios shown on Figure 2.3. Icelandic rhyolite contains an order of magnitude less total Ti than the basalts, 2.2 mol/kg vs 0.17 mol/kg respectively, which significantly offsets the Ti normalized elemental concentrations between the basalts and rhyolites. There is limited compositional overlap between the basaltic and rhyolitic samples although some of the basaltic samples have [Na+K]/[Ti] values which drift towards more evolved values.

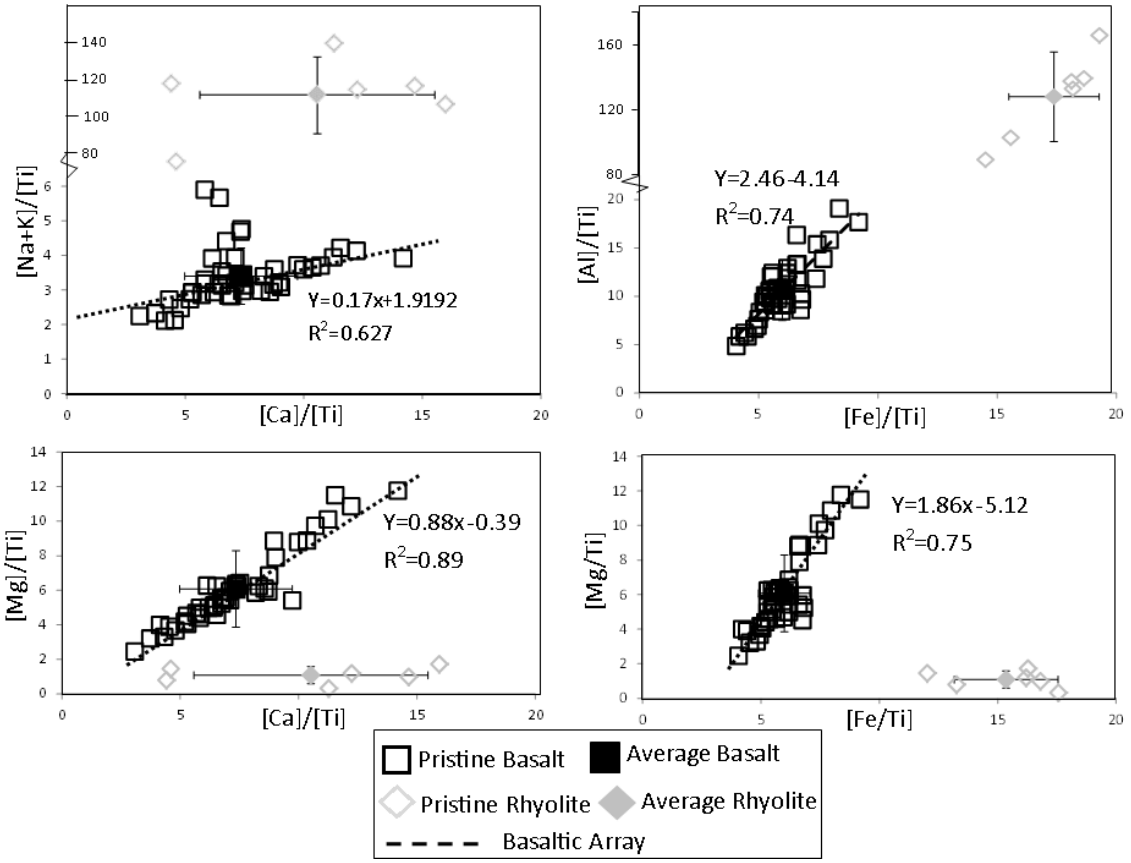

Figure 2.3. data from Jakobsson (1972), Arnorsson et al., (2002), Eiriksdottir et al., (2008), Louvat (2008) and Schuessler et al., (2009). Icelandic basalts display a limited range of variability in Ti normalized elemental space characterized by positive correlations between the various elements.

The compositional range of pristine Iceland basalt can be constrained to statistically significant correlations between Ti normalized elemental concentrations, shown as the dashed lines on Figure 3. These correlations include elemental pairs such as Mg and Ca, which have a similar mobility during chemical weathering, and elemental pairs such as Mg and Fe which have significantly different elemental mobilities (Gislason et al., 1996). For the remainder of this paper these correlations are used to define the compositional signature of pristine basalt, which will be shown as dashed black lines on the subsequent figures.

2.5.2 River Sediment Compositions

The compositions of total suspended sediment (TSS) and river bed sediment (RBS) from glacial and non-glacial rivers from Pogge von Strandmann et al., (2006) and Eiriksdottir et al., (2008) are reported relative to the basaltic compositional array in Figure 2.4. All the sediments have compositions which fall along or near the basaltic compositional array for most elements. The non-glacial TSS samples have mobile element patterns near one endmember of the basaltic compositional array while the glacial TSS samples have mobile element concentrations near the other basaltic endmember. The only potential compositional

deviation of the sediments from basaltic values is apparent in Fe/Al space. A number of the glacial samples have lower [Al]/[Ti] ratios relative to their [Fe]/[Ti] ratios than observed in pristine basalt.

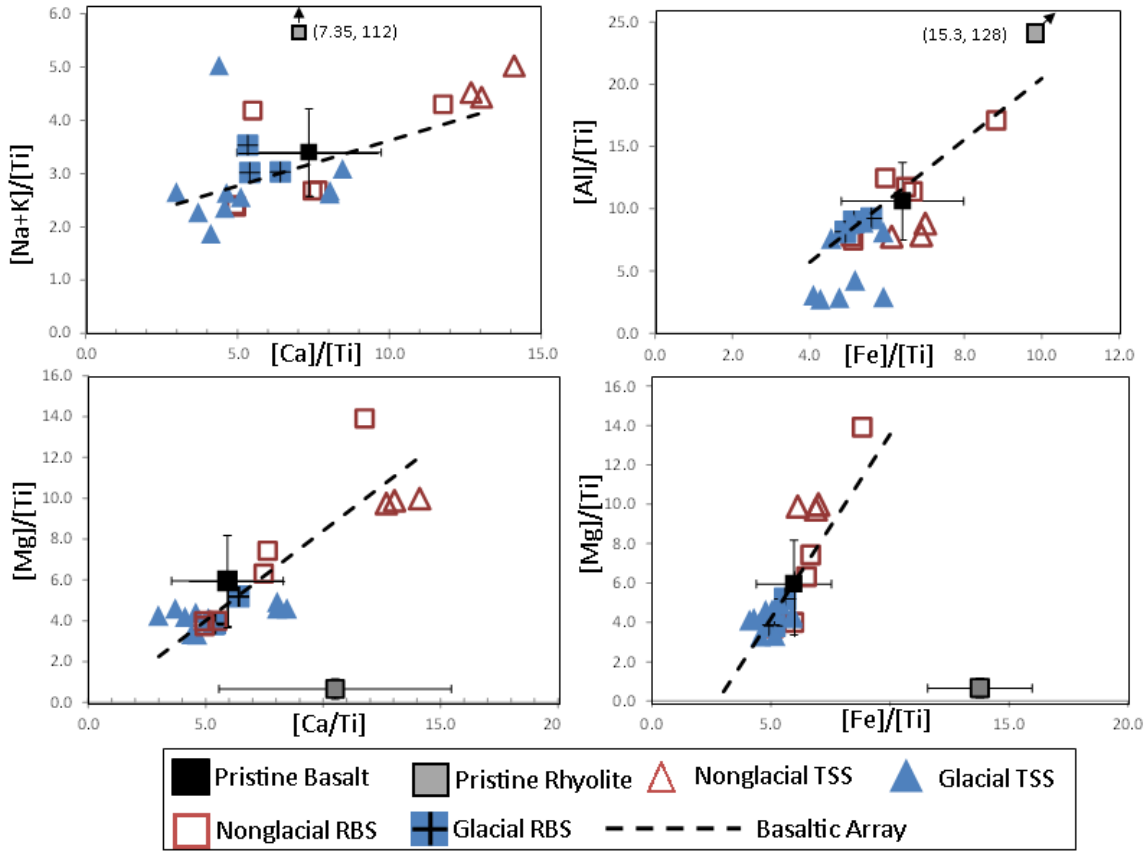

Figure 2.4. River sediment compositional data from Pogge von Strandmann et al., (2006) and Eiriksdottir et al., (2008). All the river sediments have elemental compositions consistent with those expected for pristine basalt except in terms of the proportion of [Al]/[Ti] to [Fe]/[Ti] in the glacial sediments.

2.5.3 Soil Formation

The compositions of Icelandic soil samples from Óskarsson et al., (2012) and Opfergelt et al., (2014) are reported relative to the basaltic compositional array on Figure 2.5. All the samples are from soil profiles that lie above basaltic bedrock as shown on Figure 2.2. Air borne volcanic ash, primary composed of basaltic ash, is also a major component of most Icelandic soils (Oskarsson et al., 2012). The samples are colour coded according to their Total Reserve in Bases ($TRB = \sum Na^+ + K^+ + Ca^{2+} + Mg^{2+}$ $cmol_c$ kg^{-1}). In general soil formation leads to the loss of base cations, an increase in organic carbon concentration, and the transformation of primary magnetite into secondary (oxhydr)oxides i.e. ferrihydrite and goethite.

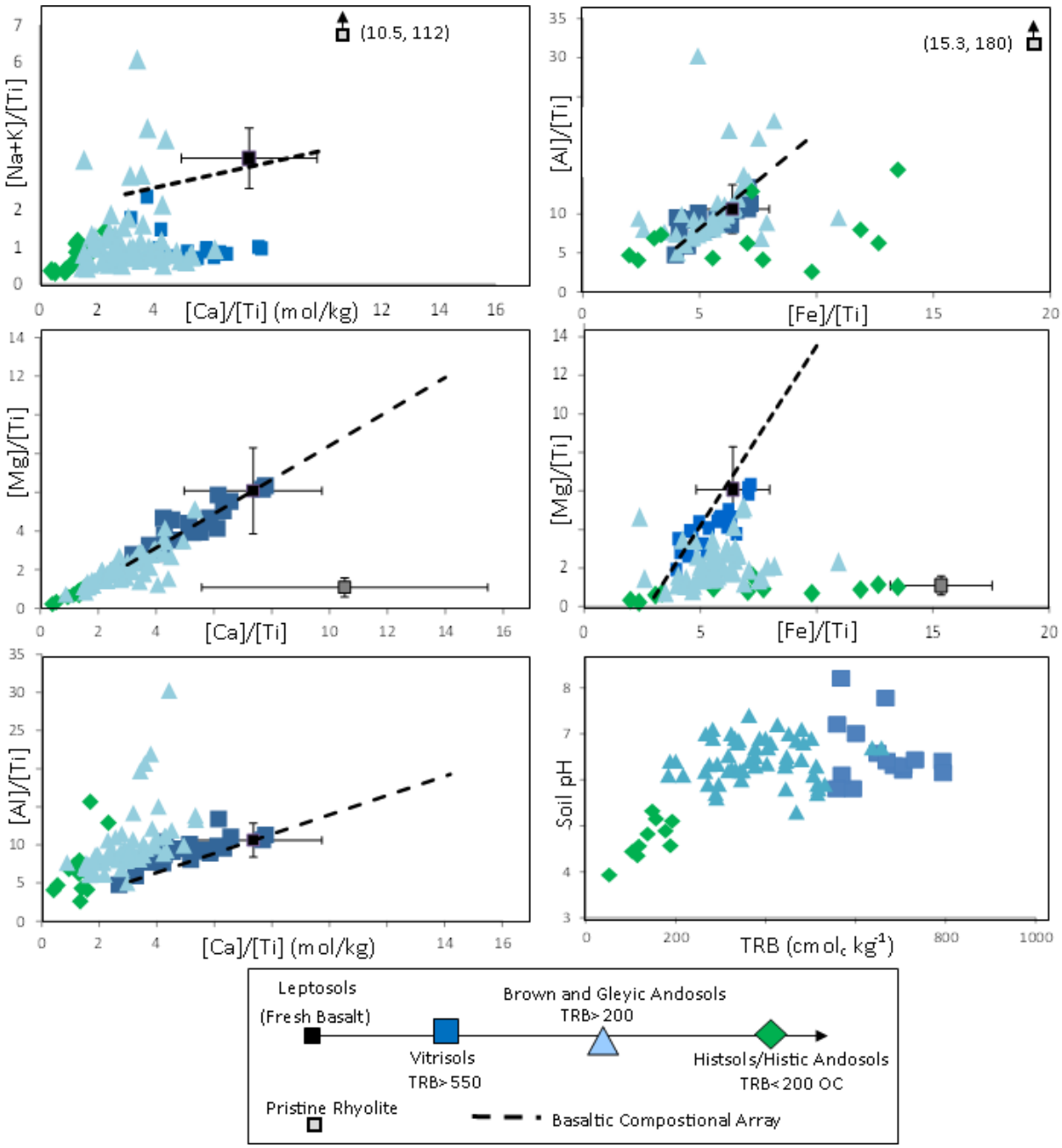

Figure 2.5. Icelandic soil composition data from (Oskarsson et al., 2012; Opfergelt et al., 2014). The dashed black lines reflect the compositional range of typical Icelandic basalt as defined in Section 2.3.2. The soils are colour coded according to their Total Reserve in Bases ($TRB = \sum Na^+ + K^+ + Ca^{2+} + Mg^{2+}$ cmol$_c$ kg^{-1}).

There is a general decrease in soil pore-water pH with decreasing TRB. Magnesium and Ca appear to behave similarly and lie on the basaltic compositional array during chemical weathering. Nearly all the soils are significantly depleted in [Na+K]/[Ti] relative to basalt. Aluminium is preferentially retained in the soils relative to Ca and Mg during chemical weathering. Iron is also preferentially retained in soils during chemical weathering relative to Mg and Ca. There is no clear and systematic pattern in the behaviour of Fe relative to Al

during chemical weathering although the soils with the lower TRB concentrations have significantly higher Fe/Al values than pristine basalt.

The trends in iron behaviour during weathering can be further explored by examining changes in iron mineralogy during weathering. Two selective iron extractions, sodium-dithionate-bicarbonate (Fe_{DCB}) and oxalate (Fe_o), were used to measure iron concentrations as a function of iron mineralogy in Icelandic soil by Opfergelt et al., (2014). The important difference between the extractions is that Fe_O includes magnetite but not goethite, while Fe_{DCB} includes goethite but not magnetite (Poulton and Raiswell 2005). Goethite is a common Fe-oxyhydroxide present during basaltic weathering (Stefansson and Gislason 2001), while magnetite is a common primary mineral phase in Icelandic basalts (Gislason and Stefansson 1993). Consequently, Fe_{DCB}/Total Iron (Fe_T) values reflect the proportion of iron oxyhydroxides to total iron within a sample. The Fe_O/Fe_{DCB} values reflect the balance of magnetite dissolution to goethite formation.

Soil Fe_{DCB}/Fe_T values show a strong positive correlation with soil clay content, increasing to in excess of 0.8 in soils with at least 60 wt.% clay (Figure 2.6A). Soil Fe_O/Fe_{DCB} shows a negative correlation with clay content in all but the most weathered soils. A few of the strongly weathered samples have unusually low Fe_O/Fe_{DCB} values given their clay content and these samples do not follow the correlation between clay content and organic carbon defined by others (Figure 2.6 B/C). Field characterizations of the outlaying samples by Opfergelt et al., (2014) suggests that they are all from reducing horizons within the soil profiles.

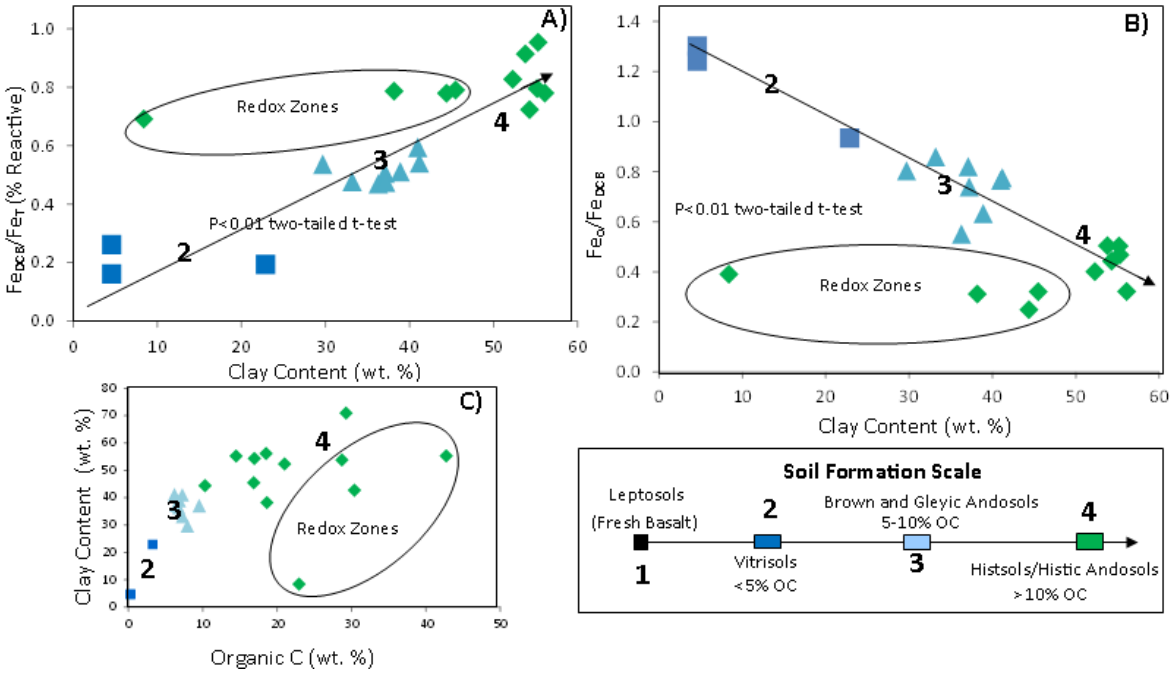

Figure 2.6. Data from Opfergelt et al., (2014). (A) The Fe_{DCB}/Total Iron (Fe_T) values, reflecting the proportion of iron oxyhydroxides to total iron within soil samples, and (B) the Fe_O/Fe_{DCB} values, reflecting the balance of magnetite dissolution to goethite formation are plotted versus the clay content of soil samples from 1) leptosol, 2) vitrisols, 3) brown and gleyic andosols and 4) histosols/histic andosols. (C) The clay content increases with the organic carbon content

2.5.4 Dissolved Load Concentrations

The chemical composition of Icelandic glacial and non-glacial rivers reported by Gislason et al., (1996), Arnorsson et al., (2002), Vigier et al., (2006), Pogge von Strandmann et al., 2006, Louvat et al., (2008), as well as new measurements (data in Supplementary Information) are summarized in Table 2.2. The data in the table includes the measured values as well as values that have been corrected for precipitation inputs. Glacial and non-glacial rivers, on average, have significantly different Cl concentrations (90µM vs. 150µm respectively, $P<0.05$). Icelandic river waters receive nearly all their Cl in affiliation with marine aerosols associated with precipitation allowing Cl to be used to correct rivers for rainwater inputs (Gislason et al., 1996).

Table 2.2. Average River water compositions ±σ. *TSS values were only measured by Pogge von Strandmann et al., (2006), Vigier et al., (2006) and in the new samples reported in the this study. As a result, only 30 glacial and 30 non-glacial samples were utilized to calculate the pH and TSS values. **Chlorine concentrations were used to correct the river values for precipitation inputs according to methods established in Gislason et al., (1996).

	Uncorrected Value		Cl Corrected value	
	Glacial n=50	Nonglacial n=57	Glacial n=50	Nonglacial n=57
Al (µM)	1.4±1.1	0.5±0.4	1.4±1.1	0.5±0.4
Ca (µM)	81±40	102±49	80±40	99±49
Cl (µM)	90±49	150±98	-	-
Fe (µM)	0.4±0.4	0.5±0.5	0.4±0.4	0.5±0.5
K (µM)	10±6	15±7	8±6	12±8
Mg (µM)	59±59	75±57	51±60	64±57
Na (µM)	236±107	280±108	168±86	149±103
TSS* (mg/L)	980±676	204±213		
pH*	8.36±0.95	7.91±0.47		

The precipitation corrected values for the individual samples location are shown in Figure 2.7. The dashed lines on Figure 2.7 correspond to the elemental ratio of pristine basalt, as defined in Section 5.1, such that the bulk dissolution of basalt during chemical weathering would result in the river waters having compositions corresponding to the lines. Overall the rivers do not have compositions consistent with such bulk dissolution. Preferential elemental mobility appears to increase along the trend Fe/Al<Mg, Ca<<Na+K. At the immobile end of this trend Fe and Al appear to behave significantly differently in glacial and non-glacial catchments. All the glacial samples possess an Al/Fe ratio that is equal to or greater than the Al/Fe ratio of basalt. The non-glacial rivers mostly display the opposite trend and are characterized by lower Al/Fe ratios than basalts across a range of Fe concentrations.

In addition to the purely chemical differences, glacial and non-glacial rivers are physically offset in terms of their total suspended sediment concentrations (TSS). Glacial rivers contain on average 4.8 times more TSS than the non-glacial rivers. The average TSS offset is consistent with a long-term record of Icelandic River data by Louvat et al., (2008). Louvat et al., (2008) found that in rivers which had been sampled a minimum of 23 times over a minimum of 7 years, glacial samples contained 923±606 mg/L TSS while non-glacial samples contained on average 150±85 mg/L TSS.

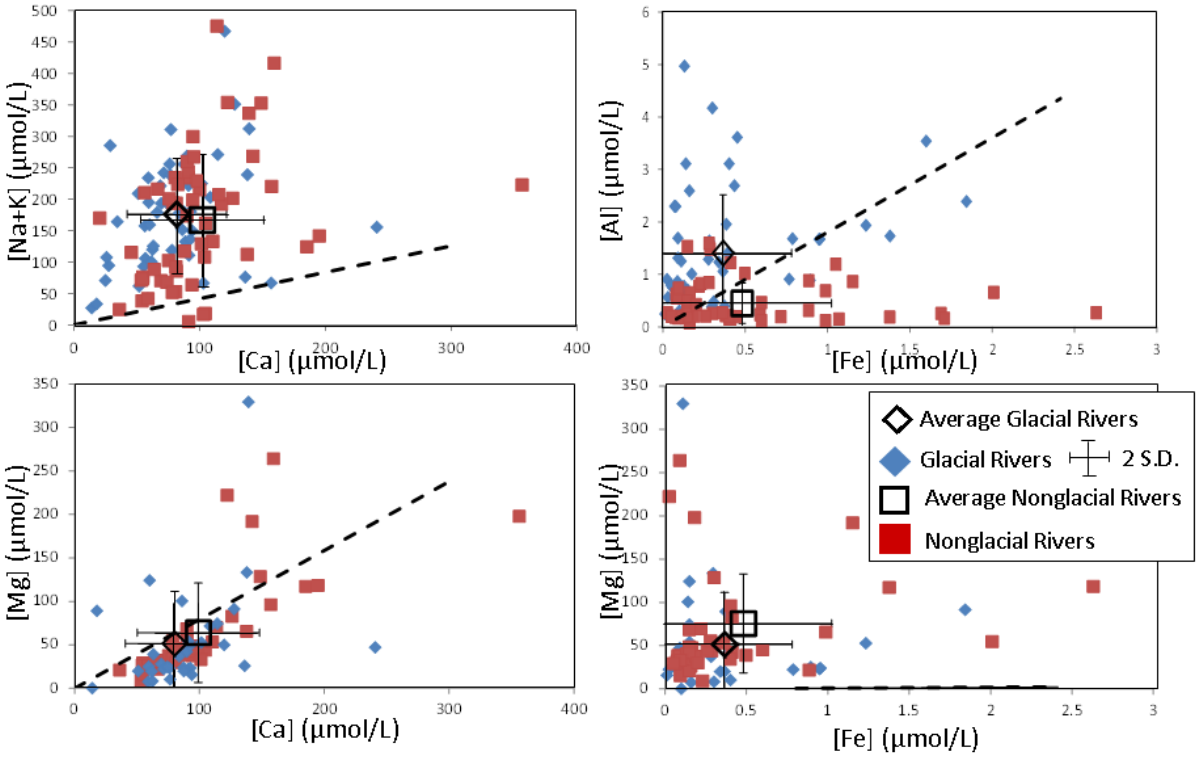

Figure 2.7. Icelandic rivers composition data from Gislason and Arnorsson (1993), Gislason et al., (1996), Arnorsson et al., (2002), Vigier et al., (2006) and Pogge von Strandmann et al., (2006). The data has been corrected for precipitation inputs. The dashed lines represent the element ratios of pristine basalt.

2.5.5 Inverse Models and Secondary Mineral Formation Rates.

The inverse chemical weathering model predicted Fe_{OOH} and Al_{OOH} formation rates are shown as functions of estimated primary mineral dissolution rates graphically in Figure 8 for glacial and non-glacial catchments. The rates are shown in molar unit concentrations, which encapsulates the general principle that chemical weathering scales with hydrologic discharge during continental weathering (e.g. Anderson et al., 1997; Eiriksdottir et al., 2008). On average, non-glacial weathering appears to significantly enhance both Fe ($P<0.02$ two-tailed t-test) and Al ($P<0.05$ two-tailed t-test) (oxyhydr)oxide formation relative to glacial weathering. The offset in Fe_{OOH} formation rates constitutes a 37% increase in iron formation in non-glacial catchments relative to glacial catchments: 32µmol/kg to 44µmol/kg.

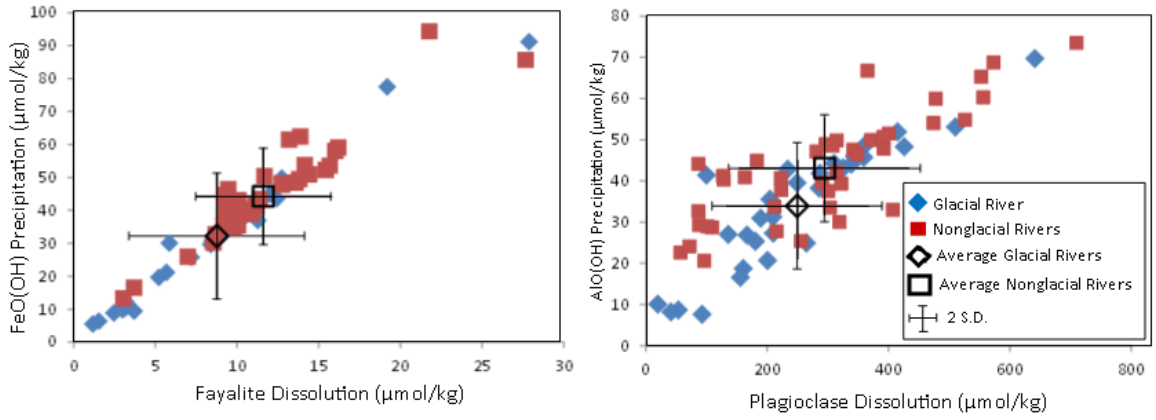

Figure 8. PHREEQC Model calculated reactive oxide formation rates. On average, non-glacial weathering significantly enhances Fe_{OOH} formation ($P<0.02$) and Al_{OOH} formation ($P<0.05$).

Sensitivity testing was conducted to determine which chemical factors were most important in terms of controlling Fe/Al_{OOH} formations. The model Fe/Al_{OOH} formation estimates are not sensitive to the measured Fe or Al concentrations of the samples; either doubling or removing the Al and Fe concentrations in the river waters from the model inputs changes the Fe/Al_{OOH} formation estimates by less than the rounding uncertainty associated with the reported data i.e. <0.1 µmol/kg). The estimates are far more sensitive to the concentrations of Mg and Ca. 'The Fe_{OOH} formation estimates effectively scale on a 1:1 basis while Al_{OOH} formation estimates scale with Ca. This is because, as shown on Figure 2.8, the model predicted Fe_{OOH} formation rates are almost entirely controlled by olivine dissolution while the Al_{OOH} formation rates are mostly controlled by plagioclase dissolution.

2.6. Discussion

2.6.1 pH and Chemical Weathering Patterns.

Gislason et al., (1996) proposed the relative mobility's of elements during Icelandic weathering decreases along the trend: Na> K>Ca, Mg >Al>Fe. This is not entirely consistent with the soil, river sediment or river water data. Figure 2.9 shows the average elemental mobility patterns of rivers in the non-glacial Borgarfjörður and glacial Vatnajökull catchment regions (see Figure 2.2). In non-glacial catchments iron is at least as mobile as Al, and in the glacial catchments the mobility is Ca is much closer to K than Mg. In total, these patterns most likely reflect the role soil formation has on continental weathering.

The mobility of Ca relative to Na decreases from the glacial to the non-glacial catchments via a process which does not seem to impact K or Mg. The most plausible explanation for the shift in Ca relative to Na is a change in plagioclase weathering. The

predicted stabilities of albite (Na-plagioclase) and anorthite (Ca-plagioclase) differ across the typical pH range or Icelandic surface and ground waters (Arnorsson et al., 2002). As shown on Figure 2.10, anorthite is always significantly under-saturated while albite is near saturated above pH values of 7 (Stefansson et al., 2011; Arnorsson et al., 2002). A shift toward more acidic conditions would therefore be expected to result in a decrease in the mobility of Ca relative to Na. The absolute pHs of the rivers do not cover the appropriate range of values, but Iceland soil porewater do span the correct range. Chemical weathering in Icelandic soils is associated with decreasing soil pore-water pH (see Figure 5). The pore water in immature soils covers a similar pH range to the Icelandic rivers, but mature soils are characterized by soil pH values as low as 4 (Opfergelt et al., 2014). If plagioclase weathering is dominantly occurring within soils, then the reduction in Ca mobility relative to Na is indicative of the pH controlled shift in continental weathering between glacial and non-glacial patterns.

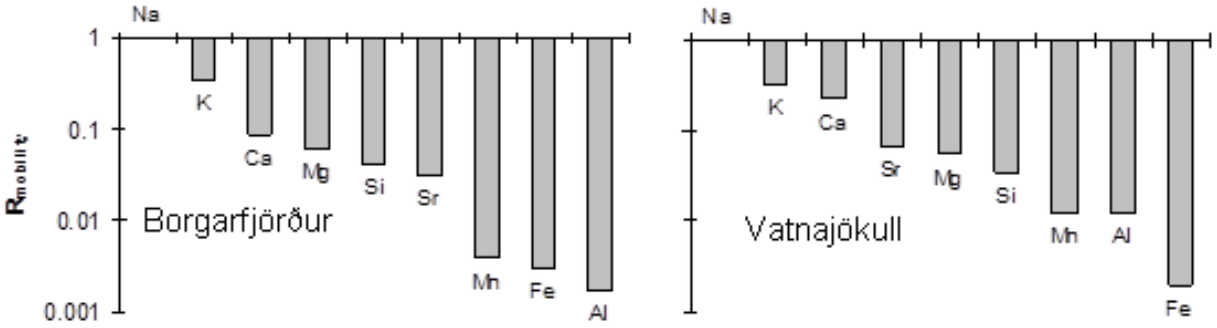

Figure 2.9 Relative mobility of major cations during basalt weathering in the Borgarfjörður and Vatnajökull catchments. $R_{mobility} = (X_{water} / Na_{water}) / (X_{RBS} / Na_{RBS})$

A key aspect of the dynamics of Ca and Na in Icelandic soil and surface water systems is that the solubility of the elements is not pH dependent. In other words, once in solution the migration of Ca and Na between (sub)glacial, soil, and/or river environments is not highly impacted by pH boundaries. This provides a clear contrast when it comes to evaluating the environmental behaviour of Al and Fe.

Temporarily ignoring organic matter dynamics, the solubility's of Fe and Al are both strongly pH dependent. Across the pH range of our river samples, pure Al is about four orders of magnitude more soluble than pure Fe (Wesolowski and Palmer 1994; Liu and Millero 1999). As pH values decrease towards acidic pore water values, the solubility of Fe increases while the solubility of Al decreases (see Figure 2.10). If, like was the case with plagioclase, most chemical weathering reactions are expected to occur in affiliation with soil formation Al mobility would be expected to be higher than Fe in glacial rivers. Additionally, Fe and Al would be expected to be effectively immobile in non-glacial rivers. This is because

while acidic pore waters will favour iron dissolution this dissolved iron would be expected to precipitate as soon as it entered the rivers.

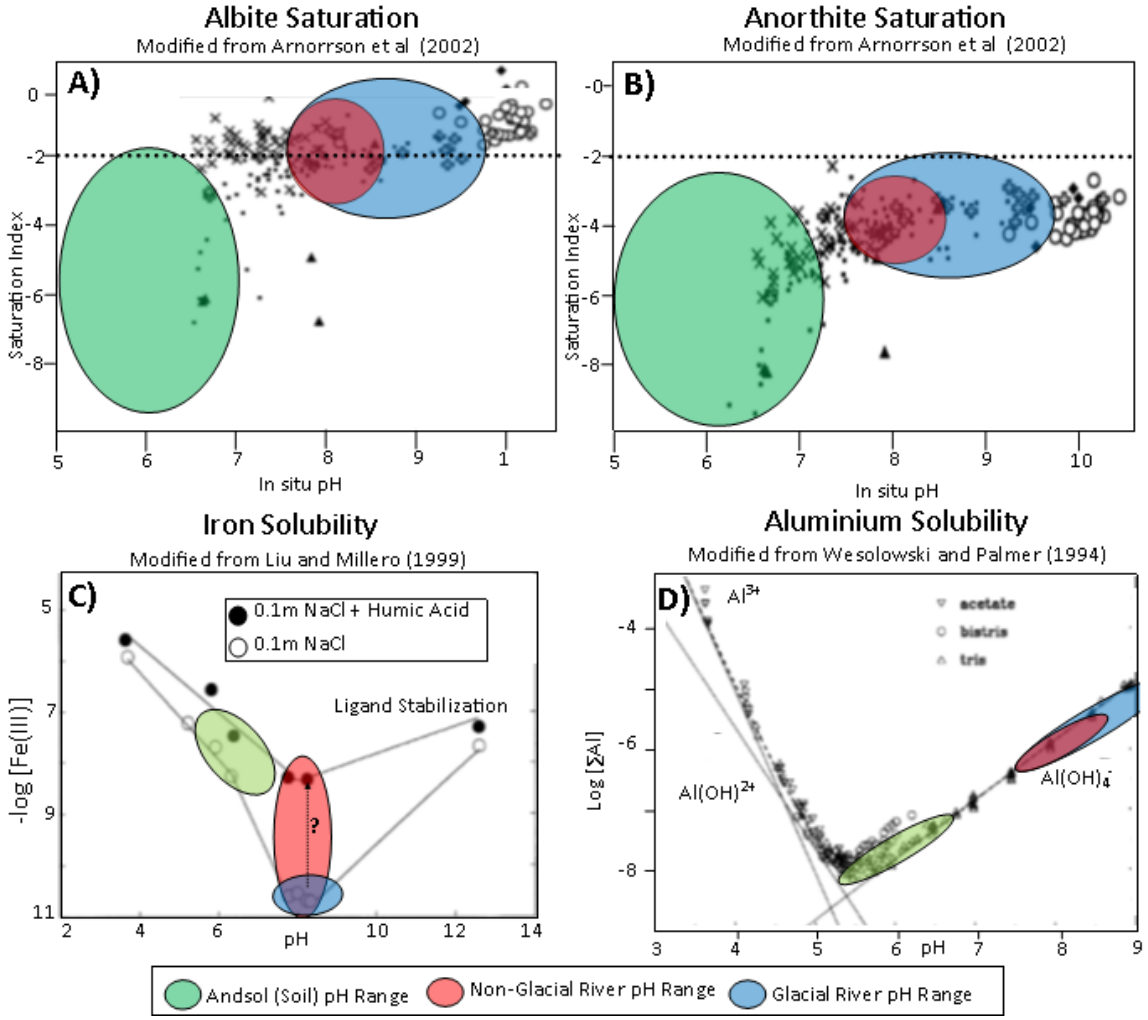

Figure 2.10. The andsol pH range is defined based on pore-water solutions from Opfergelt et al., (2014) and reflects soils typical of non-glacial catchments in Iceland. A) Albite solubility and B) Anorthite solubility in Icelandic surface waters modified from Arnorrson et al (2002). At pH>7 albite is near saturated while anorthite is significant under saturated across the pH spectrum. C) Iron solubility curve modified from Liu and Millero (1999) and D) Al solubility curve modified from Wesolowski and Palmer (1994). Iron is more soluble in the pH range of soil porewater than in the pH range of Icelandic rivers whereas Al solubility follows the opposite trend. The arrow on page C underscores the relationship between apparent iron solubility and organic ligand availability with non-glacial rivers potentially falling nearer to the ligand stabilized values.

In many surface water environments, the mobility's of Fe and Al are dominated by organic matter availability rather than the actual solubility's of Fe and Al. (Perdue et al.,

1976; Liu and Millero 1999). The presence of organic matter would be predicted to drive glacial systems to the extremes i.e. high Fe mobility in non-glacial rivers and high Al mobility in glacial rivers as organic matter stabilized the preferentially released element. This pattern of extremes can be identified within the individual samples reported on Figure 2.7, but on average non-glacial rivers do not contain significantly more iron that glacial rivers (see Table 2.2). Overall, the data appears to be better explained by the aforementioned inorganic solubility patterns. The apparent limited influence of organic matter on large scale iron mobilization in non-glacial rivers can at least in part be explained by the known relationship between organic matter accumulation and soil formation in Iceland. Opfergelt et al., (2011) showed the while Al was complexed to organic matter in pore waters of the most organic rich soils Al in most soil solutions was un-complexed. In most non-glacial catchments the total drainage area associated with organic rich soils is limited (See Figure 2.1) so, at least in Iceland, the Al flux associated with soil formation is not necessarily driven by organic matter. Additionally the overall organic matter concentrations of both glacial and non-glacial river catchments in Iceland are relatively low. Pogge von Strandmann et al., (2008) found dissolved organic carbon (DOC) concentrations of 30-50 µmol/L in glacial rivers in Iceland and DOC concentrations of 100-141 µmol/L in non-glacial rivers. The higher concentrations are very similar to the concentration of humic acid used in the experiments by Liu and Millero (1999) shown on Figure 2.10. While organic matter does increase the apparent solubility of Fe at this level the overall apparent solubility of Fe remains very low and less than Al.

The influence on pH-dependent mineral reactions during soil formation on overall chemical weathering patterns is also reflected in the inverse-weathering Fe_{OOH} and Al_{OOH} formation rate estimates. The inverse weathering models predict Fe_{OOH} formation is mainly coupled to olivine dissolution and Al_{OOH} formation is primarily coupled to plagioclase dissolution. This is a key result in terms of validating the models as the pattern is consistent with independent predictions of mineral weathering patterns in Iceland e.g. Arnorsson et al., (2002). Furthermore, the absolute stabilities of olivine and plagioclase are predicted to decrease with decreasing pH (Stefansson et al., 2001). As a result, the higher weathering rates in non-glacial catchments are best explained by the increased weathering intensity of acidic non-glacial soils relative to alkaline glacial environments. It is worth noting that this is not a result of the way the inverse models were parametrized. All the models were parametrized with the same initial rainwater pH (5.5 consistent with mean Icelandic precipitation; Gislason et al., 1996) and run to their respective final riverine pHs (which aren't significantly different) preventing the introduction of any pH bias during model parameterization. Evidently by incorporation the multi-elemental patterns of the rivers the PHREEQC calculations are able to detect the larger weathering trends.

Overall it would appear that soil formation has a measurable impact continental weathering including riverine chemistry. In the case of glacial/non-glacial differences soil formation promotes Al_{OOH} and Fe_{OOH} formation in non-glacial systems. But this does not imply non-glacial weathering increases Fe/Al_{OOH} export to nearshore marine environments.

2.6.2 Soils and River Sediments.

There is a fundamental difference between mineral formation and mineral transport. Icelandic soils trap Fe_{OOH} as it forms (Figure 2.6) opening the possibility that much of the Fe_{OOH} formed during non-glacial weathering never reaches the ocean. This possibility is underscored by the lack of chemical similarity between non-glacial river sediment and mature soils.

Figure 2.11 shows the compositions of the glacial and non-glacial sediments relative to the composition of the Icelandic soils. All the river sediments are more chemically similar to pristine basalt than to Icelandic soil material. Additionally, the compositions of the river sediment cannot be explained through the mixing of soils with different compositions. All the river sediments have higher Na+K, Mg, and Ca concentrations relative to their Fe and Al concentrations than all the soil samples. This is consistent with physical processes controlling both glacial and non-glacial river sediments independently of chemical soil formation process.

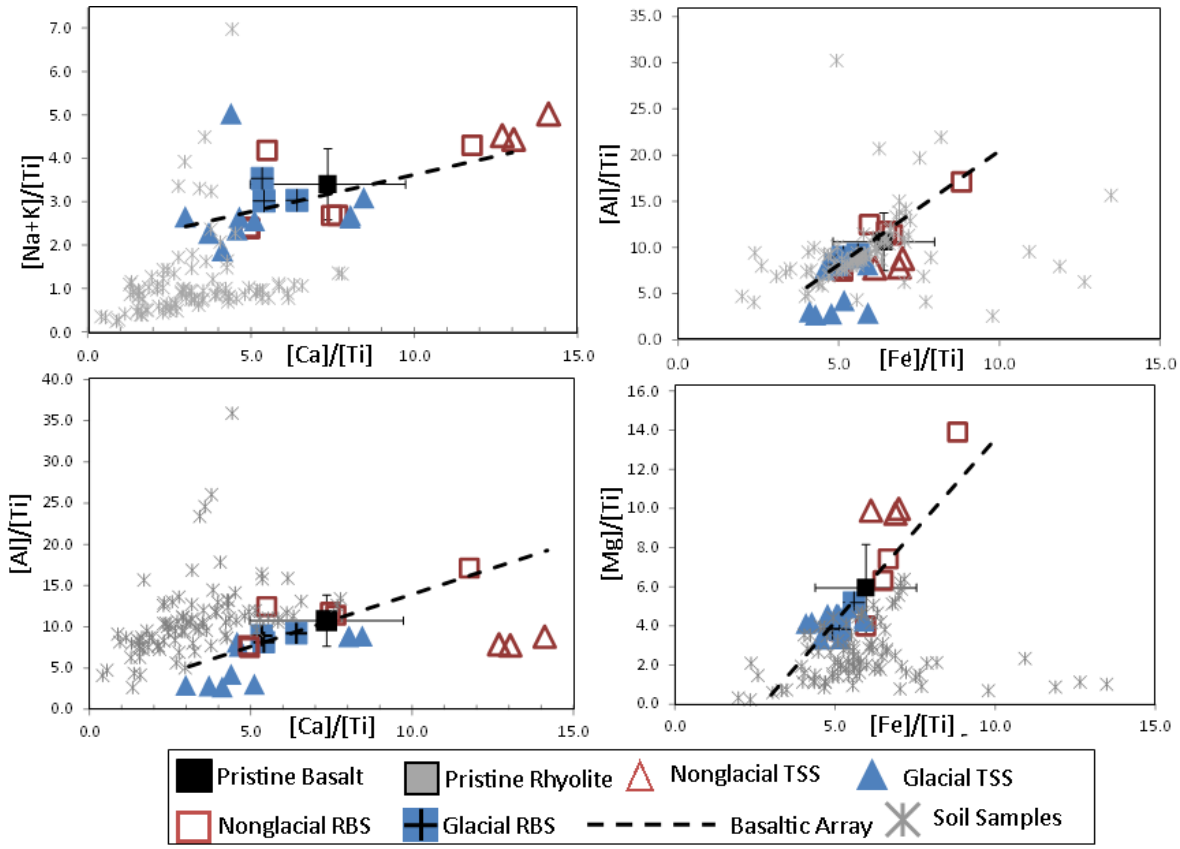

Figure 11 Icelandic river sediment and soil compositions. The river sediment data from Figure 2.5 is combined with the soil data from Figure 2.6: RBS=riverbed Sediment; TSS= total suspended sediment. The solid black lines reflect the composition of pristine Icelandic basalt. The soils are generally depleted in the mobile elements (Na, K, Mg, Ca) relative to the sediments.

The dominance of physical weathering on river sediment chemistry is not a new idea especially in the context of Fe_{OOH}. Poulton and Raiswell (2005) and Poulton and Canfield (2005) found that the Fe_{OOH} concentrations of river sediment from glacial and non-glacial catchments from around the world were best explained by physical weathering. Specifically, Fe_{OOH} concentrations were found to correspond to sediment surface area irrespective of bedrock lithology or soil formation intensity. This is consistent with more recent studies which have found high Fe_{OOH} export from glacial systems characterized by high rates of physical weathering e.g. Bhatia et al., (2013); Hawkins et al., (2014).

2.6.3 Physcial Weathering, Fe_{OOH} export and Earth's Climate

One important aspect of this study is that, whereas previous studies have shown glacial terrains can be a significant source of $Fe_{OOH,}$ we have directly compared analogous glacial and non-glacial terrains in a way which allows us to conclude glacial terrains export more Fe_{OOH} than equivalent non-glacial terrains. However, our conclusion has previously been implied based on studies of Antarctica (Martin 1990), Greenland (Bhatia et al., 2013)

and other terrains (Poulton and Canfield 2005) so the idea isn't new. Additionally, any number of previous studies have stated: chemical weathering patterns do differ between glacial and non-glacial catchments in Iceland e.g. Gislason et al., (1996); Pogge von Strandmann et al., (2006, 2012); Opfergelt et al., (2013); Opfergelt et al., (2014), but because of the environmental behaviour of Fe and Al physical processes control the secondary Fe/A_{lOOH} flux rates (Poulton and Canfield 2005). This confirms Martin (1990)'s 27 year old claim that in general physical sediment erosion by glaciers enhances marine Fe_{OOH} accumulation.

What is important to note is a significant new idea has widely gained traction since the original proposal of the Iron Hypothesis. It is now widely understood that Fe_{OOH} promotes not only primary production but also carbon burial. Marine carbon burial accounts for the sequestration of about 309 Tg C yr^{-1} (Burdgie 2007) and it accounts for about half of the total annual geologic sink of carbon (Ciais et al., 2013). Its estimated that 20% of organic carbon in marine sediments is directly stabilized by Fe_{OOH} (Lalonde et al., 2012) so significant changes in Fe_{OOH} export equate to significant changes in Earth's climate. This is a statement that is worth re-iterating because it demands a significant shift in the importance which can be attributed to studying Fe_{OOH} fluxes from glacial systems. For example Hawkins et al., (2014) concludes: "We contend that the consideration of meltwater Fe fluxes, which supplements iron from icebergs, is critical for understanding iron cycling and primary productivity in polar waters." Such a statement falls short of what we are contending as the true significant of the work by Hawkins et al., (2014), Raiswell et al., (2008) and others which is: we contended that the consideration of meltwater Fe fluxes, which supplements iron from icebergs, is critical for understanding **carbon burial** and **Earth's climate**.

2.7. Summary and Conclusions.

Direct chemical measurements of Icelandic sediments and soils and inverse stoichiometric modelling of chemical weathering in Icelandic catchments support the assertion that the chemical weathering process does differ between glacial and non-glacial catchments. The differences appear to be bi-products of the soil formation process and, more specifically, the relationship between pore-water pH and mineral weathering. However, as many authors have concluded before us, these chemical differences don't appear to have a significant effect on Fe_{OOH} and Al_{OOH} delivery to the ocean, because physical processes are more important in the context of sediment export rates. This allows us to concluded not just that glacial weathering is a significant source of (oyxhyr)oxides to the ocean, but that glacial weathering promotes the accumulation of significantly more (oyxhyr)oxides in nearshore marine environments than analogous non-glacial weathering. We assert that this

difference is not tangentially related to climate change via primary productivity but directly relates to carbon sequestration via marine carbon burial.

References

Anderson S.P., Drever J.I., Humphrey N.F. (1997) Chemical weathering in glacial environments. *Geology* **25**: 399-402.

Andersson K, Dahlqvist R., Turner D., Stople B., Larsson T., Ingri J., Andersson P. (2006) Collodial rare earth element in a boreal river: Changing sources and distributions during the spring tide *Geochimica et Cosmochimica Act*a **70**: 3261-3274.

Arnorsson S., Gunnarsson I., Stefansson A., Andresdottir A., Sveinbjornsdottir A.E. (2002). Major element chemistry of surface- and groundwaters in basaltic terrain, N-Iceland. I. Primary mineral saturation. *Geochimica et Cosmochimica Act*a.**66**(23): 4015-4046.]

Barber A, Lalonde K., Mucci, A., Gelinas Y. (2014) The role of iron in the diagenesis of organic carbon and notrigen in sediments: A long-term incubation experiment. *Marine Chem*. **162**: 1-9

Blanc Ph., Lassin A., Piantone P. Nowak C. THERMODDEM PHREEQC database. Bureau de recherches geologiques et minieres. Available from < http://thermoddem.brgm.fr/spip.php?rubrique13>

Burdige D.J. (2007) Preservation of organic matter in marine sediments: controls, mechanisms, and an imbalance in sediment organic carbon budgets? *Chemical Rev*iews **107**: 467-485.

Ciasis P and Sabine C. (2013). *Carbon and Other Biogeochemical Cycles.* In: Climate Change 2013: The Physcial Sciences Basis. Contribution of Working Group 1 to the Fifth Assessment Report of the Intergovernmental Panel on Climate Change. Cambridge University Press, United Kingdom.

Coale K.H., Johnson K.S., Chavez F.P., Buesseler K.O., Barber R.T., Brzezinski M.A., Cochlan W.P., Millero F.J., Falkowski P.G., Bauer J.E., Wanninkhof R.H., Kudeka R.M., Altabet M.A., Hales, B.E., Takahashi T., Landry M.R. Bidigare R.R., Wnad X., chase Z., Strutton P.G., Friederich G.E., Gorbunov M.Y., Lance V.P., Hilting A.K., Hiscock M.R., Demarest M., Hiscock W.T., Sullivan K.F., Tanner S.J., Gordon R.M., Hunter C.N., Elrod V.A., Fitzwater S.E., Jones J.L., Tozzi S., Koblizek M., Roberts A.E., Herndon J., Brewster J., Ladizinsky N., Smith G., Cooper D., Timothy D., Brown S.L., Selph K.E., Sheridan C.C., Twining B.S., Johnson Z.I. (2004) Southern Ocean iron enrichments experiment: carbon cycling in high- and low-si waters. *Science*, **304**: 408-414.

Conway T.M. and John S.G. (2014). Quantification of dissolved iron sources to the North Atlantic Ocean. *Nature.* **511**: 212-217.

Eiriksdottit E.S., Louvat P., Gislason S.R., Oskarsson N., Hardardottir J. (2008) Temporal variation of chemical and mechanical weathering in NE Iceland: Evaluation of a steady-state model of erosion. *Earth and Planetary Science Letters.* **272**: 78-88.

Gislason S.R. and Arnorsson S. (1993) Dissolution of primary basaltic minerals in natural waters: saturation state and kinetics. *Chemical Geology* **105**: 117-135.

Gislason S.R., Arnorsson S., Armannsson H. (1996) Chemical weathering of basalt in southwest Iceland: effects of runoff, age or rocks and vegetative/glacial cover. *American Journal of Science.,* **296**: 837-907.

Gislason S.R. and Oelkers E.H .(2003). Mechanism, rates and consequences of basaltic glass dissolution: II. An experimental study of the dissolution rates of basaltic glass as a function of pH and temperature. *Geochimica et Cosmochimica Act*a **67** (20):3817-3832.

Hawkins J.R., Washam J.L., Tranter M., Raiswell R.,Benning L.G., Statham P.J., Tedstone A., Neinow P., Lee K., Telling J., (2014). Ice sheets as a significant source of highly reactive nanoparticulate iron to the oceans. *Nature Communications*. 5:3929. DOI: 10.1038.

Jakobsson S.P. (1972) Chemistry and distribution pattern of Recent basaltic rocks in Iceland. *Lithos*. **5**: 365-386.

Kaasalainen H. and Stefansson A. (2012) The chemistry of trace elements in surface geothermal waters and steam, Iceland. *Chemical Geology*. **330-331**: 60-85.

Lalonde K., Mucci A., Ouellet A., Gelinas Y. (2012) Preservation of organic matter in sediments promoted by iron. *Nature.* **483**: 198-200.

Liu X. and Millero F.J. (1999). The solubility of iron hydroxide in sodium chloride solutions. *Geochimica et Cosmochimica Acta*. **63** (19/30):3487-3497.

Louvat P, Gislason S.R. Allegre C.J. (2008) Chemical and mechanical erosion rates in Iceland as deduced from river dissolved and solid material. *Am. J. Sci*. **308**: 679-726.

Lyven B., Hassellov M., Turner D.R., Halraldsson C., Andersson K. (2003) Competition between iron- and carbon-based colloidal carriers for trace metals in a freshwater assessed using flow filed-flow fractionation coupled to ICPMS. *Geochimica et Cosmochimica Acta* **67**(20):3791-3802.

Martin J.H. (1990) Glacial-interglacial CO2 change: the iron hypothesis. *Paleoceanography*. **5**(1):1-13

Nesbitt H.W. and Wilson R.E. (1992) Recent chemical weathering of basalts. *American Journal of Science*. **292**: 740-777.

Nordðahl H. and Petursson H.G. (2005) Relatice seal-level changes in Iceland: new aspects of the Weichselian deglaciation of Iceland. *Iceland-Modern processes and past environments*. Elsevier. 25-78.

Opfergelt S., Georg R.B., Burton K.W., Guicharnaud R., Siebert C., Gislason S.R., Hallidat A.N. (2011) Silicon isotope in allophane as a proxy for mineral formation in volcanic soils. *Applied Geochemistry*. **26**: S115-S118.

Opfergelt S., Burton K.W., Pogge von Strandmann P.A.E., Gislason S.R., Halliday A.N. (2013) Riverine silicon isotope variations in glaciated basaltic terrains: implications for the Si delivery to the ocean over glacial-interglacial intervals. *Earth and Planetary Science Letters.* **369-370**: 211-219.

Opfergelt S., Burton K.W., Georg R.B., West A.J. Guicharnaud R.A., Sigfusson B., Siebert C., Gislason S.R., Halliday, A.N. (2014). Magnesium retention on the soil exchange complex controlling Mg isotope variations in soils, soil solutions and vegetation in volcanic soils, Iceland. *Geochimica et Cosmochimica Acta* **125**: 110-130.

Oskarsson B.V., Riishuus M.S., Anralds O. (2012). Climate-dependent chemical weathering of volcanic soils in Iceland. *Geoderma*. **189-190**:635-651.

Parkhurst D.L., Appelo C.A.J. (1999) User's guide to PHREEQC-a computer program for speciation, beatch-reaction, one-dimnesional transport and inverse geochemical calculations. U.S. Geological Survey Water-Resources Investigations Report, p.312.

Perdue E.M., Beck K.C., Melmut-Reuter J. (1976) Organic complexes of iron and aluminium in natural waters. *Nature*. **260**: 418-420.

Pogge von Strandmann P.A.E., Burton K.W., James R.H., van Calsteren P., Gislason S.R., Mokaden F. (2006) Riverine behaviour of uranium and lithium isotopes in an actively glaciated basaltic terrain. *Earth and Planetary Science Letters.* **251**: 134-147.

Pogge von Strandmann P.A.E., Opfergelt S., Lai Y.-J., Sigfusson B., Gislason S.R., Burton K. (2012) Lithium, magnesium and silicon isotope behaviour accompanying weathering in a basaltic soil and pore water profile in Iceland. *Earth and Planetary Science Letters* **339-340**:11-23

Poulton S.W. and Canfield D.E. (2005) Development of a sequential extraction procedure for iron: implications for iron partitioning in continentally derived particulates. *Chemical Geology* **214**: 209-221.

Poulton S.W. and Raiswell R. (2005) Chemical and physical characteristics of iron oxides in riverine and glacial meltwater sediments. *Chemical Geology.* **218**:203-221.

Raiswell R., Benning L.G., Tranter M., Tulaczyk S. (2008) Bioavailable iron in the Southern Ocean: the significance of the iceberg conveyor belt. Geochemical Transactions. **9**:7.

Raiswell R. and Canfield D.E. (2012) The iron biogeochemical cycle past and present. *Geochemical Perspectives*, European Association of Geochemistry, 1(1)

Schuessler J.A., Schoenber R, Sigmarsson O. (2009) Iron and lithium isotope systematics of the Hekla volcanoe, Iceland- Evidence for iron isotope fractionation during magma differentiation. *Chemical Geology*. **258**: 78-91.

Schrumpf M., Kaiser K., Guggenberger G., Persson T., Kogel-Knabner I., Schulze E.-D. (2013) Storage and stability of prganic carbon in soils as related to depth, occlusion within aggregates and attachment to minerals. *Biogeosciences*. **10**: 1675-1691.

Sholkovitz E.R. and Copland D. (1981) The coagulation, solubility and adsorption properties of Fe, Mn, Cu, Ni, Cd, Co and humic acids in a river water. *Geochimica et Cosmochimica Acta*. **45**: 181-189.

Stefansson A. (2001) Dissolution of primary mineral of basalt in natural waters I. Calculation of mineral solubilities from 0C to 350C. *Chemical Geol*ogy **172**: 225-250.

Stefansson A. and Gislason S.R. (2001) Chemical weathering of basalts, southwest Iceland: Effects or rock crystallinity and secondary minerals on chemical fluxes to the ocean. *American. Journal of Science*. **301**: 513-556.

Stefansson A., Gislason S.R., Arnorsson S. (2001) Dissolution of primary minerals in natural waters II. mineral saturation state. *Chemical. Geology*. 172: 251-276.

Syvitski J.P.M., Milliman J.D. (2007). Geology, geography and humans battle for dominance over the delivery of fluvial sediment to the coastal ocean. *Geology* **115**: 1-19.

Vigier N., Burton K.W., Gislason S.R., Rogers, N.W., Duchene S., Thomas L., Hodge E., Schaefer B. (2006) The relationship between riverine U-series disequilibria and erosion rates in a basaltic terrain. *Earth and Planetary Science. Letters.* **249**: 258-273.

Vigier N., Gislason S.R., Burton K.W., Millot, R., Mokadem F. (2009) The relationship between riverine lithium isotope composition and silicate weathering rates in Iceland. *Earth and Planetary Science. Letters.* **287**: 434-411.

Wesolowski D.J. and Palmer D.A. (1994) Aluminium speciation in equilibria in aqueous solution: V. Gibbsite solubility at 50C and pH 3-9 in 0.1 molal NaCl solutions (a general model for aluminium speciation; analytical methods). *Geochimica et Cosmochimica Acta* **58**(14): 2947-2969.

Chapter 3-

Developing a New Proxy for Iron-(oxyhydr)oxides: Iron Stable Isotope Fractionation

Abstract

Poorly-crystalline iron-(oxyhydr)oxides (Fe_{OOH}) facilitate marine primary production and organic carbon burial. Practical challenges in quantifying Fe_{OOH} however restrict research into these iron-carbon interactions. The most common Fe_{OOH} minerals, including ferrihydrite and goethite, are difficult to measure by standard analytic techniques, and in general their concentrations can only be estimated based on selective chemical extractions. This study presents an alternative and novel method for estimating Fe_{OOH} concentrations based on iron stable isotope measurements. The new method is validated against dithionite-citrate-bicarbonate (DCB) extractable iron concentrations [a.k.a highly reactive iron (Fe_{HR})] in a suite of Icelandic soils. Across the sample suite the new technique systematically underestimates Fe_{OOH} concentrations by about 30% relative to the Fe_{HR} measurements. This issue of systematic underestimation can be significantly reduced by altering assumptions about the initial composition of the bedrock from which the samples were derived. Overall the new technique has the capability to provide a first-order estimates of Fe_{OOH} concentrations including in sample types such as particulate/colloidal material from aquatic environments which cannot be analysed by other techniques.

3.1 Introduction

Iron-(oxyhydr)oxides (Fe_{OOH}) moderate primary production in the Southern Ocean (Boye et al., 2010), organic carbon preservation in soils (Schrumpft et al., 2013) and organic carbon burial in marine sediments (Lalonde et al., 2012). These links between the iron and organic carbon cycles have spawned significant interest in trying to better understand Fe_{OOH} dynamics. Unfortunately, the most reactive Fe_{OOH} phase(s) tend to be amorphous and nano-particulate making them difficult to quantify by standard analytic techniques (see review by Raiswell and Canfield 2012). As a result, Fe_{OOH} concentrations are usually estimated rather than directly measured using one of a number of selective chemical extraction processes; the most common extraction techniques are dithionate-citrate-bicarbonate dissolution (Fe_{HR}), Na-acetate dissolution (Fe_{Na}) and oxalate dissolution Fe_{ox} (see review by Raiswell and Canfield 2012).

Utilizing selective extractions to estimate Fe_{OOH} has a few distinct advantages. The approach has been utilized extensively by soil scientists to explore iron-mineral-carbon

interactions, and this research provides key guidance when it comes to interpreting the extraction results (see review by Kaiser and Guggenberger 2000). More than 45 years ago selective extractions were also pioneered to explore iron-carbon-sulphur dynamics in marine environments i.e. Berner (1970). Following on from this early work, the technical details of the extractions have been studied and are well understood in relation to basic iron mineralogy (see Poulton and Canfield 2005 and Poulton and Raiswell 2005). The techniques have proven both flexible and robust to the extent they continue to help researchers push the limits of our scientific understanding of iron-carbon-climate dynamics (e.g. Lalonde et al., 2012; Bhatia et al., 2013). However, the extraction techniques also have clear limitations.

All the extraction techniques are limited by the complex relationship between the chemical reducibility of iron minerals and their real-world chemical reactivity. Maybe Fe_{ox} is the best indicator of reactive Fe_{OOH} while Fe_{HR} includes the pool of crystalline (and unreactive) iron oxides e.g. Mikkuta et al., (2006). Alternatively, maybe Fe_{HR} is actually the best indicator of Fe_{OOH} with only minimal dissolution of highly crystalline iron oxides e.g. Lalonde et al (2012); Kogel-Knabner et al., (2008); Kaiser and Guggenberger (2000). Or maybe estimating Fe_{OOH} requires looking at the pool of iron reduced by hydroxylamine e.g. Bhatia et al., (2014). On top of these inorganic mineral complexities there is an issue with organically bound iron. None of the selective reduction methods have ever been tested to determine their efficiency in extracting iron bound to various forms of organic matter so the degree to which organically bound iron is reflected in the extracted iron pools is a significant source of uncertainty. These issues are particularly acute when it comes to analysing aquatic colloidal/suspended material. Iron present within this type of material is hosted in a diverse mixture of organic and inorganic material which is not readily classified into mineral assemblages (Lyven et al 2003; Vasyukova et al., 2012).

The behaviour of iron during aquatic sampling also poses a significant practical challenge when it comes to applying the selective extraction techniques to aquatic iron samples. Iron has tendency to adsorb onto the equipment used to sample iron as well as the bottles used to store aquatic samples. It is well documented that the only way to maintain iron mass balance in aquatic sample following ultra-filtration is through the acidification of the sample (Reitmeyer et al., 1996; Hoffmann et al., 2000; Schlosser and Croot 2008). To avoid this issue, it accepted as good practice to acid rinse iron sampling equipment and to acidify aquatic samples for iron analysis even following normal (0.45/0.2µm) filtration. Many studies also dissolve filters in acid to ensure complete removal of the sample material from the filters (e.g. Ingri et al., 2006, Poitrasson et al., 2014). Sample acidification and selective iron extractions are mutually exclusive as the aim of acidification is dissolve all the solid iron phases.

What is needed is an alternative method for measuring Fe_{OOH} concentrations which: 1) is accurate; 2) is applicable to a wide range of sediment and soil samples types irrespective of mineralogy and; 3) isn't affected by intentional sample acidification. Iron stable isotope fractionation meets the final two criteria. Iron isotope measurements have been made across the range soils and sediment types (Beard et al, 2003; Homoky et al., 2009, Kiczka et al., 2011; John and Adkins 2012). This has included samples from iron poor regions of the ocean which were intentionally acidified during the sampling process e.g. Conway and John (2014). This study explores the accuracy of using iron isotope measurements to estimate Fe_{OOH} concentrations.

3.2 Sample Suite Selection

Four factors were considered when selecting samples for validating the accuracy of our new technique. The samples needed to reflect a range of Fe_{OOH} concentrations. This range needed to be balanced against an ability to understand how the samples were related to one another. Additionally, it was considered important to be able to confidently measure the Fe_{OOH} concentrations of the sample using a traditional extraction technique. Reliable independent measurements provide a clear way of assessing the accuracy of the new technique. A suite of Icelandic soils collected and characterized by Opfergelt et al., (2014) provided a good balance of these factors.

Iceland is predominately basaltic (>80%, Jakobsson 1972) and the geochemistry of Icelandic basalts has been extensively studied. Pristine Icelandic basalt does not contain any iron-carbonate minerals and possesses a minimal abundance of primary hematite (Gislason and Arnorsson 1993; Stefansson and Gislason 2001). Icelandic weathering also results in significant secondary nano-particulate goethite formation (Stefansson et al., 2001). This provides excellence coherence between the Fe_{OOH} pool expected to form in Icelandic sediments during chemical weathering and the nature of the Fe_{HR} pool predicted by Poulton and Canfield (2005) to form following the application of DCB to Icelandic basalts i.e. $[Fe_{HR}]=[Fe_{OOH}]$.

Icelandic soils can also all be related with a high degree of confidence. Iceland was completely covered by a single glacial ice sheet ~9 ka ago, which receded during the Early Holocene stabilizing to near modern conditions about 6 ka ago (Gislason et al., 1996). As a result, soil formation in Iceland is restricted to the recent geologic past. The iron isotope ratio of Icelandic basalts is also homogeneous (with respect to analytical uncertainty) (Schuessler et al., 2009). This facilitates the assumption that all sediments and soils across Iceland are

derived from a bedrock source with a uniform iron isotope composition [indistinguishable to that of the BIR-1a international iron stable isotope rock reference standard].

Against this backdrop of bedrock homogeneity Icelandic soils do provide significant geochemical variability. Since the ice sheets retreated, vegetation and soil formation processes have created significant chemical differences across the Island (Gislason et al., 1996). The chemical variability of Icelandic soils and sediments follows the spatial distribution shown on Figure 1. Based on previous studies (e.g. Opfergelt et al., 2014), the total degree of chemical weathering increases from: Leptosol<Vitrisol<Brown and Gleyic Andosol<Histic Andosol and Histosol. Samples from horizons within each of these main soil types therefore provide an ideal initial data set for calibrating iron isotopes for estimating Fe_{OOH} concentrations.

3.3 Methods

3.3.1 Field Sampling and Major Element Analysis

Six soil profiles were collected during September 2009 at location shown on Figure 3.1 and characterized by Opfergelt et al., (2014) with methods reported therein. This included measuring dithionite reducible iron (Fe_{HR}) as well as measuring the bulk normalized concentrations of the major and trace elements.

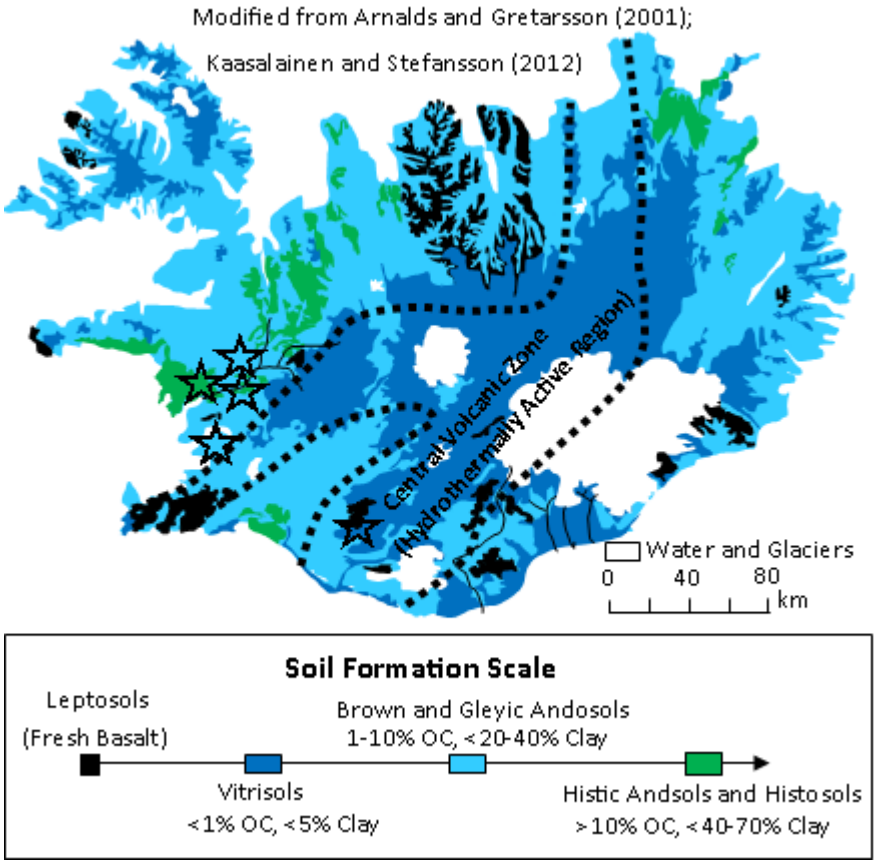

Figure 3.1. Soil map and field areas modified from Arnalds and Gretarsson (2001) and Kaaslainen and Stefansson (2012). The localities of the soil profiles collected by Opfergelt et al., (2014) are shown as stars on the map.

3.3.2 Stable isotopic analysis

The soil samples were prepared for iron stable analysis as described in Opfergelt et al., (2017). Iron stable isotope compositions are reported in δ^{56}Fe notation, which represents the per mil deviation of the measured $^{56}Fe/^{54}Fe$ ratios relative to that of the bracketing standard, IRMM-014. In order to verify mass dependence both δ^{56}Fe and δ^{57}Fe values were measured. Iron fractionation factors are reported in Δ^{56} Fe notation, which represents the per-mil offset of two δ^{56}Fe values relative to each other i.e. $\Delta^{56}\ Fe_{A\text{-}B} = \delta^{56}Fe_A - \delta^{56}Fe_B$.

3.4. Model Development and Calculations

3.4.1 Linking Fe_{OOH} formation and Iron Cycling.

Inorganic iron is effectively insoluble in oxygenated low temperature environments including near surface soils (Nesbitt and Wilson 1999, Stefansson et al., 2001) and aquatic environments (Liu and Millero 1999). Organic ligands can stabilize aqueous iron (Johnson 1997; Millero 1998) creating a ‘dissolved’ iron pool, but iron remains less mobile than nearly every other element (see previous chapter for discussion). Iron’s low mobility is primarily a

result or rapid Fe_{OOH} precipitation following the the dissolution of iron from primary minerals (Stefansson et al., 2001) This allows iron cycling during chemical weathering to be simplified into three equations which are listed below and illustrated on Figure 3.2.

1) $Fe_i = Fe_{OOH} + Fe_{aq} + Fe_p$:The sum of the (oxyhydr)oxide iron pool (Fe_{OOH}), the aqueous iron pool (Fe_{aq}) and the primary iron pool (Fe_P) is determined by the concentration of iron initially present in the system (Fe_i).

2) $[Fe_T] = \frac{Fe_p + Fe_{OOH}}{1 - \frac{Fe_{OOH} + Fe_{aq}}{Fe_i}}$: the bulk normalized concentration of iron in a sediment sample is the ratio of the sedimentary iron pool (Fe_p+Fe_o) and the total composition of the sediment following mineral dissolution ($1 - (\frac{Fe_o + Fe_{aq}}{Fe_i})$. This assumes iron is the most immobile element during chemical weathering.

3)$[Fe_{OOH}] = [Fe_T] \times \frac{Fe_{OOH}}{Fe_{OOH} + Fe_p}$: the bulk normalized concentration of Fe_{OOH} ([Fe_{OOH}]) is the relative amount of Fe_{OOH} to total iron ($\frac{Fe_{OOH}}{Fe_{OOH} + Fe_p}$) multiplied by the total iron concentration ([Fe_T])

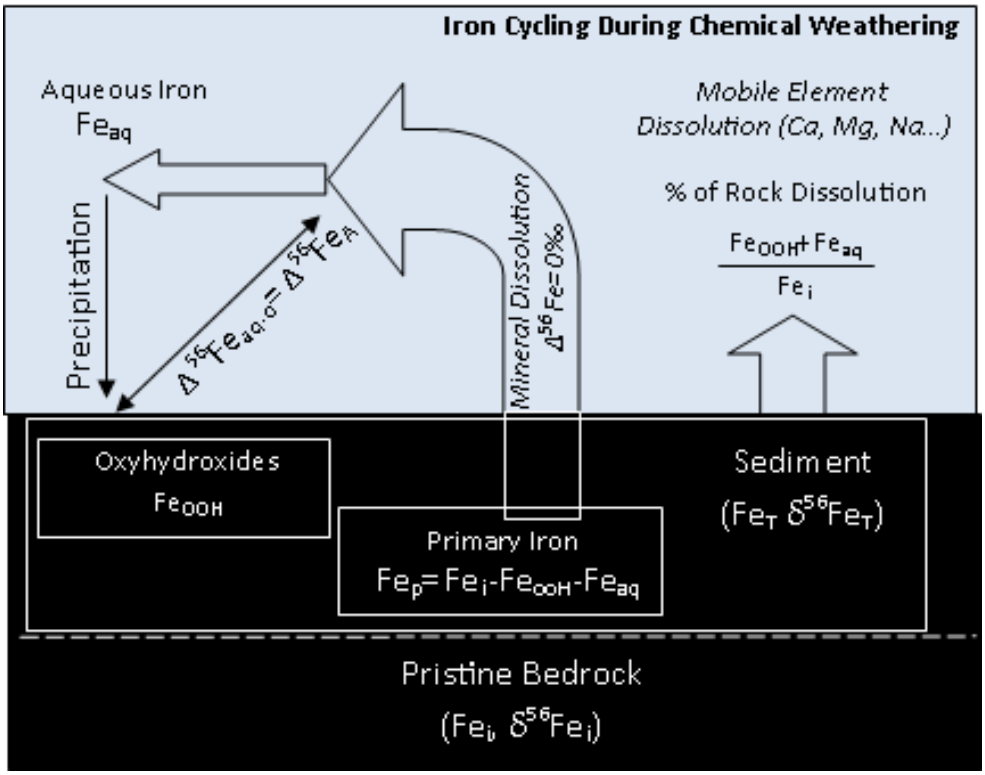

Figure 3.2. Box model of iron isotope fractionation during chemical weathering

Combining the first two equations makes it possible to determine the ratio of Fe_{OOH} to total sedimentary iron within any sample given the initial iron concentration of the sample [Fe_i]

and the bulk normalized residual iron concentration of sample [Fe_T]: ($\frac{Fe_{OOH}}{Fe_{OOH}+Fe_p} = 1 - \frac{Fe_i}{Fe_T}$). This ratio can then be used in Equation 3 to derive a bulk normalize Fe_{OOH} concentration.

The two key parameters required to solve to the equations are [Fe_T] and [Fe_i]. The value of [Fe_T] is just the concentration of iron in the sediment sample so it can be directly measured. The value of [Fe_i], the initial amount of iron in the system, can't be directly measured but it can be back-calculated based on other measurements of the system. The most intuitive way to derive a value for Fe_i value involves measuring the mobile element concentrations of the samples. This approach will be shown in the next section to validate the conceptual framework of the model. However, there is little if any advantage to this approach relative to conducting selective iron extractions. An alternative method of deriving Fe_i values is to measure the iron isotope composition of the sediment phase.

As illustrated on Figure 3.2 iron isotope fractionation can be directly tied into our model of iron cycling. This allows the derivation of the three equations listed below:

4) $\delta^{56}Fe_T = \left(\frac{Fe_p}{Fe_p+Fe_o}\right) * (\delta^{56}Fe_i) + \left(\frac{Fe_o}{Fe_p+Fe_o}\right) * (\delta^{56}Fe_O)$: The iron isotope composition of the residual bulk sediment pool ($\delta^{56}Fe_R$) is the mass balanced composition of primary iron pool (Fe_p, $\delta^{56}Fe_i$) and precipitated iron (oxyhydr)oxide pools (Fe_O, $\delta^{56}Fe_O$).

5) $\Delta^{56}Fe_{aq-s} = \delta Fe_{aq} - \delta Fe_s$: The iron isotope composition of the aqueous (δFe_{aq}) and solid (δFe_s) iron pools during chemical weathering differ based on one of the fractionation factors derived in the previous section ($\Delta^{56}Fe_{aq-s}$)

6) $\delta^{56}Fe_i = \left(\frac{Fe_o}{Fe_{aq}+Fe_o}\right) * (\delta^{56}Fe_o) + \left(\frac{Fe_{aq}}{Fe_{aq}+Fe_o}\right) * (\delta^{56}Fe_{aq})$: The initial amount of iron in a system (Fe_i) is dependent on the concentration of iron in the bedrock ([Fe_i])

Used in combination with the first three equations these final isotope equations provide a constraint on the possible [Fe_i] value of any given sediment. This allows Fe_{OOH} concentration estimates to be made based on iron concentration and iron isotope measurements Section 3.4.2 outlines the isotope approach to estimating Fe_i and Fe_{OOH}.

3.4.2 Intial model validation

Model validation was first conducted using total element concentration data for all the input values. Our model of iron cycling during chemical weathering assumes that iron is immobile relative to the other elements. This assumption dictates that bulk normalized iron concentrations always increase during chemical weathering. The increase in bulk normalized

iron concentrations is driven by the loss of more mobile elements making it possible to back calculate the initial concentration of iron of a sample by tracing the loss of the more mobile elements.

The total reserve in bases (TRB=ΣCa+Na+K+Mg) of a sediment provides a good indication of the loss of mobile elements. Opfergelt et al., (2014) measured the TRB of the soil samples utilized throughout this study as reported on Table 3.1. If, as we are assuming, iron is the least mobile element in the system then the initial iron concentration must equal the total iron concentration of the sediment multiplied by the change in TRB i.e. $[Fe_i] = [Fe_T] \times \frac{TRB}{TRBi}$ where TRB_i is the initial TRB concentration of the sample. Table 3.1 contains these calculations for all the Icelandic soil samples as well as the resulting Fe_{OOH} estimates. Opfergelt et al., 2014 also measured the Fe_{HR} concentrations of the soil profiles making it is possible to directly compare our estimates to the Fe_{HR} measurements as shown on Figure 3.3. Perfect coherence between Opfergelt et al., 2014's reduction based estimates and our estimates would result in a best line y=x; R^2=1. Our estimates are within 6% of this ideal fit.

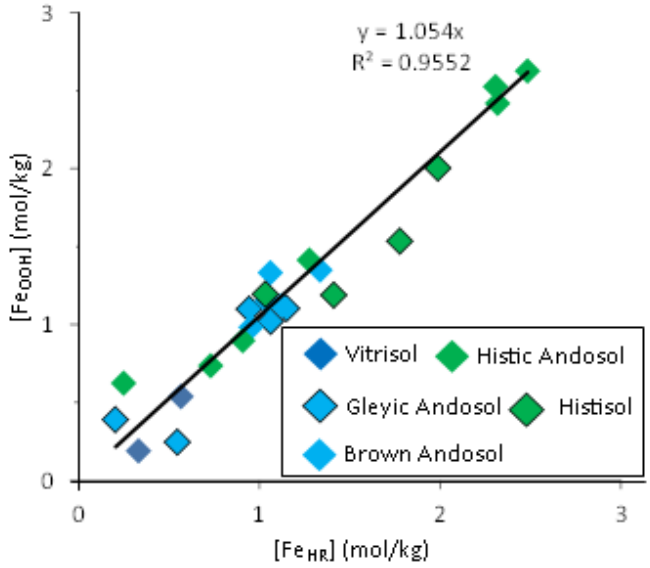

Figure 3.3. Calibrating Fe_{OOH} concentration estimates against Fe_{HR} concentration measurements. The line in the diagram is the best-fit line illustrating the similarity between the two independent data-sets.

Table 3.1. Results Summary. **A)** Data from Opfergelt et al., (2014) **B)** calculated as $[Fe_i] = [Fe_T] \times \frac{TRB}{TRBi}$ **C)** calculated using [Fei] estimated based on TRB values **D)** Data from Opfergelt et al., (2017) **E)** calculated using the iron isotope values to estimate [$_{Fei}$] **F)** The Brown Andosol horizons were assumed to originate for basalt with [Fei]=1.24 mol/kg while the Histsol and Histic Andsol samples were assumed to originate form Icelandic Rhyolite **G)** The average of 44 pristine Icelandic basalts from Jakobson (1972), Arnorrsson et al., (2002), and Eiriksdottir et al., (2008) **H)** From Craddock and Dauphas (2001).

Soil Type	Horizon	$[Fe_T]$[A)] mol/kg	TRB [A)] $cmol_c/kg$	Fe_{HR}[A)] mol/kg	$[Fe_i]$[B)] TRB based mol/kg	$[Fe_{OOH}]$[C)] mol/kg	$\Delta^{56}Fe$‰[D)]	±2σ ‰[D)]	$[Fe_{OOH}]$[E)] isotope based mol/kg	$[Fe_{OOH}]$[F)] refined mol/kg
Parent Basalt		1.64[G)]	733.6		1.64[G)]		0.053[H)]	0.015[H)]		
Vitrisol	A	2.08	666.9	0.33	1.89	0.19	0.053	0.047	0.31	
	B/c	2.18	568.1	0.57	1.69	0.54	0.053	0.047	0.04	
Gleyic Andosol	A1	1.87	333.4	0.94	0.85	1.10	0.067	0.027	0.74	
	A2	2.13	377.0	1.15	1.09	1.10	0.067	0.047	0.55	
	Bw1	2.08	274.5	1.06	0.78	1.02	0.093	0.033	0.41	
	C	2.13	648.9	0.55	1.88	0.25	-0.060	0.033	0.18	
	2Bw1	1.06	479.6	0.20	0.69	0.39	0.007	0.033	0.20	
Brown Andosol	A1	2.00	402.7	0.95	1.10	0.98	0.053	0.053	0.59	0.82
	A2	2.09	369.6	1.12	1.05	1.12	0.080	0.067	0.50	0.93
	Bw1	2.19	376.9	1.04	1.13	1.15	0.093	0.027	0.39	1.02
	Bw2	2.25	317.2	1.34	0.97	1.35	0.113	0.067	0.23	1.09
	Bw3/C	2.28	324.5	1.06	1.01	1.33	0.080	0.040	0.36	1.11
Histisol	o1	2.15	265.6	1.78	0.78	1.53	0.447	0.047	0.54	1.83
	o2	1.50	192.2	1.03	0.39	1.19	0.373	0.047	0.50	1.18
	o3	2.53	188.0	1.99	0.65	2.00	-0.013	0.013	0.43	2.21
	o4	1.81	282.5	1.41	0.70	1.19	0.080	0.047	0.67	1.50
Histic Andosol	A1	2.96	148.2	2.31	0.60	2.53	0.253	0.053	0.30	2.64
	A2	1.77	177.5	1.28	0.43	1.41	0.080	0.020	0.47	1.45
	Bw1	3.13	137.7	2.48	0.59	2.62	-0.220	0.047	0.19	2.81
	Bw2	2.94	156.0	2.32	0.62	2.42	-0.240	0.093	0.05	2.62
	o1	0.99	103.4	0.91	0.14	0.89	-0.107	0.100	0.39	0.68
	Redox	1.03	332.0	0.25	0.47	0.62	-0.033	0.033	0.05	0.71
	O2	0.77	52.4	0.73	0.05	0.73	-0.400	0.047	0.59	0.45

3.4.2 Replacing TRB with Iron Isotopes

The total amount of elemental data required to trace TRB restricts the practicality of the approach. Iron isotopes offer an alternative means of solving the model equations to calculate sediment Fe_{OOH} concentrations. Iron has four stable isotopes (^{54}Fe, ^{56}Fe, ^{57}Fe and ^{58}Fe) that are fractionated in a mass-dependent manner during low-temperature chemical weathering (Skulkan et al., 2002; Kiczka et al., 2011). More specifically, iron re-precipitation following mineral dissolution promotes the formation of aqueous and immobile-solid iron pools which are fractionated relative to each other (Skulkan et al., 2002). The fractionation factor ($\Delta^{56}Fe_{aq\text{-}s}$) which encapsulates this process can have one of six generalized environmentally dependent based on published experimental data which is summarized on Table 3.2.

Table 3.2. Summary of published iron isotope fractionation experiments. (A) Experiments conducted under either oxidizing or reducing conditions and the measured experimental values are reported ± their published uncertainty. The measured values have then been converted into the opposing redox conditions utilizing the experimentally derived value for redox fractionation *Wiederhold et al., (2006) reported their values in $\delta^{57/54}$ notation and did not report uncertainty so the values have been converted to $\delta^{57/54}$ assuming $\delta^{57/54}=1.5*\delta^{56/54}$ and utilizing an uncertainly reported from their standards.

Fe_{aq}-Fe_{aq}	Experimental Conditions	$\Delta^{56}Fe_{II-III}$		Source
	Equilibrium Redox Fractionation			
	Fe(II)-Fe(III) (15 days)	-3.01 ±0.08		Johnson et al 2002; Wu et al 2011
Fe_{aq}-Fe_s	Iron System	$\Delta^{56}Fe_{aq-s}$ (A)		Reference
		Oxic	Anoxic	
	Kinetic Iron Cycling			
	Fe_{aq}-Geothite(exchange)	1.95	-1.05±.0.08	Beard et al 2010
	Fe_{aq}-Fesurface	1.83	-1.18±.0.1	Beard et al 2010
	Fe_{aq}-Magnetite	1.76	-1.24±0.14	Frierdich et al 2014
	Fe_{aq}-Ferrihydrite	1.44	-1.56±0.48	Croal et al 2004
	Fe_{aq}-Geothite	1.31	-1.7±0.2*	Weiderhold et al 2006
	Fe_{aq}-Hematite	1.32 ±0.24	-1.68	Skulkan et al 2002
	Generalized Value	+1.5	-1.5	
	Ligand Stabilized Iron Cycling			
	Fe_{aq}+OM-Geothite	0.34±0.15*	-2.66	Weiderhold et al 2006
	Fe_{aq}+Silica-Ferrihyrdite	0.53	-2.58±0.14	Wu et al 2011
	Fe_{aq}+OM-Ferrihydrite	0.6±0.15	-2.4	Dideriksen et al 2008
	Generalized Value	+0.49	-2.51	
	Equilibrium Iron Cycling			
	Fe_{aq}-Hematite	-0.10 ±0.40	-3.2	Skulkan et al 2002
	Fe_{aq}-Ferrihydrite	-0.17	-3.18±0.08	Wu et al 2011
	Fe_{aq}-Goethite	-0.29	-3.30±0.98	Crosby et al 2005
	Fe_{aq}-Hematite	0.06	-2.95±0.38	Crosby et al 2005
	Generalized Value	-0.15	-3.15	

The six generalized values reflect the combined influences of redox and thermodynamic factors on iron isotope fractionation. In general, anoxic conditions promote redox fractionation between the aqueous and solid iron pools. This causes the aqueous iron pool to become preferentially enriched in the lighter isotope of iron relative to the residual sedimentary iron pool. Kinetic iron precipitation has the opposite effect as kinetic precipitation preferentially removes the light isotope of iron from solution. Ligands, including organic matter, stabilize aqueous iron preventing true equilibration between the aqueous and residual solid iron pools. Thus, iron

cycling in environments with high organic matter concentrations adheres to a pattern which is intermediate to true kinetic and equilibrium systems.

Of the six generalized iron cycling environments, only two are needed to cover the vast majority of low temperature weathering environments: oxic cycling in the presents of organic ligands ($\Delta^{56}Fe$=+0.49‰) and oxic-equilibrium iron cycling ($\Delta^{56}Fe$=-0.15‰). [Kinetic iron reduction is also an environmentally plausible scenario for certain low temperature environments e.g. Reidel et al., (2013). Kinetic reduction is predicted to result in sediment samples which are strongly enriched in the heavy isotopes of iron ($\Delta^{56}Fe_{aq\text{-}s}$=-1.5‰).] The opposing nature of isotope fractionation with and without organic ligands allows a single fractionation factor to be selected to describe the weathering history of any sediment; samples with isotope compositions less than the bedrock [δFe^{56}<0.053‰ in the case of Iceland] can only be described by organic iron cycling while samples with isotope compositions greater that the bedrock can only be described by equilibrium iron cycling. Carrying these assumptions through Equations 1-6 (listed in Section 4) it is possible to calculate the initial iron isotope composition of a sample ($\delta^{56}Fe_i$) for any given values of [Fe_T] and [Fe_i].

Icelandic basalt has a known and well defined $\delta^{56}Fe_i$ value such that any value of [Fe_i] which yields an incorrect value for $\delta^{56}Fe_i$ can immediately be eliminated. [Section 3.5.2 will discuss the limits of this of assuming bedrock $\delta^{56}Fe_i$ values]. In this way, the value of [Fe_i] can be restricted within a narrow range of potential values which yield the correct value of $\delta^{56}Fe_i$ based on Equations 1-6. Existing data on Icelandic basalts can then be used choose the most likely value of [Fe_i] from within the range of potential values.

The average of 44 pristine Icelandic basalts from Jakobson (1972), Arnorrsson et al., (2002), and Eiriksdottir et al., (2008) is: [Fe]=1.64±0.4 (2σ) (mol/kg). On this basis, we set 1.64 mol/kg as the default value for [Fe_i] meaning the [Fei] value within the range of acceptable values (as determined by solving the equations for $\delta^{56}Fe_i$) which was closest to 1.64 was used to estimate [Fe_{OOH}].

The estimates for [Fe_{OOH}] utilizing this approach are reported on Table 3.1 for all the soil horizons. Figure 3.4 shows the results of this isotope based approach relative to the Fe_{HR} concentrations measured by Opfergelt et al., (2014) in the same samples. The error bars on Figure 4.5 reflect the propagation of analytic uncertainty from the isotope measurements to the Fe_{OOH} estimates. There is a statistically significant correlation (P<0.001) between our estimates

and the Fe_{HR} concentrations across the samples, but our estimates are also systematically lower than the Fe_{HR} concentrations. On average the [Fe_{OOH}] estimates are more than 30% lower than the Fe_{HR} concentrations across the sample suite.

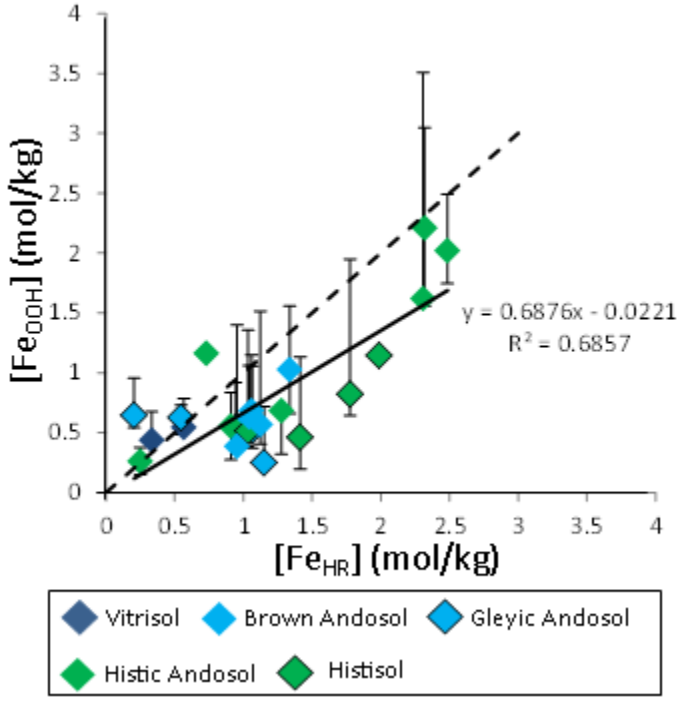

Figure 3.4. Calibrating Fe_{OOH} concentration estimates against Fe_{HR} concentration measurements. The solid line in the diagram is the best-fit line illustrating the similarity between the two independent data-sets. The dashed line defines the theoretic perfect fit relationship.

3.5 Discussion

3.6.1 Istopes vs. mobile elements.

Our model reliably reproduces the Fe_{HR} concentrations of the soil samples when parameterized with bulk normalized iron and mobile element concentrations. The 5% difference between our model estimates and Opfergelt's (2014) Fe_{HR} concentrations falls within the analytic uncertainty envelope of the original concentration measurments. However, this approach offers no clear advantage over selective extraction based Fe_{HR} measurements. Samples which can be analysed for TRB are also going to be appropriate for analysis by selective extraction, and the selective extraction data will be associated with a higher degree of confidence. More directly, having to measure TRB values in samples is not a viable solution to extending Fe_{OOH} concentration estimates to aquatic samples. The results illustrate the potential

of the model to describe iron cycling during chemical weathering, but an alternative means of solving the model for [Fe_i] and [Fe_{OOH}] is needed.

Iron isotopes offer an alternative means of estimating [Fe_i] with-in the same model to derive Fe_{OOH} concentrations. The clear drawback with the isotope based approach is its lack of accuracy. In sample suites where there is truly no other way to estimate Fe_{OOH} concentrations the approach is still useful. For example it is well documented that iron in aquatic samples is split between organic and inorganic particulates which have distinct affiliations with carbon and/or biological processes e.g. Ingri et al., 2000, Leyven et al., 2003, Boye et al., 2010, Vasyukova et al., 2012. At the same time, most studies still default to lumping all this iron together as 'dissolved' iron due to a lack of suitable alternatives (see review by Raiswell and Canfield 2012). The ability to estimate the fraction of Fe_{OOH} within such 'dissolved' iron pools to within ~30% would represent a significant improvement in the characterization of these samples. In the context of more traditional soil and bulk sediment samples however the ~30% uncertainty needs to be reduced.

The accuracy of the isotope based measurement can be improved by changing the assumed composition of the initial bedrock. Our initial estimates assumed all the soils were derived from basaltic bedrock with an initial composition equivalent an average value. This is an impossible assumption to test as there is no way to sample the actual initial bedrock composition of these soils. Furthermore the total iron concentrations of the samples suggest that our average basalt composition may not be a good representation for several of the soil profiles.

The average TRB corrected initial iron concentration for the Histisol and Histic Andosol samples is 0.49 mol/kg (Table 3.1). This is well outside the iron concentration range of typical Icelandic basalt ([Fe]=1.64±0.4 mol/kg) and is close to the initial iron concentration found in Icelandic rhyolite: 0.32±0.04 mol/kg (Schuessler et al., 2009). Rhyolite also has a slightly heavier initial iron concentration that pristine basalt ($\delta^{56}Fe$=0.168±0.021‰ Schuessler et al., 2009) consistent with the heavier isotope compositions of the Histisol soil horizons. Additionally, the soil horizons from the Brown Andosol soil profile have TRB corrected [Fe_i] values near the low end of the average basaltic range. Figure 3.5 shows how our Fe_{OOH} estimates change if the Histisol and Histic Andosol samples are assumed to have been derived from Icelandic Rhyolite and the Brown Andosol samples are assumed to have been derived from basalt with [Fe_i]= 1.24 mol/kg. The modified Fe_{OOH} estimates (reported on Table 3.1) are clearly closer to the sample

Fe_{HR} concentrations, and on average are with 2% of the measurements. These refinements are not however without their problems.

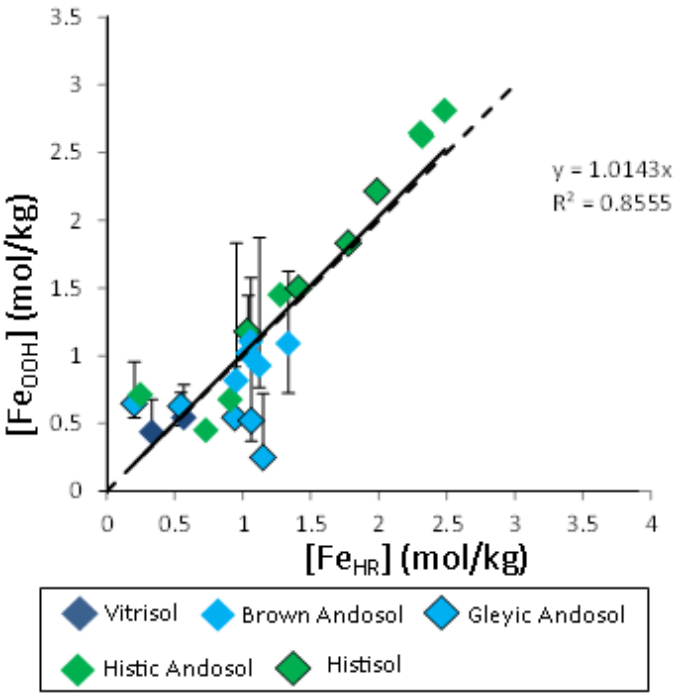

Figure 3.5 Calibrating Fe_{OOH} concentration estimates against Fe_{HR} concentration measurements. The difference between this figure and Figure 3.4 is that the [Fe_{OOH}] values for the Histic Andosol and Histisol horizons have been adjusted assuming the horizons originated from rhyolitic bedrock and the values for the Brown Andosol horizons have been adjusted assuming an [Fe_i] of 1.24 mol/kg.

An alternative explanation of the low apparent initial iron concentrations of the most weathered soil horizons is the onset of preferential oxide dissolution during the later stages of chemical weathering. The onset of acidic and/or reducing conditions in mature soil horizons could create conditions favouring preferential and quantitative dissolution of iron oxides. The preferential removal of iron oxides from sediments would induce the trend of decreasing apparent initial iron concentration with increasing extent of weathering as seen in our dataset. Unfortunately, the preferential dissolution process cannot be identified by isotope measurements. Mineral dissolution alone does not induce iron isotope fraction (Skulkan et al., 2002) such that preferential oxide dissolution does not leave an identifiable signal in the iron isotope record. This makes it impossible to identify samples which may have undergone preferential oxide dissolution without adding an additional layer of assumptions and uncertainties to the model estimates.

Overall, the methodologic uncertainty of the isotope based Fe_{OOH} concentration estimates is appears to be inversely correlated to the compositional similarity between the samples and bedrock. In this way, the approach appears to be far better suited for application to immature sediment which have a high degree of chemical similarity to the bedrock from which they were derived than strongly weathered soils.

3.6.2 Moving Beyond Basalts.

Our sample set only covered soils derived from a single bedrock type. The inherent nature of iron isotope fractionation however allows the model to be extrapolated to sediments derived from all crustal terrains. This is because iron isotope fractionation is inversely dependent on mineral crystallization temperature, and at low temperature there is no need to correct for bedrock and/or organic matter compositional variability within the model.

Above 500°C mineral equilibrium fractionation factors are smaller than the analytic sensitivity of iron isotope ratio measurements due to the inverse relationship between isotope fractionation and crystallization temperature (Blanchard et al., 2009). In the real world, this means that primary minerals within crustal terrains are expected to all have the same iron isotope ratios. Magmatic differentiation does induce bulk iron stable isotope fractionation between large igneous bodies (Weyer et al., 2005; Schuessler et al., 2009), but igneous minerals within a given terrain are not significantly fractionated relative to each other. Therefore, primary mineralogy is not a significant control of iron isotope compositions in crustal terrains. Sedimentary terrains might not adhere to this same principle as iron carbonates, iron-sulphides and iron-oxides formed at low temperatures are expected to be measurably fractionated relative to one another (Blanchard et al., 2009).

Even at low temperatures there is no need to consider bedrock composition during crustal weathering under most circumstances. Based on the the published experimentally derived iron isotope fraction factors (Table 3.2) the systematic uncertainty associated with deriving iron isotope fractionation factors for a given environment is greater than any mineral specific control on isotope fractionation. Systems which contain magnetite as the solid phase are indistinguishable from systems which contain ferrihydrite as the solid phase. Similarly, for the environments which contain ligands there is no significant difference between the experiment which used silica to stabilize aqueous iron i.e. Wu et al (2011) and the experiments which utilized organic siderophores i.e. Dideriksen et al., (2008). [This is consistent with the fact that studies of anoxic ground waters have traditionally argued organic matter stabilizes the light

isotopes of iron (Ingri et al., 2006) while studies of oxic surface waters have argued organic matter stabilized the heavy isotopes of iron (Ilinia et al., 2013)]. In the context of our model is means our generalized $\Delta^{56}Fe_{aq\text{-}s}$ values can be taken as environmentally representative without the need to further account for compositional differences in the bedrock and/or organic matter between real-world environments. Again, this is might be limited to comparisons between iron oxides as iron sulphides and/or iron carbonates have the theoretical potential to significantly alter iron isotope fractionation (Blanchard et al., 2009).

Despite the potential effects of low temperature carbonates and/or sulphide cycling in iron isotope fractionation sedimentary terrains display a restricted range of iron isotope compositions (Beard et al., 2003). Extreme iron fractionation has been identified in sedimentary rock from Greenland, but why this is true is a matter of debate (Dauphaus et al., 2004, 2007). Previous studies have therefore widely assumed that on a global scale iron isotope fractionation in sedimentary rocks is negligible e.g. Conway and John (2014). Therefore, our model can confidently be extended to all may also be broadly applicable to sedimentary terrain albeit with a higher degree of uncertainty than when it is used in crustal terrains.

3.7 Summary and Conclusion

Iron isotope and iron concentration measurements provide a simple, if imperfect, method of estimating the concentrations of secondary iron (oxyhydr)oxides in sediment samples. The reliability of the estimates is inversely correlated with the similarity between the sediment samples and the bedrock from which the sediments were derived. Given that iron isotope and iron concentration measurements can be applied to a greater array of samples than traditional selective extractions our new method opens the door to studying iron cycling and Fe_{OOH} formation in new systems. Specifically, the future application of this technique to samples of aquatic suspended and colloidal material Fe_{OOH} content could help unlock the role iron plays in moderating the carbon cycle.

3.8 References.

Arnalds O. and Gretarsson E. (2001) Soil Map of Iceland, second editions. Agricultural Research Institute Reykjavik. Available from: <ww.rala.is/desert>.

Arnorsson S., Gunnarsson I., Stefansson A., Andresdottir A., Sveinbjornsdottir A.E. (2002). Major element chemistry of surface- and groundwaters in basaltic terrain, N-Iceland. I. Primary mineral saturation. *Geochem. Cosmochem. Act.* **66**(23): 4015-4046.

Beard B.L.., Johnson C.M., Von Damm, K.L., Poulson, R.L. (2003) Iron isotope constraints on Fe cycling and mass balance in oxygenated Earth oceans. *Geo*l. 31(7): 629-632.

Beard B.L., Handler R.M., Scherer M.M., Wu L., Czaja A.D., Heimann A., Johnson C.M. (2010) Iron isotope fractionation between aqueous ferrous iron and goethite. Ear Plan Sci Lett. 295: 241-250.

Berner R.A. (1970) Sedimentary Pyrite Formation. *American Journal of Science* **268**: 1-23.

Bhatia M.P., Kujawinski E.B., Das S.B., Breier C.F., Henderson P.B., Charette M.A. (2013) Greenland meltwater as a significant and potentially bioavailable source of iron to the ocean. *Nat. Geosci*. **6**: 271-278.

Boye M., Nishioka J., Croot P., Laan P., Timmermans K.R., Strass V.H., Takeda S., de Barr H.J.W. (2010) Significant portion of dissolved organic Fe complexes in fact is Fe colloids. *Mar. Chem.* **122**: 20-27.

Conway T.M. and John S.G. (2014). Quantification of dissolved iron sources to the North Atlantic Ocean. *Nature.* **511**: 212-217.

Craddock P.R. and Dauphas N. (2010) Iron isotopic composition of geological reference materials and chondrites. *Geostand. Geoanaly. Res*. **35**(1):101-123.

Crosby H.A., Johnson C.M., Roden, E.E., Beard B.L. (2005) Coupled Fe(II)-Fe(III) electron and atom exchange as a mechanism for Fe isotope fractionation during dissimilatory iron oxide reduction. *Environ. Sci. Technol*. **39**: 6698-6704.

Dauphas N., van Zuilen M., Wadhwa M., Davis A.M., Marty B., Janney P.E. (2004) Clues from Fe Isotope Variations on the Origin of Early Archean BIFs from Greenland. *Science* **306**: 2077-2080.

Dauphas N., van Zuilen M., Busigny V., Lepland A., Wadhwa M., Jannet P.E. (2007) Iron istope, major and trace elements characterizations of early Archean supracrustal rocks from SW Greenland: Protolith identification and metamorphic overprint. *Geochem. Cosmochem Act*. **71**: 4745-4770.

Dideriksen K., Baker, J.A., Stipp S.L.S. (2008) Equilibrium Fe isotope fractionation between inorganic aqueous Fe(III) and the siderophore complex, Fe(III)-desferioxamine B. *Earth Plan Sci Let*. **269**: 280-290.

Eiriksdottir E.S., Louvat P., Gislason S.R., Oskarsson N., Hardardottir J. (2008) Temporal variation of chemical and mechanical weathering gin NE Iceland: Evaluation of a steady-state model of erosion. *Earth Planet. Sci Lett.* **272**: 78-88.

Frierdich A.J., Beard B.L., Scherer M.M., Johnson C.M. (2014) Determination of the Fe(II)aq-mangnetite equilibrium iron isotope fractionation factor using the three-isotope method and multi-direction approach to equilibrium. *Earth and Planetary Science Letters* **391**:77-86

Gislason S.R. and Arnorsson S. (1993) Dissolution of primary basaltic minerals in natural waters: saturation state and kinetics. *Chem. Geo.* **105**: 117-135

Gislason S.R., Arnorsson S., Armannsson H. (1996) Chemical weathering of basalt in southwest Iceland: effects of runoff, age or rocks and vegetative/glacial cover. *Amer. Journ. Sci.,* **296**: 837-907.

Homoky W.B., Severmann S., Mills, R.A., Statham P.J., Fones G.R. (2009) Pore-fluid isotopes reflect the extent of benthic Fe redox recycling: evidence from continental shelf and deep-sea sediments. Geology 37: 751-754

Hoffmann S.R., Shafer M.M., Babiarz C.L., Armstrong D.E. (2000) A critical evaluation of tangential-flow ultrafiltration for trace metal studies in freshwater systems: 1. organic carbon. *Environ. Sci. Technol.* **34**: 3420-3427.

Ingri J., Malinovsky D., Rodushkin I., Baxter D.C., Widerlund A., Andersson P., Gustafsson O., Forsling W., Ohlander B. (2006) Iron isotope fractionation in river colloidal matter. Earth Plan Sci Lett. 245: 792-798.

John S.G. and Adkins J. (2012) The vertical distribution of iron stable isotopes in the North Atlantic near Burmuda. *Global Biogeochem Cycles*. **26**: GB2034.

Johnson K.S., Gordon R.M., Coales K.H. (1997) What controls dissolved iron concentrations in the worlds ocean? *Marine Chem*. **57**: 137-161

Johnsson C.M., Skulkan J.L., Beard B.L., Sun H., Nealson K.H., Braterman P.S. (2002) Isotopic fractionation between Fe(III) and Fe(II) in aqueous solutions. *Earth Plant. Sci. Lett.* **195**: 141-153

Jakobsson S.P. (1972) Chemistry and distribution pattern of Recent basaltic rocks in Iceland. *Lithos*. **5**: 365-386.

Kaasalainen H. and Stefansson A. (2012) The chemistry of trace elements in surface geothermal waters and steam, Iceland. *Chem. Geo*. **330-331**: 60-85.

Kaiser K. and Guggenberget G. (2000) The role of DOM sorption to mineral surfaces in the preservation of organic matter in soils. *Organic Geochem.* **31**:711-725

Kiczka M., Wiederhold J.G., Frommer J., Voegelin A., Kraemer S.M., Bourdon B., Kretzschmar R. (2011) Iron speciation and isotope fractionation during silicates weathering and soil formation in an alpine glacier forefield chronosequence. *Geochem Cosmochem Act*. **75**:5559-5573.

Kogel-Knabner I., Guggenberger G, Kleber M., Kandeler E., Kalbitz K, Scheu S., Eusterhues K, Leinweber P. (2008) Organo-mineral associations in temperate soils: integrating biology, mineralogy and organic matter chemistry. *J. Plant Nutr. Soil Sci*. **171**: 61-82.

Lalonde K., Mucci A., Ouellet A., Gelinas Y. (2012) Preservation of organic matter in sediments promoted by iron. *Nature.* **483**: 198-200.

Liu X. and Millero F.J. (1999). The solubility of iron hydroxide in sodium chloride solutions. *Geochim Cosmochem. Act.* **63** (19/30):3487-3497.

Lyven B., Hassellov M., Turner D.R., Halraldsson C., Andersson K. (2003) Competition between iron- and carbon-based colloidal carriers for trace metals in a freshwater assessed using flow filed-flow fractionation coupled to ICPMS. Geochem Cosmo Act. **67**(20):3791-3802.

Mikutta R., Kleber M., Torn M.S., Jahn R. (2006) Stabilization of soil organic matter: association with minerals or chemical recalcitrance? *Biogeochem*. **77**: 25-56.

Millero, FJ. (1998). Solubility of Fe(III) in seawater. *Earth Planet Sci Lett*. **154**: 323-329.

Nesbitt H.W. and Wilson R.E. (1992) Recent chemical weathering of basalts. *Amer. Journ. Sci*. **292**: 740-777.

Opfergelt S., Burton K.W., Georg R.B., West A.J. Guicharnaud R.A., Sigfusson B., Siebert C., Gislason S.R., Halliday, A.N. (2014). Magnesium retention on the soil exchange complex controlling Mg isotope variations in soils, soil solutions and vegetation in volcanic soils, Iceland. *Geochem Cosmo. Acta*. **125**: 110-130.

Opfergelt S., Williams H.M., Cornelis J.T., Guivharnaud R.A., Georg R.B., Siebert C., Gislason S.R., Halliday A.N., Burton K.W. (2017). Iron and silicon isotope behaviour accompanying weathering in Icelandic soils with implications for Fe mobilization from peat-bearing soils. *Geochem. Cosmochem. Act* (in-press).

Poitrasson F., Viera L.C., Seyler P, dos Santos Pinheiro G.M., Mulholland D.S., Bonnet M.-P., Martinez J-M., Lima B.A., Boaventura G.R., Chmeleff J., Dantas E.L., Guyot J-L., Mancini L., Pimentel M.M., Santos R.V., Sondag F., Vauchel P. (2014) Iron isotope composition of the bulk waters and sediment from the Amazon River Basin. *Chem Geol*. **377**: 1-11.

Poulton S.W. and Canfield D.E. (2005) Development of a sequential extraction procedure for iron: implications for iron partitioning in continentally derived particulates. *Chem. Geo*. **214**: 209-221.

Poulton S.W. and Raiswell R. (2005) Chemical and physical characteristics of iron oxides in riverine and glacial meltwater sediments. *Chem Geo.* **218**:203-221.

Raiswell R. and Canfield D.E. (2012) The iron biogeochemical cycle past and present. Geochemical Perspectives, European Association of Geochemistry, 1(1)

Reitmeyer R., Powell R.T., Landing W.M., Measures C.I. (1996) Colloidal aluminium and iron in seawater: an intercomparison between various cross-flow ultrafiltration systems. *Marine Chem*. **55**: 75-91.

Schrumpf M., Kaiser K., Guggenberger G., Persson T., Kogel-Knabner I., Schulze E.-D. (2013) Storage and stability of organic carbon in soils as related to depth, occlusion within aggregates and attachment to minerals. *Biogeosci*. **10**: 1675-1691.

Schlosser C. and Croot P.L.. (2008) Application of cross-flow filration for determining the solubility of iron species in open ocean seawater. Limnol. Oceanogr: Methods. 6: 630-642.

Schuessler J.A., Schoenber R, Sigmarsson O. (2009) Iron and lithium isotope systematics of the Hekla volcanoe, Iceland- Evidence for iron isotope fractionation during magma differentiation. *Chemical Geology*. **258**: 78-91.

Skulan J.L., Beard B.L., Johnson C.M. (2002). Kinetic and equilibrium Fe isotope fractionation between aqueous Fe(III) and hematite. *Geoch. Cosmo. Act*. **66**(17): 2995-3015.

Stefansson A. and Gislason S.R. (2001) Chemical weathering of basalts, southwest Iceland: Effects or rock crystallinity and secondary minerals on chemical fluxes to the ocean. *Americ. Journ. Sci*. **301**: 513-556.

Stefansson A., Gislason S.R., Arnorsson S. (2001) Dissolution of primary minerals in natural waters II. mineral saturation state. *Chem. Geol*. **172:** 251-276.

Vasyukova E., Pokrovsky O.S., Viers J., Dupre B. (2012) New operational method of testing colloid complexation with metals in natural waters. *Appl. Geochem*. **27**: 1226-1237.

Wiederhold J.G., Kraemer S.M., Teutsch N., Borer P.M., Halliday A.N., Kretzschmar R. (2006). Iron isotope fractionation during proton-promoted, ligand-controlled, and reductive dissolution of Goethite. *Environ. Sci. Technol*. **40**: 3787-3793.

Weyer S., Anbar A.D., Brey G.P., Munker C., Mezger K., Woodland A.B. (2005) Iron isotope fractionation during planetary differentiation. *EPSL*. **240**: 251-264.

Wu L., Beard B.L., Roden E.E., Johnson C.M. (2011) Stable iron isotope fractionation between aqueous Fe(II) and hydrous ferric oxide. *Environmental Science and Technology*. **45**: 1847-1852

Chapter 4

Estimating the Effects of Weathering on Reactive Iron Fluxes from Iceland

Abstract

This study compares the continental weathering patterns of glacial and non-glacial catchments in Icelandic on the basis of iron isotope measurements, total suspended sediment concentration data and sediment iron (oxyhydr)oxide estimates. The iron isotope measurements indicate organic matter influences iron cycling in non-glacial catchments while iron cycling in the non-glacial catchments is an inorganic process. The amount of iron affiliated with organic matter in the non-glacial systems is however only a small proportion of the total iron pool transported within the river systems. Overall, the large difference in physical sediment transport rates between glacial and non-glacial rivers is the dominant driver of iron export differences between glacial and non-glacial rivers. On average the glacial rivers contain 3.5 times more total sediment and 2.5 times more iron (oxyhydr)oxide than analogous non-glacial rivers on a flow-normalized basis. Globally total sediment accumulation and iron (oxyhydr)oxide accumulation rates correlate with organic carbon preservation in nearshore marine environments. Our results are therefore consistent with the hypothesis that glaciers enhance marine organic carbon burial by enhancing marine sediment and Fe_{OOH} accumulation.

4.1 Introduction

There is a strong positive correlation between organic carbon (OC) accumulation and total sediment accumulation in marine sediments as shown on Figure 4.1. This raises two related questions: Does the relationship between marine sediment accumulation and organic carbon accumulation mean that processes which enhance marine sedimentation increase carbon burial?; and if so, is there a positive feedback between glaciers and organic carbon sequestration? There is no doubt that glaciers enhance physical weathering rates relative to analogous non-glaciated terrains (Anderson et al., 2000; van de Flierdt et al., 2002). Whether or not the increase in physical weathering corresponds to an increase in OC burial depends on why sediment accumulation and organic carbon accumulation are so closely correlated.

There is no universally accepted explanation for why OC accumulation and total sediment accumulation are so strongly correlated in marine sediment. Some authors have suggested the

correlation is a product of redox dynamics e.g. Canfield (1994). Another theory is that non-specific mineral-organic matter surface interactions promote the protection of otherwise labile OC (e.g. Mayer 1994, Hedge and Keil 1995, Greathouse et al., 2014). More recently there has been a shift away from non-specific mineral-OM dynamics towards specific iron-OC dynamics to explain how inorganic minerals promote OC accumulation (e.g. Lalonde et al 2012, Barber et al., 2014). Iron (oxyhydr)oxides (Fe_{OOH}) have been singled out as the key phase(s) controlling OC burial (Schrumpf et al., 2013).

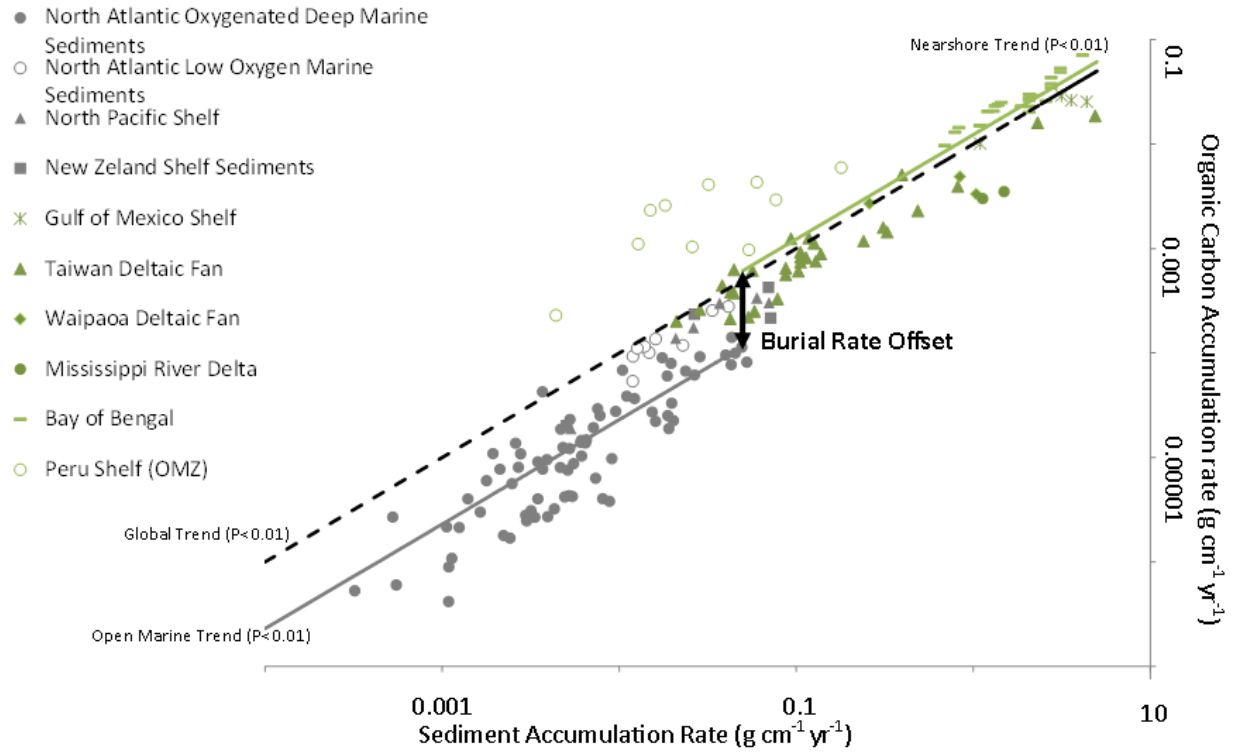

Figure 4.1: Sediment and organic carbon accumulation. Organic carbon accumulation in marine environments adheres to strong linear relationship with total sediment accumulation. Open ocean locations tend to fall below this line while estuarine locations tend to fall above the line consistent different environments having different relative carbon burial efficiencies. The data in the figure is from Talwani et al., (1976), Lyendyk et al., (1978), Barker et al., (1990), Barron et al., (1991), Eadie et al., (1994), Thiede et al., (1996), Saunders et al., (1998), Barker et al., (1999), Raymo et al., (1999), Flemmings et al., (2006), Kao et al., (2006), Aller et al., (2008) and Brackley et al., (2010), Fulthorpe et al., (2011), Dale et al., (2015) and Peketi et al., (2015).

Iron (oxyhydr)oxide concentrations have traditionally been measured utilizing selective chemical reduction techniques leading them to be described as highly reactive iron (Fe_{HR}). Reactive iron concentrations have been widely shown to correlate with the OC preservation

potentials of soils irrespective of all other environmental factors (Kaiser and Guggenberget 2000; Mikutta et al., 2006; Kogel-Knabner 2008; von Lutzow et al., 2008; Schrumpft et al., 2013). More recently Lalonde et al., (2012) showed the same trend exists in marine sediments. The theory that Fe_{OOH} actively controls, rather than passively correlates with, OC burial is supported by the unique ability for Fe_{OOH} to account for what is labelled as the 'burial rate offset' on Figure 4.1. This offset is a way of describing the fact that different environments tend to have slightly different relationships between OC and sediment accumulation.

The burial differences between marine environments are only weakly linked to absolute differences in primary production and/or redox conditions (see reviews by Blair and Aller 2012 and Burdige 2007). Environments with higher than average sediment normalized OC accumulation rates do however contain higher than average sediment normalized Fe_{OOH} accumulation rates. Sediment redox cycling promotes Fe_{OOH} formation in environments with anoxic and/or poorly oxygenated bottom waters leading to high OC and Fe_{OOH} preservation on a sediment normalized basis (Canfield et al., 1993; Riedel et al., 2013). Marine upwelling also enhances Fe_{OOH} formation (Hedges and Keil 1995) because the upwelling waters are rich in iron which precipitates near the surface. The direct protection of OC by Fe_{OOH} therefore provides a means for accounting for the known marine OC accumulation patterns.

If OC preservation in sediments is dependent on specific secondary Fe_{OOH} phases then predicting OC burial rates requires knowing the composition of sediments exported to the ocean as well as the total sediment export rates. This study compares the physical and chemical weathering dynamics of glacial and non-glacial river catchments in Iceland to determine how glaciers alter both the extent and nature of iron in alluvial sediments.

4.2 Icelandic Geology, Weathering, and Reactive Iron Formation

Chemical and physical weathering rates are strongly dependent on geologic variables in addition to local climatic conditions (Anderson et al., 1997, Syvitski and Milliman 2007). It is therefore necessary to control for geologic factors when assessing the impact of climatic shifts on terrestrial weathering patterns. This includes constraining initial bedrock iron isotope compositions when using iron isotope ratios to investigate iron cycling dynamics. Iceland is one of the best locations in the world for controlling for the influence of geology when comparing glacial and non-glacial catchments.

Iceland is a geologically young and active island formed primarily (>80%) of basaltic lavas with a mixed mid-ocean ridges-ocean island melt source composition. All known pristine Icelandic basaltic lavas have an iron isotope composition within uncertainty of the USGS BIR-1a Icelandic basalt international iron-isotope reference standard, $\delta^{56/54}Fe=0.053\pm0.015$ (Schuessler et al., 2009; Craddock and Dauphas 2010). Non-basaltic portions of the island are composed of more evolved lavas, predominantly rhyolites, and are focused near the most active volcanic centres. Magmatic evolution appears to involved iron isotope fractionation such that Icelandic rhyolites have iron isotope compositions around $\delta^{56/54}Fe=0.15\pm0.03$ (Schuessler et al., 2009).

Pristine Icelandic lavas do not contain primary Fe_{OOH} minerals restricting Fe_{OOH} to secondary mineral formation during chemical weathering (Stefansson et al., 2001). This means that differences in the iron isotopic compositions and Fe_{OOH} concentrations of sediments in glacial and non-glacial basaltic can be confidently attributed to differences in weathering rather than variations in initial bedrock chemistry. As for chemical weathering, iron is one of the least mobile elements during mineral dissolution in Icelandic environments (Stefansson and Gislason 2001). Iron's low mobility is largely due to secondary Fe_{OOH} formation during primary mineral dissolution (Stefansson et al., 2001).

4.3 Methods

4.3.1 Field Sampling

River samples were collected during September 2003, August 2005, September 2009, September 2010, August 2012, August 2013, and September 2014 at locations shown in Figure 4.2. The 2003 and 2005 samples were collected and characterized by (Pogge von Strandmann et al., 2006, 2008, 2011). The 2012 and 2013 samples were collected using the same methodology. Water samples were collected from near the water surface in the centre of the flow, facilitated by road bridges. For filtered and suspended sediment samples 15L of waters was collected and quickly filtered shortly after sampling, through 0.2µm Millipore filters, using a pressurized teflon unit. The filters were preserved and later the suspended particulate matter (SPM) was physically removed from the filters for analysis. Separate samples were collected for total suspended sediment (TSS), filtering a known volume of water through a 0.2µm filter. Riverbed sediment (RBS) samples were also collected as grab sample from within the active streambed where possible.

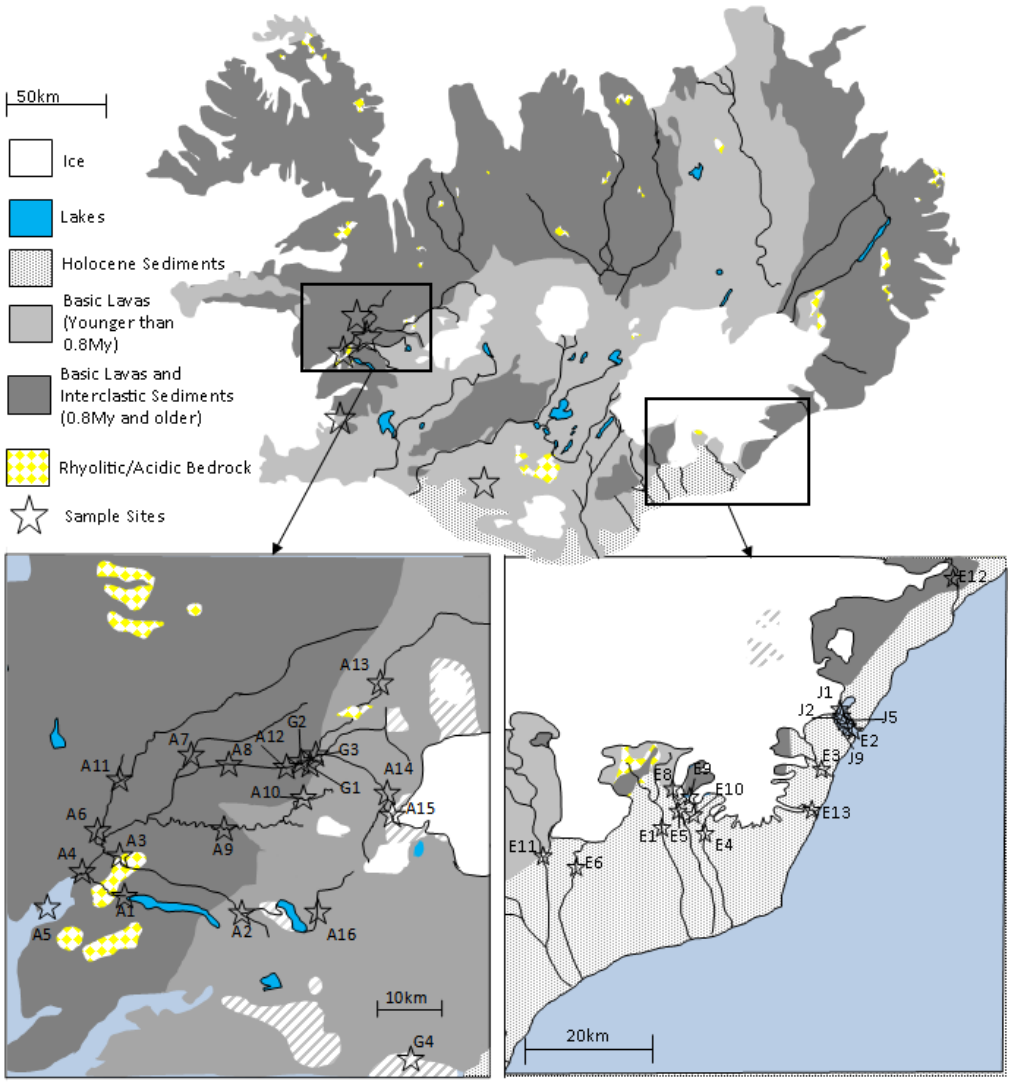

Figure 4.2. Soil map and field areas modified from the Icelandic Institute of Natural Histories Bedrock Geology Map of Iceland. The samples sites on the upper map show the locations of the soil profiles collected by Opfergelt et al., (2014) and used to calibrate the weathering models. The sample sites on the lower figures show the locations of the water samples.

4.3.2 Filterable Iron and Total Carbon Concentrations:

Iron concentrations in the filtered water samples were measured on a Thermo-Fisher X-series inductively coupled mass spectrometer (ICP-MS) utilizing a collision-cell to reduce oxide interferences at Durham University. The concentrations were calibrated against high purity synthetic Fe-standards which were doped with sodium (250µmol/L) and calcium (100µmol/L) to more accurately match the sample matrix. The certified reference standard SLRS-5 was used check the accuracy of the measurements, and external reproducibility was better than ±5%. The

total carbon concentrations of a number of the suspended sediments samples were measured on a Thermo-Finnigan MAT 253 isotope-ratio mass spectrometry at Durham University.

4.3.3 Stable isotopic analysis:

All samples were prepared for iron stable analysis according to established methods reported in Williams et al., (2004). Known volumes (500ml-1L) of the 0.2μm filtered waters were dried down for Fe_F analysis. Suspended and riverbed sediments were transferred into glass vials using a teflon coated spatula and 18.2 MΩ water and dried at 60°C. All samples were treated with a mixture of concentrated teflon-distilled HNO_3 and HF to ensure total sample digestion as well as complete oxidation of any organic matter. Digested samples were then taken through two treatments of HCl dissolution/evaporation prior to column chemistry. The samples were then brought up in 1 mL of 6 N HCl and half the samples was loaded onto 1mL of preconditioned BioRad AGX-1 X4 resign stored in 2mL columns. The columns were rinsed four volumes of 6 N HCL before being eluted in seven volumes of 2N HCL. After sample elution another volume of 2N HCl was added to the columns, collected and concentration checked for iron to ensure quantitative purification. Following elution the samples were dried and refluxed in a mixture of ultra-pure H_2O_2 and HNO_3 to oxidize any resin which may have leaked through the columns. Following oxidation the samples were prepared in 0.1 N HNO_3 for MC-ICPMS analysis. Total procedural blanks, processed in parallel with the samples were below the detection limit (<0.1μgFe) which is negligible relative to the quantities of processed sample iron (>200μg).

All the samples were diluted to within 10% of the sample-standard bracketing iron standard solution using the beam estimated intensity prior to analysis. All sediment analyses were carried out using sample standard bracketing against IRMM-14 at 2μg/g on an Thermo Neptune Plus multi-collector inductively coupled plasma mass spectrometer (MC-ICPMS) on medium resolution-mode with an Elemental Scientific Apex desolvator introduction system. A number of the measurements were conducted using a Fe^{57}-Fe^{58} double spike technique described by Millet et al., (2012) and run at 3 μg/g total iron (1.5μg/g sample, 1.5μg/g spike) with all other parameters the same as the non-spiked analyses. Each sample analysis consisted of at least 30 individual measurements (2 second integration times) and analyses were always repeated at least once within a session and during at least two different sessions. All errors are reported as 2 standard deviations (2σ) of the average value.

Iron isotope compositions are primarily reported in $\delta^{56}Fe$ notation, which represents the per mil deviation of the measured $^{56}Fe/^{54}Fe$ ratios relative to that of the bracketing standard, IRMM-014. In order to verify mass dependence during analysis, when utilising sample-standard bracketing, both the measured $\delta^{56}Fe$ and $\delta^{57}Fe$ values are reported in the data section. Iron fractionation factors are reported in Δ^{56} Fe notation, which represents the per mil offset of two $\delta^{56}Fe$ relative to each other i.e. $\Delta^{56}\ Fe_{A\text{-}B} = \delta^{56}Fe_A - \delta^{56}Fe_B$.

The BIR-1a USGS standard and internal FeCl lab standard were analysed multiple times during every analytical session to monitor stability and external reproducibility. The long-term external reproducibility of the value for the BIR-1a standard was $\delta^{56}Fe$=0.049±0.043, $\delta^{57}Fe$=0.105±0.080 (n=30; 2 σ) well within the accepted range of values for the standard ($\delta^{56}Fe$=0.053±0.015‰, $\delta^{57}Fe$=0.087±0.023, Craddock and Dauphaus 2011). The long term reproducibility of the value for the laboratory internal FeCl standard was consistent with previously published values of this standard (Williams et al., 2012; Williams and Bizimis 2014).

4.3.4 Iron isotope based Fe_{OOH} concentrations

Iron cycling during chemical weathering to be simplified into six equations which are listed below (see the previous chapter for a detailed discussion of the model):

1) $Fe_i = Fe_{OOH} + Fe_{aq} + Fe_p$:The sum of the (oxyhydr)oxide iron pool (Fe_{OOH}), the aqueous iron pool (Fe_{aq}) and the primary iron pool (Fe_P) is determined by the concentration of iron initially present in the system (Fe_i).

2) $[Fe_T] = \frac{Fe_p + Fe_{OOH}}{1 - \frac{Fe_{OOH} + Fe_{aq}}{Fe_i}}$: the bulk normalized concentration of iron in a sediment sample is the ratio of the sedimentary iron pool (Fe_p+Fe_o) and the total composition of the sediment following mineral dissolution ($1 - (\frac{Fe_o + Fe_{aq}}{Fe_i})$. This assumes iron is the most immobile element during chemical weathering.

3)$[Fe_{OOH}] = [Fe_T] \times \frac{Fe_{OOH}}{Fe_{OOH} + Fe_p}$: the bulk normalized concentration of Fe_{OOH} ($[Fe_{OOH}]$) is the relative amount of Fe_{OOH} to total iron ($\frac{Fe_{OOH}}{Fe_{OOH} + Fe_p}$) multiplied by the total iron concentration ($[Fe_T]$)

4) $\delta^{56}Fe_T = \left(\frac{Fe_p}{Fe_p+Fe_o}\right) * (\delta^{56}Fe_i) + \left(\frac{Fe_o}{Fe_p+Fe_o}\right) * (\delta^{56}Fe_O)$: The iron isotope composition of the residual bulk sediment pool ($\delta^{56}Fe_R$) is the mass balanced composition of primary iron pool (Fe_p, $\delta^{56}Fe_i$) and precipitated iron (oxyhydr)oxide pools (Fe_O, $\delta^{56}Fe_O$).

5) $\Delta^{56}Fe_{aq-s} = \delta Fe_{aq} - \delta Fe_s$: The iron isotope composition of the aqueous (δFe_{aq}) and solid (δFe_s) iron pools during chemical weathering differ based on one of the fractionation factors derived in the previous section ($\Delta^{56}Fe_{aq-s}$)

6) $\delta^{56}Fe_i = \left(\frac{Fe_o}{Fe_{aq}+Fe_o}\right) * (\delta^{56}Fe_o) + \left(\frac{Fe_{aq}}{Fe_{aq}+Fe_o}\right) * (\delta^{56}Fe_{aq})$: The initial amount of iron in a system (Fe_i) is dependent on the concentration of iron in the bedrock ([Fe_i])

Solving the equations requires measuring the iron isotope composition ($\delta^{56}Fe_T$) and bulk normalized iron concentration ([Fe_T]) of the target sediment samples. It is also necessary to parameterize the equations with the iron isotope composition of the pristine bedrock ($\delta^{56}Fe_i$) and the environmentally relevant iron cycling iron isotope fractionation factor ($\Delta^{56}Fe_{aq\text{-}s}$) to refine the estimated initial iron concentration of the sample (Fe_i). The full details of this process along with a validation test of the method in Icelandic soils are provided in the previous chapter which should be consulted for more information. In this study, we are assuming $\delta^{56}Fe_i$ is equivalent to the isotope composition of the BIR-1a international iron isotope references standard, which is an Icelandic Basalt ($\delta^{56}Fe_i$=0.053 ‰ Craddock and Dauphas 2010). $\Delta^{56}Fe_{aq\text{-}s}$ is assumed to be either -0.15‰, reflecting equilibrium iron cycling, or +0.49, reflecting iron cycling in the presence of organic matter (see Chapter 3 for further details).

4.3. Results

4.3.1 Total Suspended Sediments and Filterable Fe Concentrations

The concentrations of total sediment (TSS), filterable iron (Fe_F<0.2µm) and suspended particulate iron (Fe_{SPM}<0.2µm) are reported in Table 4.1 alongside the calculated proportion of the total iron load which is transported in the Fe_F pool (%Fe_F). On average glacial rivers contain 3.5 times more TSS than non-glacial rivers: 1099 mg/L and 310 mg/L respectively. On average the non-glacial rivers contain higher Fe_F concentrations than the glacial rivers, but the difference is not statistically significant (P>0.1). There is also no statistically significant difference in Fe_{SPM} concentrations between glacial and non-glacial sediments. The large offset in TSS and insignificant differences in Fe_F concentrations between glacial and non-glacial rivers equate to a

higher relative fraction of the total iron load in the glacial rivers being transported in the sediment phase. However, even in the non-glacial most of the total iron in the systems is affiliated with the sedimentary load (average non-glacial % Fe_F=4.77%).

There is significant inter-annual variability in the data (e.g. Gislason et al., 1996) including at locations collected over multiple years. The 2003 TSS values are consistently higher than values collected over subsequent years. In general, the 2003 samples also have lower Fe_F concentrations that the remaining samples.

Table 4.1 Riverine total suspended sediment (TSS) and filterable iron (Fe_F<0.2µm) concentrations. A) Discharge normalized percentage of iron within the filterable iron pool relative to the total iron pool. Values market with (-) were not determined.

Sample Source	Sample	[Fe_F] (µmol/L)	TSS (mg/L)	[Fe_{SPM}] (mol/kg)	% Fe_F A)
Glacial Rivers	A12-12	0.47	1531	1.31	0.02
	A14-12	0.33	2047	1.62	0.01
	A16-03	0.31	364	1.41	0.06
	G2-03	0.01	517	1.09	0.00
	E1-03	0.13	1890	1.55	0.00
	E3-03	0.95	1380	1.88	0.04
	E4-14	0.84	1650	1.26	0.04
	E5-03	0.06	2790	0.15	0.02
	E5-12	0.11	780	0.69	0.02
	E5-14	0.79	181	1.55	0.28
	E6-03	-	1570	-	-
	E6-14	0.37	335	1.82	0.06
	E8-12	0.02	1294	0.28	0.01
	E10-12	0.37	768	1.68	0.03
	E11-12 (East)	0.55	910	1.45	0.04
	E12-12	0.49	238	1.69	0.12
	E13-12	0.05	432	1.34	0.01
	Average	0.37	1099	1.30	0.05
Nonglacial River	A3-03	1.85	522	1.87	0.19
	A6-03	0.22	525	1.39	0.03
	A6-13	0.73	12	1.69	3.40
	A7-03	-	558	-	-
	A7-13	0.63	1	1.49	29.54
	A8-03	0.24	635	1.06	0.04
	A8-10	0.21	-	1.26	-
	A8-12	0.21	145	1.20	0.12
	A8-13	0.02	83	0.54	0.05
	Average	0.51	310	1.31	4.77

4.3.2 Riverine Isotope Compositions

The iron isotope compositions of the SPM samples are reported on Table 4.2. In the glacial samples $\delta^{56}Fe_{SPM}$ values vary from -0.015≤ $\delta^{56}Fe$≤0.232. The compositional range of the non-glacial samples is -0.049≤ $\delta^{56}Fe$≤0.127. The average isotopic compositions of the glacial and non-glacial SPM are $\delta^{56}Fe$=0.055±0.04 and $\delta^{56}Fe$=0.053±0.06 respectively which is within error of the isotopic value of fresh basalt ($\delta^{56}Fe$=0.049±0.04 for the BIR-1a reference standard).

The composition of glacial SPM does not vary significantly between samples collected from rivers, from ice and from a glacial estuary.

The iron isotope compositions of the riverbed sediment samples (RBS) are reported on Table 4.4. All the samples are isotopically equal to or heavier than pristine basalt. The compositions of the glacial samples range from $0.047 \leq \delta^{56}Fe \leq 0.131$ (average $\delta^{56}Fe = 0.096 \pm 0.03$), and the compositions range of the non-glacial samples is $0.056 < \delta^{56}Fe < 0.470$ (average $\delta^{56}Fe = 0.260 \pm 0.16$).

The total carbon concentrations (organic + inorganic) are also reported on Table 4.3 along with iron isotope measurements of selected Fe_F and Aeolian sand samples. All the SPM sample contain <0.3 wt. % carbon. The sand sample has an isotope composition within error of pristine basalts. The Fe_F samples from the two measured glacial samples are slightly enriched in the lighter iron isotopes relative to pristine basalt. The isotopic compositions of the Fe_F samples are also lighter than the compositions of the SPM pools with which they were co-collected. The non-glacial Fe_F samples display the opposite patterns. The samples have iron isotope compositions which are enriched in the heavy isotopes of iron compared to both pristine basalt and the SPM pools collected in the same total water samples.

Table 4.2. Iron isotope compositions of the SPM samples

Suspendend Particulate Material (>0.2um)					
Sample Source	Sample	δ56	2sd	δ57	2sd
Fresh Basalt	BIR-1a	0.049	0.04	0.105	0.08
Glacial Rivers	A12-12	0.064	0.09	0.064	0.09
	A14-12	0.061	0.08	0.043	0.01
	A15-12	0.061	0.13	0.043	0.01
	A16-03	0.077	0.04	0.115	0.04
	G2-03	0.042	0.03	0.062	0.04
	G3-03	0.107	0.04	0.159	0.16
	E1-03	0.052	0.04	0.078	0.04
	E1-12	0.043	0.05	0.056	0.10
	E3-03	0.002	0.04	-0.025	0.04
	E3-09	0.051	0.04	0.077	0.04
	E4-14	-0.015	0.04	-0.050	0.04
	E5-03	0.101	0.04	0.151	0.04
	E5-09	0.027	0.04	0.009	0.07
	E5-12	0.037	0.03	0.055	0.09
	E5-14	0.002	0.04	0.139	0.05
	E6-03	0.085	0.04	0.127	0.04
	E6-09	0.101	0.02	0.157	0.02
	E6-14	0.032	0.02	0.038	0.05
	E8-12	0.045	0.08	0.097	0.07
	E10-12	0.030	0.02	0.062	0.08
	E11-13 (East)	0.015	0.05	0.000	0.05
	E12-12	0.024	0.01	0.036	0.04
	E13-12	0.048	0.08	0.034	0.14

Suspendend Particulate Material (>0.2um)					
Sample Source	Sample	δ56	2sd	δ57	2sd
Glacial Ice	A15-12 Ice	-0.001	0.04	-0.015	0.01
	E4-14 ice	0.001	0.08	0.019	0.01
	E9-12 Ice	0.092	0.05	0.090	0.04
	J ice	0.075	0.01	0.131	0.09
Glacial Estuary	E2-05	0.101	0.02	0.152	0.06
	E2-12	0.057	0.10	0.056	0.12
	J1	0.232	0.11	0.318	0.18
	J2	0.120	0.04	0.209	0.06
	J5	0.005	0.09	0.065	0.10
	J9	0.053	0.01	0.112	0.01
Non-glacial River	A3-10	-0.049	0.03	-0.105	0.01
	A6-03	0.080	0.05	0.150	0.08
	A6-13	0.122	0.02	0.280	0.08
	A7-03	0.035	0.04	0.053	0.07
	A7-13	0.011	0.04	0.079	0.08
	A8-03	0.090	0.01	0.225	0.09
	A8-10	0.024	0.04	0.036	0.06
	A8-12	0.035	0.05	0.016	0.01
	A8-13	0.127	0.06	0.188	0.09
Mixed Source Estuary	A5-10	0.038	0.04	0.008	0.01

Table 4.3 Iron isotope compositions of the RBS, Fe_F and sand samples as well as SPM total carbon concentrations.

Bed Load Material					
Weathering Extent	Sample	δ56	2sd	δ57	2sd
Fresh	BIR-1a	0.052	0.04	0.105	0.08
Glacial Rivers	A14-12	0.094	0.03	0.162	0.00
	E1-03	0.121	0.01	0.180	0.08
	E4-14	0.097	0.04	0.140	0.04
	E5-03	0.106	0.03	0.184	0.10
	E5-14	0.089	0.01	0.081	0.05
	E8-12(I)	0.068	0.07	0.040	0.05
	E8-12(II)	0.131	0.04	0.196	0.08
	E10-12	0.094	0.07	0.131	0.11
	E12-12	0.114	0.05	0.165	0.05
	E13-12	0.047	0.07	0.092	0.08
Non-glacial Rivers	A4-14	0.056	0.03	0.098	0.03
	A4-05	0.115	0.04	0.172	0.06
	A6-13	0.208	0.16	0.630	0.08
	A3-03	0.327	0.12	0.340	0.11
	A7-03	0.383	0.06	0.620	0.05
	A8-03	0.470	0.04	0.700	0.05

Aeolean Basaltic Sand					
Weathering Extent	Sample	δ56	2sd	δ57	2sd
Aeolean Sand	Westman	0.085	0.091	0.115	0.07

Filterable Iron (<0.2µm)					
Weathering Extent	Sample	δ56	2sd	δ57	2sd
Glacial Rivers	E5-12	0.036	0.05	0.030	0.05
	E13-12	0.000	0.04	-0.020	0.04
Non-glacial Rivers	A6-13	0.253	0.04	0.340	0.04
	A7-13	0.116	0.05	0.150	0.05
	A8-12	0.188	0.05	0.250	0.05

Suspendend Particulate Material (>0.2um)		
Sample Source	Sample	Total Carbon wt%
Glacial	A12	0.04
	A14(I)	0.05
	A14(II)	0.02
	A15 ice course	0.03
	A15 ice fine	0.11
	E1	0.10
	E5	0.14
	E8	0.14
	E10	0.18
	E11	0.12
	E12	0.11
Non-Glacial	A3-09	0.22
	A8	0.11

4.3.3 Fe_{OOH} concentrations

Table 4.4 list the total iron concentrations ([Fe]) and Fe_{OOH} concentration estimates for all the RBS samples. On average the non-glacial RBS samples have higher Fe and Fe_{OOH} concentrations, but the differences are not statistically significant (P>0.2 t-test).

Table 4.5 list the Fe_{OOH} concentration estimates for all the SPM samples. The flow normalized fluxes of Fe_{OOH} from the rivers were determined by multiplying the TSS concentrations by the estimated Fe_{OOH} concentration of the sediment pool. The non-glacial samples contain higher Fe_{OOH} concentrations on average than the glacial samples, but the difference is not statistically significant (p>0.1, t-test). Due to the significant difference between the TSS concentrations in glacial and non-glacial rivers the glacial export at least 2.5 times more Fe_{OOH} than non-glacial rivers on a flux normalized basis.

Table 4.4 River bedload sediment Fe_{OOH} estimates. *These locations are downstream of both glacial and non-glacial tributaries but have dominantly non-glacial catchment areas.

Bed Load Material							
System	**Sample**	**[Fe] mol/kg**	**[FeOOH] mol/kg**	**System**	**Sample**	**[Fe] mol/kg**	**[Fe_{OOH}] mol/kg**
Glacial Rivers	**A14-12**	**1.42**	0.42	**Non-glacial Rivers**	**A4-12***	**1.57**	0.07
	E1-03	**1.34**	0.64		**A4-05***	**2.51**	1.11
	E4-14	**0.96**	0.36		**A6-13**	**1.41**	0.91
	E5-03	**1.85**	0.65		**A3-03**	**1.67**	1.17
	E5-14	**1.63**	0.43		**A7-03**	**2.29**	0.65
	E8-12(I)	**1.40**	0.20		**A8-03***	**1.36**	0.46
	E8-12(II)	**1.74**	0.94		**Average**	**1.79**	**0.73**
	E10-12	**1.16**	0.36				
	E12-12	**2.73**	1.13				
	E13-12	**1.31**	0.11				
	Average	**1.55**	**0.57**				

Table 4.5 Fe_{OOH} concentration and flux estimates. *These locations are downstream of both glacial and non-glacial tributaries but have dominantly non-glacial catchment areas.

Suspended Particulate Material (>0.2um)					
Sample Source	Sample	[Fe] mol/kg	[Fe_{OOH}] mol/kg	TSS (mg/L)	Fe_{OOH} Flux (µmol/L)
Glacial Rivers	A12-12	1.31	0.11	1531	168.0
	A14-12	1.62	0.12	2047	245.0
	A15-12	1.24	0.14	-	-
	A16-03	1.41	0.31	364	112.7
	G2-03	1.09	0.09	517	46.4
	G3-03	1.21	0.51	-	-
	E1-03	1.55	0.05	1890	94.8
	E1-12	1.48	0.08	-	-
	E3-03	1.88	0.24	1380	331.9
	E3-09	1.92	0.28	-	-
	E4-14	1.26	0.26	1650	427.3
	E5-03	0.70	0.30	2790	832.3
	E5-09	2.10	0.46	-	-
	E5-12	0.69	0.09	780	70.1
	E5-14	1.55	0.25	181	45.3
	E6-03	1.55	0.35	1570	549.5
	E6-09	1.90	0.60	-	-
	E6-14	1.82	0.18	335	60.3
	E8-12	0.28	0.03	1294	39.1
	E10-12	1.68	0.08	768	61.3
	E11-13	1.45	0.15	910	136.1
	E12-12	1.69	0.19	238	45.1
	E13-12	1.34	0.04	432	17.2
	Average	1.42	0.21	1099	193.1

Suspended Particulate Material (>0.2um)					
Sample Source	Sample	[Fe] mol/kg	[Fe_{OOH}] mol/kg	TSS (mg/L)	Fe_{OOH} Flux (µmol/L)
Glacial Ice	A15-12 Ice	0.89	0.19	-	-
	E4-14 ice	1.51	0.21	-	-
	E9-12 Ice	1.56	0.46	-	-
	J ice	2.13	0.49	-	-
	Average	1.52	0.33		-
Glacial Estuary	E2-05	1.78	0.58	203	117.6
	E2-12	1.93	0.29	24	6.9
	J1	1.95	1.55	23.6	36.6
	J2	1.16	0.56	-	-
	J5	1.45	0.15	-	-
	J9	1.31	0.11	-	-
	Average	1.60	0.54	83	45.1
Estuary	A5-10	1.07	0.07	-	-
Nonglacial River	A3-10	1.87	0.47	522	245.1
	A6-03	1.39	0.29	525	152.3
	A6-13	1.69	0.69	12.2	8.4
	A7-03	-		558	-
	A7-13	1.49	0.29	0.36	0.1
	A8-03*	1.06	0.36	635	228.6
	A8-10*	1.26	0.16	-	-
	A8-12*	1.20	0.10	145	14.5
	A8-13*	0.54	0.34	83	28.2
	Average	1.31	0.34	310	80.3

4.4 Discussion

4.4.1 The 2003 Data

A published long term record of Icelandic River data by Louvat et al., (2008) suggests our 2003 samples are anomalously high even against decadal scale variability. Louvat et al., (2008) found in rivers which had been sampled a minimum of 23 times over a minimum of 7 years glacial samples contained 923±606 mg/L TSS while non-glacial samples contained on average 150±85 mg/L TSS. If the data from 2003 is removed our TSS data falls close to these values (924±621 mg/L and 60±67 mg/L glacial and non-glacial respectively). The 2003 samples were collected following a major storm event created by the merger of Hurricane Fabian with a major extra-tropical storm in the North Atlantic (Pasch et al., 2003). The storm event impacted all of Iceland and may account for the high TSS values in 2003.

The decision was made to not remove the 2003 samples during analysis even though they may reflect abnormal river flow conditions. Including the 2003 was determined as one way to intentionally minimize the glacial and non-glacial differences by reducing the TSS offset from a factor of 6, consistent with Louvat et al., (2008), to a factor of 3.5. In doing so we ensure that our estimated glacial-non-glacial differences are highly conservative, and reduce the possibility that our final estimates overstate the true impact of weathering changes on iron (oxyhydr)oxide export to the ocean.

4.4.2 Iron Cycling Patterns: Fe_F and Fe_{SPM}

Organic matter and/or plant activity has been identified as the cause of significant differences in the behaviour of aluminium, silica (Opfergelt et al., 2011) and magnesium (Opfergelt et al., 2014 during chemical weathering in Iceland. For more than 4 decades it has also been known that the environmental behaviour of iron is highly dependent on organic matter i.e. Purdue and Beck (1976). Glacial catchments in Iceland are known to be poorer in OM than non-glacial catchments (Gislason et al., 1996) leading the expectation that organic matter might cause iron to behave differently during chemical weathering in glacial and non-glacial catchments. The iron isotope data is consistent with organic matter influencing iron cycling in the non-glacial catchments but not in the glacial catchments.

Figure 4.3 shows the relative compositions of the Fe_F, Fe_{SPM} and Fe_{RBS} pools in all the locations where the pools were sampled at the same time. Suspended particulate material is expected to be more chemically reactive than RBS due its much larger surface area to volume

ratio and its constant mixing within the river. The relative fractionation between the Fe_F and Fe_{SPM} pools ($\Delta^{56}Fe_{F\text{-}SPM}$) therefore provides an indication of iron cycling within the active river system. The Fe_F pools in non-glacial rivers are significantly heavier than both pristine basalt and the co-occurring Fe_{SPM} pools. This is consistent with organically bound iron being the primary component of the Fe_F pool.

Organic ligands preferentially bind the heavier isotopes of iron in oxygenated environments (Dideriksen et al., 2008; Wiederhold et al., 2006). [In anoxic environments ligands preferentially stabilize the light isotopes due to redox controls on iron isotope fractionation (Wu et al., 2011)]. In the absence of organic matter, equilibrium iron cycling under oxidizing conditions is associated with the opposite isotope fractionation patter; the light isotopes of iron are preferentially retained in solution although the difference is just above analytic uncertainty (Skulkan et al., 2002, Wu et al., 2011). This inorganic pattern provides a good explanation of the glacial samples as the glacial Fe_F pools are slightly enriched in the light iron isotopes relative to their corresponding Fe_{SPM} pools.

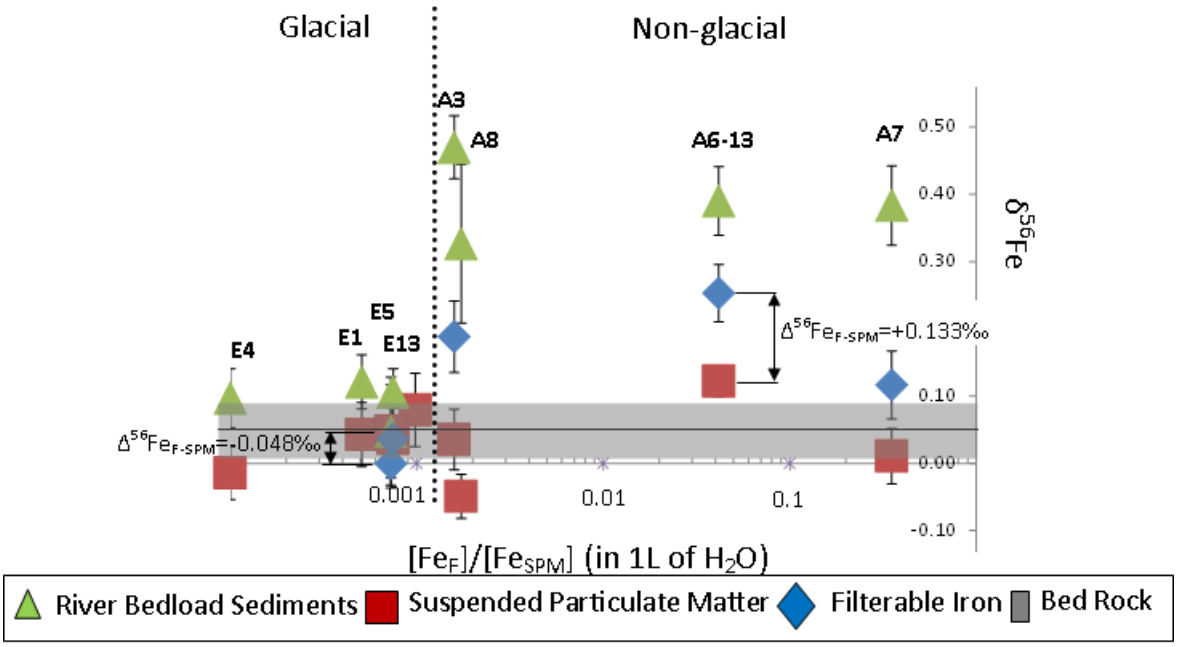

Figure 4.3. Environmental Iron cycling. Glacial and non-glacial river systems are distinguishable both in terms of their Fe_F/Fe_{SPM} and $\Delta^{56}Fe_{F\text{-}SPM}$ values. This is consistent with organic ligands stabilizing iron in the non-glacial catchments but not in the glacial catchments.

The x-axis of Figure 4.3 is the relative portioning of iron between the Fe_F and Fe_{SPM} pools. A higher percentage of the total iron pool is associated with Fe_F in non-glacial rivers than

in glacial rivers. This patterns is again consistent with non-glacial rivers having higher organic matter concentrations than glacial rivers. However, even in the sample with the highest [Fe_F]/[Fe_{SPM}] more than 70% of total iron in system is associated with the suspended sediments (Table 4.2). From a mass balance prospective, this limits the overall influence organic matter ultimately has on the total iron flux differences between glacial and non-glacial systems. While organic matter does appear to be stabilizing Fe_F in the non-glacial rivers, the pool of ligand stabilized iron represents only a small fraction of the total iron pool in these systems.

4.4.3 Iron Cycling Patterns: Fe_F and Fe_{SPM}

Figure 4.4 shows how the iron concentrations and iron isotope compositions of the RBS and SPM samples compare to each other and to the compositions of Icelandic soils from Opfergelt et al., (2014, 2017). The glacial RBS and all SPM samples have similar ranges of iron concentrations and iron isotope compositions (see Figures 4.3 and 4.4). This range overlaps with the expected range of immature sediments with a high degree of chemical similarity to the bedrock. As a discussed in the previous chapter this makes the SPM samples a good samples suite for estimating Fe_{OOH} concentrations via the iron istope approach. The non-glacial RBS samples do not fall within this compositional range, and have compositions which are more similar to the soil horizons. Such a pattern is consistent with the inclusion of more mature soil material into the bedload fraction of non-glacial rivers. The potentital mixing of soil material into the non-glacial RBS significantly decreases the reliability of the iron isotope measurements for estimating Fe_{OOH} concentrations in the samples (see previous chapter for full discussion).

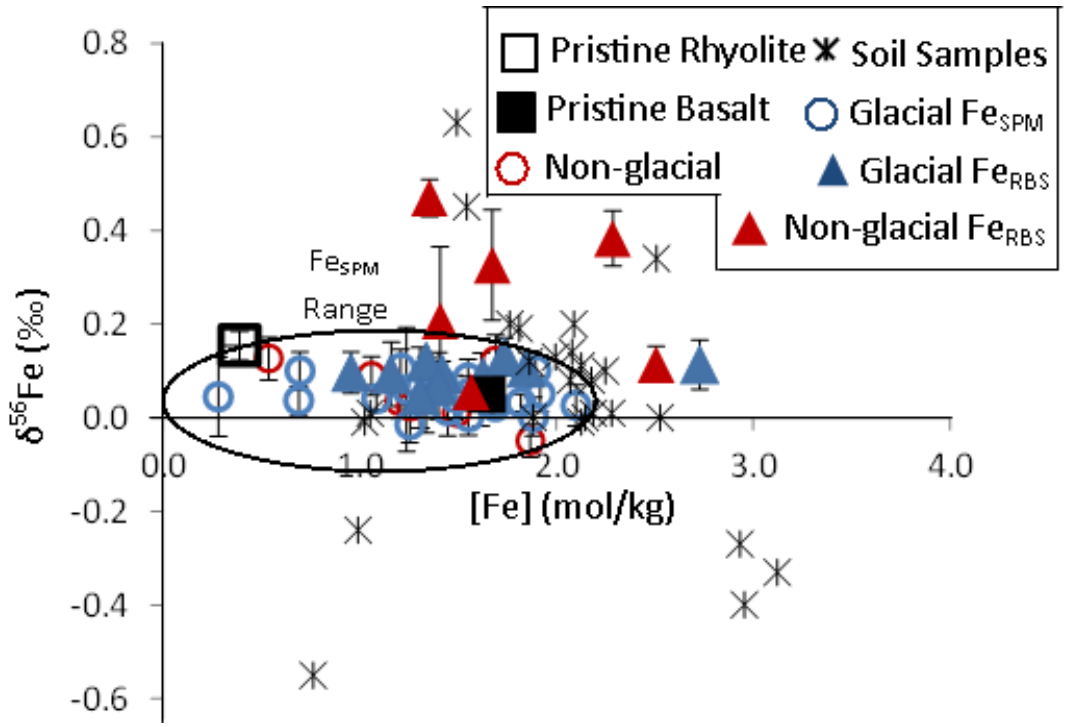

Figure 4.4 Compositional range of Icelandic soils and river sediments. Soil compositions from Opfergelt et al., 2014, 2017.

4.4.4 Proglacial Weathering

The pattern of glacial weathering discussed in Section 4.4.2 would inherently limit glacial sediments to iron isotope compositions $\delta^{56}Fe>0.053‰$. There are a few samples which contradict this pattern i.e. $\delta^{56}Fe_{SPM}<0.053‰$. These outlying samples all come from glacial rivers which drain the Vatnajökull icsheet. In this region of Iceland, glacial meltwaters pool in significant lakes before draining into the rivers. Biologic activity within the lakes might be creating sufficient quantities of organic matter to influence iron cycling and the composition of the local sediments. Ligand stabilization would account for the isotope compositions of the outlaying samples, and indicate the melt-water lakes represent a transitional glacial/non-glacial environment.

4.4.5 Coastal iron (oxyhydr)oxide exports

Iron mixes in a strongly non-conservative manner in estuaries resulting in the near complete deposition of alluvial iron in nearshore marine environments (Berquist and Boyle 2009). Discharge normalized nearshore Fe_{OOH} deposition rates can therefore be derived by adding the Fe_{OOH} concentrations contained with the SPM and Fe_F pools per litre of water. Table

4.6 presents the average estimated Fe_{OOH} flux rates for glacial and non-glacial systems in Iceland. On average glacial rivers are estimated to deposit 239% more Fe_{OOH} in nearshore marine environments than analogous non-glacial rivers.

Table 4.6 Total Fe_{OOH} flux estimates.

System	TSS	Fe_{OOH} sediment	Fe_F	Total Fe_{OOH} flux
	mg/L	µmol/L	µmol/L	µmol/L
Glacial	1099	193.1	0.37	193.5
Non-glacial	310	80.3	0.53	80.8
Relative Difference (%)	354.5	240.5	69.8	239.4

In general, interglacial periods are associated with wetter climates than glacial periods (Coale et al., 2004). Wetter climates may mean higher terrestrial hydrologic flux rates, but the link between de-glaciation and increased precipitation accumulation in Iceland is not easy to quantify. From 1835-2000, climate change has driven a statistically significant increase in average temperatures across Iceland while having no statistically significant impact on total precipitation rates (Hanna et al., 2004). Therfore it is not possible to readily quantify the difference in total hydrologic discharge between peak glacial and non-glacial conditions, and flux normalized data provides the best available means for comparing the climate systems.

The Icelandic data fits well into established global patterns surrounding the impact of glaciers on continental weathering. In general, glacial terrains are associated with higher physical weathering rates but near equal chemical weathering rates relative to analogues non-glacial terrains (Anderson et al., 1997). That is not to say chemical weathering difference do not occur between glacial and non-glacial catchments, but that most of the differences are due to minor phase weathering dynamics (van de Flierdt et al., 2002; Anderson et al., 2000). Iron cycling is not controlled by the weathering of accessory minerals, and therefore Fe_{OOH} formation does not significantly differ between glacial and non-glacial terrains. This claim is supported by reactive iron (Fe_{HR}) concentration data from Poulton and Canfield (2005) and Poulton and Raiswell (2005) on glacial and non-glacial sediments from catchments around the world. Those studies concluded that physical sediment characteristics, namely sediment surface area, controls sediment Fe_{HR} concentrations, and that the controls do not significantly differ between glacial and non-glacial system. The studies also recognized the implications of such a claim in the context of global Fe_{OOH} export dynamics; the physical weathering differences between

glacial and non-glacial weathering must equate to significant differences in the relative Fe_{OOH} export rates of glacial and non-glacial terrains.

4.5 Conclusion.

Organic matter availability creates a small difference in the way iron behaves in non-glacial catchments in Iceland relative to glacial catchments. The difference is detectable in the iron isotope concentrations of the non-glacial sediments, but overall organically bound iron constitutes a minor component of the total iron cycle. Physical sediment erosion is the primary source of Fe_{OOH} to rivers and subsequently to nearshore marine environments. The enhanced physical erosion rates associated with glacial weathering allow glacial rivers to deliver far more Fe_{OOH} to the ocean than analogous non-glacial rivers. Barring a complete revision of the factors which control the correlation between marine total sediment and marine organic carbon accumulation, the preferential export of total sediment and Fe_{OOH} from glaciated catchments constitutes a significant positive climate feedback mechanism.

4.6 References.

Aller C A, Blair N E, Brunskill G J (2008). Early diagenetic cycling, incineration, and burial of sedimentary organic carbon in the central Gulf of Papua (Papua New Guinea). Journ. Geophys. Res. **113**: F01S09

Anderson S.P., Drever J.I., Humphrey N.F. (1997) Chemical weathering in glacial environments. Geology 25: 399-402.

Anderson S.P., Drever J.I., Frost C.D., Holden P. (2000) Chemical weathering in the foreland of a retreating glacier. Geoch. Cosmo Act. 64(7): 1173-1189.

Barker, P. F., Kennett, J. P., et al, 1990. Proc. ODP, Sci. Results, 113: College Station, TX (Ocean Drilling Program).

Barker, P.F., Camerlenghi, A., Acton, G.D., et al., 1999. *Proc. ODP, Init. Repts.,* 178 [Online]. Available from World Wide Web: <http://www-odp.tamu.edu/publications/178_IR/178TOC.HTM>.

Barron, J., Larsen, B., et al., 1991. Proc. ODP, Sci. Results, 119: College Station, TX (Ocean Drilling Program).

Barber A, Lalonde K., Mucci, A., Gelinas Y. (2014) The role of iron in the diagenesis of organic carbon and notrigen in sediments: A long-term incubation experiment. *Marine Chem*. **162**: 1-9

Bergquist B.A. and Boyle E.A. (2006) Iron isotopes in the Amazon River system: weathering and transport signatures. Ear Plan Sci Lett **248**: 54-68.

Blair N.E. and Aller R.C. (2013) The fate of terrestrial organic carbon in the marine environment. *Annu. Rev. Marine Sci*. **4**: 401-423.

Brackley H.L., Blair N.E., Trustman N.A., Carter L, Leithold E.L. Canuel E.A., Johnston J.H., Tate K.R. (2010) Dispersal and transformation of organic carbon across an episodic high sediment discharge continental margin, Waipaoa Sedimentary System, New Zealand. Marine Geology. **270**: 202-212

Burdige D.J. (2007) Preservation of organic matter in marine sediments: controls, mechanisms, and an imbalance in sediment organic carbon budgets? *Chem. Rev.* **107**: 467-485.

Canfield D.E., Thamdrup B, Hansem J.W. (1993) The anaerobic degradation of organic matter in Danish coastal sediments: Iron reduction, manganese reduction and sulfate reduction. *Gechem Cosmochem Act*, **57**:3867-3883.

Canfield D.E. (1994) Factors influencing organic carbon preservation in marine sediments. *Chem. Geo*. **114**: 315-329.

Coale K.H., Johnson K.S., Chavez F.P., Buesseler K.O., Barber R.T., Brzezinski M.A., Cochlan W.P., Millero F.J., Falkowski P.G., Bauer J.E., Wanninkhof R.H., Kudeka R.M., Altabet M.A., Hales, B.E., Takahashi T., Landry M.R. Bidigare R.R., Wnad X., chase Z., Strutton P.G., Friederich G.E., Gorbunov M.Y., Lance V.P., Hilting A.K., Hiscock M.R., Demarest M., Hiscock W.T., Sullivan K.F., Tanner S.J., Gordon R.M., Hunter C.N., Elrod V.A., Fitzwater S.E., Jones J.L., Tozzi S., Koblizek M., Roberts A.E., Herndon J., Brewster J., Ladizinsky N., Smith G., Cooper D., Timothy D., Brown S.L., Selph K.E., Sheridan C.C., Twining B.S., Johnson Z.I. (2004) Southern Ocean iron enrichments experiment: carbon cycling in high- and low-si waters. *Science*, **304**: 408-414.

Craddock P.R. and Dauphas N. (2010) Iron isotopic composition of geological reference materials and chondrites. *Geostand. Geoanaly. Res*. **35**(1):101-123.

Dale A.W., Sommer S., Lomnitz U., Montes I., Treude T., Liebetrau V., Gier J., Hensen C., Dengeler M., Stolpovsky K., Bryant L.D., Wallmann K. (2015) Organic carbon production, mineralisation and preservation on the Peruvian margin. *Biogeosciences*. **12**: 1537-1559.

Dideriksen K., Baker, J.A., Stipp S.L.S. (2008) Equilibrium Fe isotope fractionation between inorganic aqueous Fe(III) and the siderophore complex, Fe(III)-desferioxamine B. *Earth Plan Sci Let*. **269**: 280-290.

Eadie B.J., McKee, B.A., Lansing M.B., Robbins J.A., Metz, S., Trefry J.H. (1994) Records of nutrient-enhanced coastal ocean productivity in sediments from the Louisiana continental shelf. *Estuaries.* **17**(4): 754-765.

Flemings, P.B., Behrmann, J.H., John, C.M., and the Expeditions 308 Scientists, 2006. Proc. IODP, 308:College Station Tx (Integrated Ocean Drilling Program Management International Inc.) doi:10.2204/iodp.proc.308.2006.

Fulthorpe, C.S., Hoyanagi, K., Blum, P., and the Expedition 317 Scientists, (2011). Proc. IODP, 317:Yokyo (Integrated Ocean Drilling Program Management International, Inc). doi:10.2204/iodp.proc.317.2011

Gislason S.R., Arnorsson S., Armannsson H. (1996) Chemical weathering of basalt in southwest Iceland: effects of runoff, age or rocks and vegetative/glacial cover. *Amer. Journ. Sci.,* **296**: 837-907.

Greathouse J.A., Johnson K.L., Greenwell H.C. Interactions of natural organic matter with layered minerals: recent developmentsw in computational methods at the nanoscale (2014) *Minerals*. **4**:519-540

Hanna E., Jonsson T. Box J.E. (2004) An analysis of Icelandic climate since the nineteenth Century. *Int. J. Climatol*. **24**: 1193-1210.

Hedges J.I. and Keil R.G. (1995) Sedimentary organic matter preservation: an assessment and speculative synthesis. *Mar. Chem*. **49**: 81-115.

Johnson K.S., Gordon R.M., Coale K.H. (1997) What controls dissolve iron concentrations in the world ocean*? Mar. Chem*. **57**: 137-161.

Jakobsson S.P. (1972) Chemistry and distribution pattern of Recent basaltic rocks in Iceland. *Lithos*. **5**: 365-386.

Kaiser K. and Guggenberget G. (2000) The role of DOM sorption to mineral surfaces in the preservation of organic matter in soils. *Organic Geochem.* **31**:711-725

Kao S-J, Shiah F-K, wangs C-H, Li K-K (2006) Efficient trapping of organic carbon in sediments on the continental margin with high fluvial sediment input off southwestern Taiwan. *Continental Shelf Research*. **26**(20): 2520-2537.

Keil R.G., Montlucon D.B., Prahl F.G., Hedges J.I. (1994) Sorptive preservation of labile organic matter in marine sediments*. Nature*. **370**: 549-552.

Kogel-Knabner I., Guggenberger G, Kleber M., Kandeler E., Kalbitz K, Scheu S., Eusterhues K, Leinweber P. (2008) Organo-mineral associations in temperate soils: integrating biology, mineralogy and organic matter chemistry. *J. Plant Nutr. Soil Sci*. **171**: 61-82.

Kulm, L. D., von Huene, R., et al, 1973, Initial Reports of the Deep Sea Drilling Project, Volume 18, Washington (U.S. Government Printing Office)

Lalonde K., Mucci A., Ouellet A., Gelinas Y. (2012) Preservation of organic matter in sediments promoted by iron. *Nature.* **483**: 198-200.

Louvat P, Gislason S.R. Allegre C.J. (2008) Chemical and mechanical erostion rates in Iceland as deduced from river dissolved and solid material. *Am. J. Sci*. **308**: 679-726.

Luyendyk, B.P., Cann, J.R., et a. 1978. Intial Reports of the Deep Sea Drilling Project, v. 49: Washington (US Government Printing Office)

Liu X. and Millero F.J. (1999). The solubility of iron hydroxide in sodium chloride solutions. *Geochim Cosmochem. Act.* **63** (19/30):3487-3497.

Mayer L.M. (1994) Surface area control of organic carbon accumulation in continental shelf sediements. Geoch. Cosmoch. Act. 58(4):1271-1284.

Millet M-A. Baker J.A., Payne C.E. (2012) Ultra-precise stable Fe isotope measurments by high resolution multiple-collector inductively couple plasma mass spectrometry with a 57Fe-58Fe double spike. *Chem. Geol*. **304-305**:18-25.

Millero F.J. (1998) Solubility of Fe(III) in seawater. *Earth Plan. Sci. Lett*. **154**: 323-329.

Mikutta R., Kleber M., Torn M.S., Jahn R. (2006) Stabilization of soil organic matter: association with minerals or chemical recalcitrance? *Biogeochem*. **77**: 25-56.

Nesbitt H.W. and Wilson R.E. (1992) Recent chemical weathering of basalts. *Amer. Journ. Sci*. **292**: 740-777.

Opfergelt S., Eiriksdottir E.S., Burton K.W., Einarsson A., Siebert C., Gislason S.R., Halliday A.N. (2011) Quantifying the impact of freshwater diatom productivity on silicon isotopes and silicon fluxes: Lake Myvatn, Iceland. *EPSL*. **305**: 73-82.

Opfergelt S., Burton K.W., Pogge von Strandmann P.A.E., Gislason S.R., Halliday A.N. (2013) Riverine silicon isotope variations in glaciated basaltic terrains: implications for the Si delivery to the ocean over glacial-interglacial intervals. *EPSL.* **369-370**: 211-219.

Opfergelt S., Burton K.W., Georg R.B., West A.J. Guicharnaud R.A., Sigfusson B., Siebert C., Gislason S.R., Halliday, A.N. (2014). Magnesium retention on the soil exchange complex controlling Mg isotope variations in soils, soil solutions and vegetation in volcanic soils, Iceland. *Geochem Cosmo. Acta*. **125**: 110-130.

Opfergelt S., Williams H.M., Cornelis J.T., Guivharnaud R.A., Georg R.B., Siebert C., Gislason S.R., Halliday A.N., Burton K.W. (2016). Iron and silicon isotope behaviour accompanying weathering in Icelanid soils with implications for Fe mobilization from peat-bearing soils. *Geochem. Cosmochem. Act* (in-press).

Pasch R.J., Blake E.S., Brown D.P. (2003) Tropical Cyclone Report, Hurrican Fabian, National Hurrican Center.

Peketi A., Mazumdar A., Joao H.M., Patil D.J., Usapkar A. Dewangan P. (2015) Coupled C-S-Fe geochemistry in a rapidly accumulation marine sediment system: Diagenetic and depositional implications. *Geochem. Geophys, Geosyst*. **16**: 2865-2883.

Pogge von Strandmann P.A.E., Burton K.W., James R.H., van Calsteren P., Gislason S.R., Mokaden F. (2006) Riverine behaviour of uranium and lithium isotopes in an actively glaciated basaltic terrain. *Ear. Plan. Sci. Lett.* **251**: 134-147.

Pogge von Strandmann P.A.E., Burton K.W., Porcelli D., James R.H., van Calsteren P. Gislason S.R. (2011) Transport and exchange of U-series nuclides between suspended material, dissolved load and collods in rivers draining basaltic terrains. *EPSL*. **301**: 125-136.

Pogge von Strandmann P.A.E., Burton K.W., James R.H., Calsteren P.V., Gislason S.R., Sigusson B. (2008) The influence of weathering processes on riverine magnesium isotopes in a basaltic terrain. *Earth Palent. Sci. Lett*. **276**:187-197.

Pogge von Strandmann P.A.E., Opfergelt S., Lai Y.-J., Sigfusson B., Gislason S.R., Burton K. (2012) Lithium, magnesium and silicon isotope behaviour accompanying weathering in a basaltic soil and pore water profile in Iceland. *EPSL* **339-340**:11-23

Poulton S.W. and Canfield D.E. (2005) Development of a sequential extraction procedure for iron: implications for iron partitioning in continentally derived particulates. *Chem. Geo*. **214**: 209-221.

Poulton S.W. and Raiswell R. (2005) Chemical and physical characteristics of iron oxides in riverine and glacial meltwater sediments. *Chem Geo.* **218**:203-221.

Raiswell R., Tranter M., Benning L.G. Siegert M., De'ath R., Huybrechts P., Payne T. (2006) Contributions from glacially derived sediment to the global iron (oxyhydr)oxide cycle: implication for iron delivery to the oceans. *Geoch. Cosmo. Act.* **70**: 2764-2780.

Raiswell R., Benning L.G., Tranter M., Tulaczyk S. (2008) Bioavailable iron in the Southern Ocean: the significance of the iceberg conveyor belt. Geoch. Tans. 9:7.

Raiswell R. and Canfield D.E. (2012) The iron biogeochemical cycle past and present. *Geochemical Perspectives*, European Association of Geochemistry, **1**(1)

Raymo, M.E., Jansen, E., Blum, P., and Herbert, T.D. (Eds.), 1999. *Proc. ODP, Sci. Results,* 162: College Station, TX (Ocean Drilling Program).

Riedel T., Zak D., Beister H., Dittmar T. (2013). Iron traps terrestrially derived dissolved organic matter at redox interfaces. *Preced. Nation. Acad. Sci* **110**(25):10101-10105.

Saunders, A.D, Larsen, H.C., and Wise, S.W., Jr. (Eds.), 1998. Proc. ODP, Sic. Results, 152:College Station, TX (Ocean Drilling Program)

Schrumpf M., Kaiser K., Guggenberger G., Persson T., Kogel-Knabner I., Schulze E.-D. (2013) Storage and stability of prganic carbon in soils as related to depth, occlusion within aggregates and attachment to minerals. *Biogeosci*. **10**: 1675-1691.

Schuessler J.A., Schoenber R, Sigmarsson O. (2009) Iron and lithium isotope systematics of the Hekla volcanoe, Iceland- Evidence for iron isotope fractionation during magma differentiation. *Chemical Geology*. **258**: 78-91.

Skulan J.L., Beard B.L., Johnson C.M. (2002). Kinetic and equilibrium Fe isotope fractionantion between aqueous Fe(III) and hematite. Geoch. Cosmo. Act. 66(17): 2995-3015.

Stefansson A., Gislason S.R., Arnorsson S. (2001) Dissolution of primary minerals in natural waters II. mineral saturation state. *Chem. Geol*. 172: 251-276.

Stefansson A. and Gislason S.R. (2001) Chemical weathering of basalts, southwest Iceland: Effects or rock crystallinity and secondary minerals on chemical fluxes to the ocean. *Americ. Journ. Sci*. **301**: 513-556.

Syvitski J.P.M., Milliman J.D. (2007). Geology, geography and humans battle for dominance over the delivery of fluvial sediment to the coastal ocean. *Geology* **115**: 1-19.

Talwani, M., Udintsev, G., et al., 1976. Initial Reports of the Deep Sea Drilling Project, Volume 38, Washington (U.S. Government Printing Office), 1256 p

Thiede, J., Myhre, A.M., Firth J.V., Johnson G.L., and Ruddiman, W.F. (Eds.), 1996/ Proc. ODP Sci. Results. 151: College Station, TX (Ocean Drilling Program).

van de Flierdt T., Frank M., Lee D., Halliday A.N. (2002) Glacial weathering and the hafnium isotope composition of seawater. *Ear. Plan. Sci. Lett*. **201**:639-647.

von Lutzow M., Kogel-Knabner I., Ludwig B., Matzner E., Flessa H., Ekschmitt K., Guggenberger G., Marschner B., Kalbitz K. (2008) Stabilization mechanisms of organic matter in four temperate soils: development and application of a conceptual model. *J. Plant Nutr. Soil Sci*. **171**: 111-124.

Williams H.M., McCammon C.A., Peslier A.H., Halliday A.N., Teutsch N., Leevasseur S., Burh J-P. (2004) Iron Isotope Fractionation and the Oxygen Fugacity of the Mantle. *Science*. **304**: 1656-1659.

Wiederhold J.G., Kraemer S.M., Teutsch N., Borer P.M., Halliday A.N., Kretzschmar R. (2006). Iron isotope fractionation during proton-promoted, ligand-controled, and reductive dissolution of Geothite. *Environ. Sci. Technol*. **40**: 3787-3793.

Williams H.M, Wood, B.J., Wade J., Frost D.J., Tuff J. (2012) Isotopic evidence for internal oxidation of the Earth's mantle during accretion. *Earth Planet. Sci. Lett.* **321-322**:54-63.

Williams H.M. and Bizimis M. (2014). Iron isotope tracing of mantle heterogeneity with the source regions of oceanic basalts. *Earth Plant. Sci*. **404**: 396-407

Wu L., Beard B.L., Roden E.E., Johnson C.M. (2011) Stable iron isotope fractionation between aqueous Fe(II) and hydrous ferric oxide. *Environmental Science and Technology*. **45**: 1847-1852

Chapter 5

Estimating the Effects of Weathering on Reactive Iron Fluxes from Greenland

Abstract

This study presents sediment concentrations, total iron concentrations and iron isotope measurements from glacial and non-glacial catchments in Greenland to compare continental weathering patterns between analogous glacial and non-glacial terrains. The iron stable isotope compositions of the sediment and water samples indicate that organic ligands impact the behaviour of iron during continental weathering in non-glacial but not in glacial systems. This chemical weathering difference does not appear to have a significant impact on the iron (oxyhydr)oxide export rates of glacial and non-glacial systems. Total (oxyhydr)oxide export, estimated from the data, broadly scales with total sediment export and glacial rivers contain 100 times more sediment than non-glacial rivers on a flow normalized basis. The preservation of organic matter in nearshore marine sediments depends on the accumulation total sediment and/or iron (oxhydr)oxides from continental weathering. Therefore, our data supports the hypothesis that glacial weathering increases nearshore marine organic carbon burial, relative to non-glacial weathering, thereby enhancing the positive feedback between glacial advance and Earth's climate.

5.1 Introduction

Do glaciers enhance organic carbon sequestration? Glacial environments are poor in organic matter (OM) such that their relationship with organic carbon burial has received little attention. However, OM preservation is not readily accounted for by organic processes (see reviews by Burdige 2007, Blair and Aller 2012 and Kögel-Knabner et al., 2008). Globally two inorganic variables are far better indicators of OM preservation than any other biologic or environmental factors.

The first inorganic variable which provides a strong indication of organic matter preservation is total sediment accumulation. There is a strong correlation between sediment accumulation and organic carbon (OC) concentrations proposed to be the bi-product of OC preservation by inorganic minerals (Mayer 1994, Kiel et al., 1994, Hedges and Kiel 1995, Blair and Aller 2012). Sedimentation rates have also been proposed as a key control of sediment redox dynamics

which would allow increases in sedimentation rates to further enhance OM preservation (Canfield 1994).

The second variable which is a strong predictor of OM accumulation is (oxyhydr)oxide (Fe_{OOH}) accumulation. Berner (1970) was the first study to show a clear correlation between the concentrations of Fe_{OOH} and organic carbon (OC) preservation in marine sediments. More recently Lalonde et al., (2012) dubbed the relationship the 'Rusty Carbon Sink' and Figure 5.1a summarizes the existing published data on the phenomena. There is a statistically significant correlation between organic carbon concentrations and extractable iron (a functionally defined approximation of Fe_{OOH}) within alluvial and marine environments. Organic carbon and Fe_{OOH} concentrations are also significantly correlated in terrestrial soils (Figure 5.1b). The correlation between Fe_{OOH} and organic carbon has been found to be so universal in soils that Schrumpf et al., (2013) concluded Fe_{OOH} concentrations are a robust indicator of soil OM preservation irrespective of all other environmental factors.

This study reports total sediment and Fe_{OOH} discharge rates from glacial and non-glacial catchments in Greenland. The Fe_{OOH} discharge rates are estimated based on iron isotope and iron concentration measurements of samples of filterable iron (Fe_F<0.2µm), suspended particulate iron (SPM>0.2µm) and riverbed sediments (RBS). The iron isotope data is also used to investigate differences in iron cycling dynamics between glacial and non-glacial rivers. Comparing these factors between the glacial and non-glacial systems provides an indication of the feedback between glacial-interglacial change, organic carbon burial and Earth's climate.

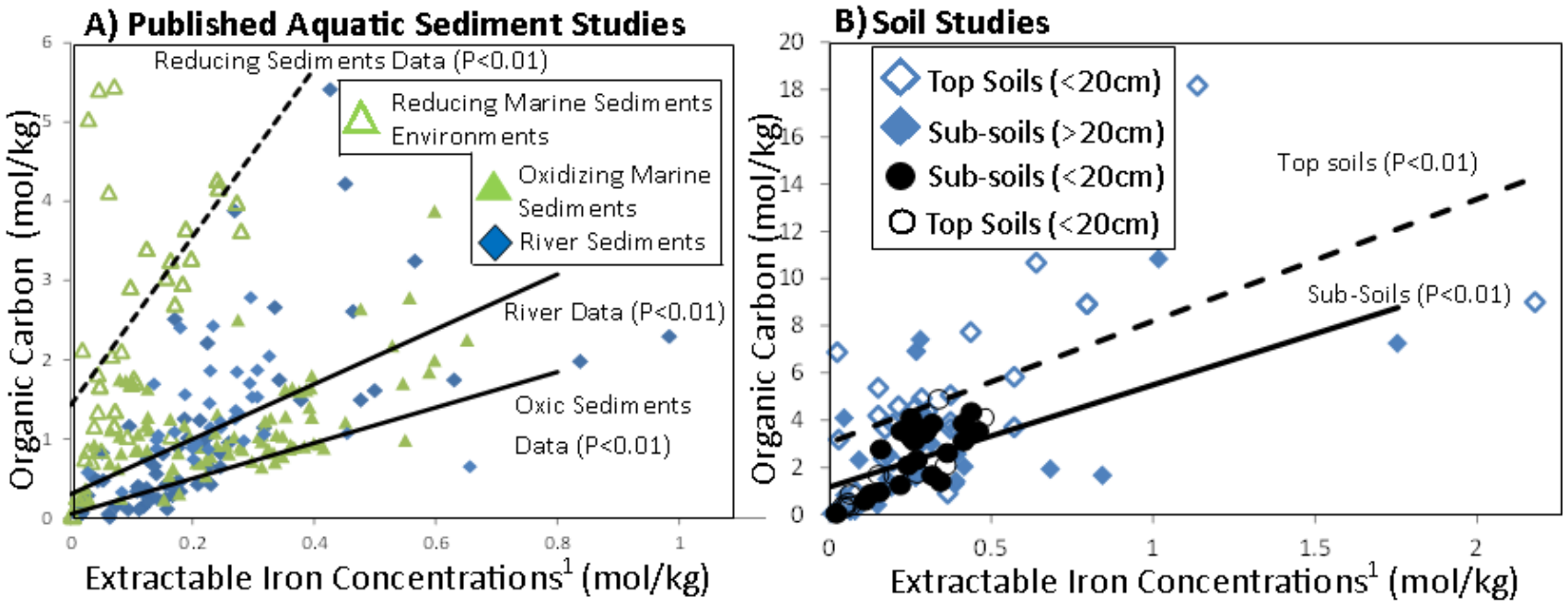

Figure 5.1. Organic Carbon Preservation and Chemically Reactive Iron. A) Aquatic sediment data from: Berner (1970), Poulton and Raiswell et al., (2005), Lalonde et al., (2012), Sabadini-Santos et al., (2014), and Sheng et al., (2015). B) Modified from Kaiser and Guggenberg (2000), whose data is shown in black, with additional data shown in blue from: Kiem and Kögnel-Knabner (2002) Mikkuta et al., (2006), Xu-hui et al.,(2007), Lutzow et al.,(2008), Thompson et al., (2011) and Song et al., (2012) shown in blue. (1) The Chemical extractable iron concentrations reflect a combination of oxalate, dithionate and HCL soluble iron measurements reflecting the different methodologies of the different studies

5.2 Greenlandic Geology and Weathering Regimes

Lithology has a major impact on continental weathering (Syvitski and Milliman 2007) making it important to control for geologic factors when comparing weathering patterns between locations. South-west Greenland is one region where significant areas of glacial and non-glacial weathering occur over a very similar lithology. South-west Greenland is primarily composed of Proterozoic tonalite-trondhjemite-granodiorite (TTG) orthogenesis (Gool and Marker 2007). Greenlandic TTGs are characterized by a low degree of iron stable isotope variability (Dauphas et al., 2009), and a relatively low degree of overall geochemical variability (Kalsbeek 2001). Given the scale of South-west Greenland some level of heterogeneity is expected, and the region does contain a number for supracrustal formations with distinctive geochemical properties (Dauphaus et al., 2004, 2009; Gool and Marker 2007). However, bedrock composition is expected to have a minimal impact on the differences in the weathering patterns between glacial and non-glacial catchments in South-west Greenland. Additonally relative to other regions where glacial and non-glacial catchments persist on equivalent bedrock, South-west Greenland offers the most extreme glacial and non-glacial endmember environments for comparison.

The Greenland Ice Sheet covers about 80% of the Greenland's total surface area. Surface meltwaters penetrate through the ice sheet and form sub-glacial drainage networks (McMillian et al., 2007). Where the sub-glacial networks emerge from the glacial front they feed large rivers characterized by seasonally variable discharge rates and high suspended sediment concentrations (McMillian et al., 2007). The combination of past glacial erosion and limited post-glacial vegetation means the rivers have few natural barriers before they drain into the ocean. Greenland's post-glacial geography and climate favours the formation of non-glacial systems which have few similarities to these glacial systems.

Permafrost coverage prevents groundwater formation throughout Greenland and forces all hydrologic flow into surface systems (Jorgensen and Andreasen 2007). While Greenland has low average annual temperatures, precipitation accumulation rates across South-west Greenland are near zero (Bales et al., 2009) i.e. evaporation rates are as high as precipitation rates. This has led to the formation of largely static lakes which dominate the pro-glacial landscape. Many of the lakes have become (semi)-saline as evaporation exceeds precipitation in some locations (Anderson et al., 1998*).* Many of the lakes are also organic rich environments (Bhatia et al., 2013, Palmtag 2015) and can be redox stratified (Anderson et al., 1998). From a

theoretical standpoint, many of the environmental differences between these lakes and typical (sub)glacial drainage systems are expected to cause continental weathering patterns to differ between glacial and non-glacial regions of Greenland.

Figure 5.2 shows the locations of the samples used in this study. Figure 5.2 also highlights the geo-spatial relationship between glaciated regions, lake dominated pro-glacial catchments, and the North Atlantic. The actual transition from glacial and non-glacial environments compared in this study occurs on a km to sub-km scale. This maximizes the ability extrapolate the effect of glacial retreat/advance on continental weathering from the differences in the glacial and non-glacial samples.

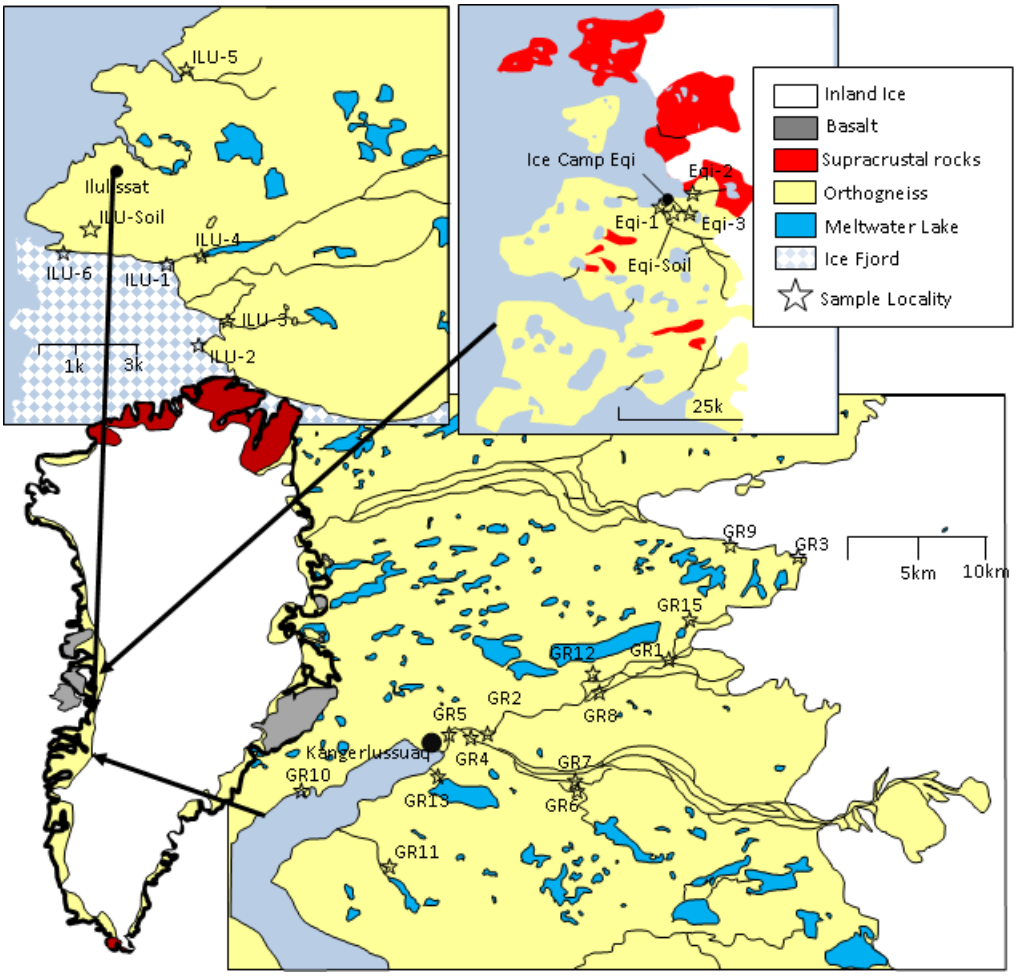

Figure 5.2. Geologic map of South-west Greenland modified from Gool and Marker (2007) including sampling localities.

5.2 Methods:

5.2.1 Field Sampling

Field sampling in the Illulissat and Eqi field areas was conducted using the same methodology Wimpenny et al., (2010) utilized for collecting samples in the Kangerlussuaq field area. Riverine samples were collected from the surface near centre of the flow in 15L pre-cleaned containers. The large water samples were quickly filtered, through 0.2µm cellulose-acetate Millipore filters, using a pressurized PFA unit. The filters were preserved and the suspended particulate matter (SPM) was later removed for analysis. Temperature, pH, alkalinity, and conductivity were measured in field at the same locations using handheld probes. Total suspended sediment (TSS) concentrations were measured by filtering 100mL of water through a preweighed 0.2µm and then drying and reweighing the filters. Where possible riverbed sediments (RBS) were taken from within the river and bedrock samples were collected from adjacent outcrops.

Glacial ice samples were collected from within the Ilulissat ice fjord by placing pieces of glacial ice into pre-cleaned plastic bags. The ice as allowed to melt for 24 hours and then the remaining ice was transferred into a second bag and fully melted. The initial melt samples were discarded reduce the potential of surface contamination during sampling. The melt water was then filtered and treated like the riverine samples. In all cases, some sediment was retained within the melt-bags after filtration, and this sediment was also recovered from the bags following filtration.

5.2.2 Elemental Analysis

Iron concentrations in the filtered water samples were measured on a Thermo-Fisher X-series inductively coupled plasma-mass spectrometry (ICP-MS) with a collision-cell to reduce oxide interferences at Durham University. The concentrations were calibrated against high purity synthetic Fe-standards which were doped with sodium (250µmol/L) and calcium (100µmol/L) to more accurately match the sample matrix. The certified reference standard SLRS-5 was used check the accuracy of the measurements and external reproducibility was better than ±5%.

Total nitrogen and carbon concentrations were measured on an Isotope Ratio Mass Spectrometer according to methods described in Hilton et al., (2010). The iron concentrations of

the suspended and riverbed samples were also measured during stable isotope analysis as described below.

5.2.3 Stable isotopic analysis:

All samples were prepared for iron stable analysis according to established methods reported in Williams et al., (2004). Suspended sediments and bed load sediments were transferred into glass vials using a teflon coated spatula and mili-Q water and dried at 60^{o}C. All samples were treated with a mixture of concentrated teflon-distilled HNO_3 and HF to ensure total sample digestion as well as complete oxidation of any organic matter. Digested samples were then taken through two treatment of HCl dissolution/evaporation prior to column chemistry. The samples were loaded onto preconditioned BioRad AGX-1 X4 and rinsed four times with 1 mL 6 N HCL before being eluted in 7mL of 2N HCL. After sample elution another 1mL of 2N HCl was added to the columns, collected and concentration checked for iron to ensure quantitative purification. Following elution the samples were dried and refluxed in a mixture of ultra-pure H_2O_2 and HNO_3 to oxidize any resin which may have leaked through the columns. Following oxidation the samples were prepared in 0.1 N HNO_3 for MC-ICPMS analysis. Total procedural blanks, processed in parallel with the samples were below the detection limit (<0.1µgFe) which is negligible relative to the quantities of processed sample iron (>200µg).

All the samples were diluted to within 10% of the sample-standard bracketing iron standard solution using the beam estimated intensity prior to analysis. All sediment analysis were carried out using sample standard bracketing against IRMM-14 at 2ppm at medium resolution on an Neptune Plus multi-collector inductively coupled plasma mass spectrometer (MC-ICPMS) with an Apex desolvator introduction system. The a number of the measurements were conducted using a Fe^{57}-Fe^{58} double spike technique described by Millet et al., (2012) and run at 3 ppm total iron (1.5ppm sample, 1.5ppm spike) with all other parameters the same as the non-spiked analysis. Each sample analysis consisted of at least 30 individual measurements and analyses were always repeated at least once within a session and during at least two different sessions. All errors are reported as 2 S.D. of the average analysis value.

Iron stable isotope compositions are primarily reported in $\delta^{56}Fe$ notation, which represents the per mil deviation of the measured $^{56}Fe/^{54}Fe$ ratios relative to that of the bracketing standard, IRMM014. In order to verify mass dependence both $\delta^{56}Fe$ and $\delta^{57}Fe$ values are reported. Iron fractionation factors are reported in Δ^{56} Fe notation, which represents the per-mil offset of two $\delta^{56}Fe$ relative to each other i.e. $\Delta^{56}\ Fe_{A-B} = \delta^{56}Fe_A - \delta^{56}Fe_B$.

The BIR-1a USGS standard and internal FeCl lab standard were analysed multiple times during every analytical session to monitor stability and external reproducibility. The long-term external reproducibility of the value for the BIR-1a standard was $\delta^{56}Fe$=0.049±0.04, $\delta^{57}Fe$=0.105±0.08 (n=30; 2σ) well within the accepted range of values for the standard ($\delta^{56}Fe$=0.053±0.015‰, $\delta^{57}Fe$=0.087±0.023, Craddock and Dauphaus 2010). The long-term reproducibility of the value for the laboratory internal FeCl standard was $\delta^{56}Fe$=-0.693±0.04, $\delta^{57}Fe$=-1.008±0.08 (n=158; 2σ) consistent with previously published values of this standard (Williams et al., 2012; Williams and Bizimis 2014).

5.1.4 Measuring Reactive Iron

Iron cycling during chemical weathering to be simplified into six equations which are listed below (see Chapter 3 of a detailed discussion of the method):

1) $Fe_i = Fe_{OOH} + Fe_{aq} + Fe_p$:The sum of the (oxyhydr)oxide iron pool (Fe_{OOH}), the aqueous iron pool (Fe_{aq}) and the primary iron pool (Fe_P) is determined by the concentration of iron initially present in the system (Fe_i).

2) $[Fe_T] = \frac{Fe_p + Fe_{OOH}}{1 - \frac{Fe_{OOH} + Fe_{aq}}{Fe_i}}$: the bulk normalized concentration of iron in a sediment sample is the ratio of the sedimentary iron pool (Fe_p+Fe_o) and the total composition of the sediment following mineral dissolution ($1 - (\frac{Fe_o + Fe_{aq}}{Fe_i})$. This assumes iron is the most immobile element during chemical weathering.

3)$[Fe_{OOH}] = [Fe_T] \times \frac{Fe_{OOH}}{Fe_{OOH} + Fe_p}$: the bulk normalized concentration of Fe_{OOH} ([Fe_{OOH}]) is the relative amount of Fe_{OOH} to total iron ($\frac{Fe_{OOH}}{Fe_{OOH} + Fe_p}$) multiplied by the total iron concentration ([Fe_T])

4) $\delta^{56}Fe_T = \left(\frac{Fe_p}{Fe_p + Fe_o}\right) * (\delta^{56}Fe_i) + \left(\frac{Fe_o}{Fe_p + Fe_o}\right) * (\delta^{56}Fe_O)$: The iron isotope composition of the residual bulk sediment pool ($\delta^{56}Fe_R$) is the mass balanced composition of primary iron pool (Fe_p, $\delta^{56}Fe_i$) and precipitated iron (oxyhydr)oxide pools (Fe_O, $\delta^{56}Fe_O$).

5) $\Delta^{56}Fe_{aq-s} = \delta Fe_{aq} - \delta Fe_s$: The iron isotope composition of the aqueous (δFe_{aq}) and solid (δFe_s) iron pools during chemical weathering differ based on one of the fractionation factors derived in the previous section ($\Delta^{56}Fe_{aq-s}$)

6) $\delta^{56}Fe_i = \left(\frac{Fe_o}{Fe_{aq}+Fe_o}\right) * (\delta^{56}Fe_o) + \left(\frac{Fe_{aq}}{Fe_{aq}+Fe_o}\right) * (\delta^{56}Fe_{aq})$: The initial amount of iron in a system (Fe_i) is dependent on the concentration of iron in the bedrock ([Fe_i])

Solving the equations requires measuring the iron isotope composition ($\delta^{56}Fe_T$) and bulk normalized iron concentration ([Fe_T]) of the target sediment samples. It is also necessary to parameterize the equations with the iron isotope composition of the pristine bedrock ($\delta^{56}Fe_i$) and the environmental specific iron cycling iron isotope fractionation factor ($\Delta^{56}Fe_{aq\text{-}s}$) to refine the estimated initial iron concentration of the sample (Fe_i). The full details of this process along with a validation test of the are provided in the Chapter 3 of this thesis which should be consulted for more information. In this study, we are assuming $\delta^{56}Fe_i$ is equivalent to the average iron isotope composition of Greenlandic TTG as reported by Dauphas et al., 2004 and Dauphas et al., 2009 ($\delta^{56}Fe_i$ =0.074‰). $\Delta^{56}Fe_{aq\text{-}s}$ is assumed to be either: -0.15‰, reflecting equilibrium iron cycling; +0.49, reflecting iron oxidation in the presence of organic matter; or-1.5‰ reflecting anoxic sediment reductions.

5.3 Results

5.3.1 Bulk Riverine Compositions

The physical and chemical properties of the water samples are reported in Table 5.1. The samples cluster into three distinct groups: glacial, iron rich non-glacial (GR11, GR12 and GR14) and iron poor non-glacial.

The glacial locations have high TSS concentrations, high pH values, and intermediate Fe_F concentrations compared to the non-glacial samples. The iron isotope composition of the Fe_F pool was analysed in two of the samples and both samples are slightly enriched in the light isotopes of iron relative to Greenlandic bedrock (data presented in the next section). Most of the non-glacial samples lower Fe_F concentrations that the glacial samples. The samples from GR11, GR12 and GR14 are however significantly enriched in Fe_F compared to all the other samples. The iron isotope composition of the Fe_F pool from GR11 was measured and is significantly enriched in the heavy isotopes of iron relative to Greenlandic bedrock.

Table 5.1. Bulk Riverine Measurements. N.D.= not determined ** The glacial fjord samples are not included in the overall glacial average.

Sample	Type	[Fe_F] umol/L	TSS mg/L	pH	Conductivity µS	Alkalinity meq/L	$\delta^{56}Fe_F$ ‰	σ	$\delta^{57}Fe_F$ ‰	σ
GR1	Glacial	0.23	435	8.48	9	0.07				
GR2	Glacial	0.12	598	7.91	14	0.10	0.063	0.04	0.075	0.04
GR3	Supraglacial	0.06	229	6.32	3	0.02				
GR4	Glacial	0.09	846	7.11	18	0.12				
GR5	Glacial	0.10	399	7.18	10	0.15				
GR7	Glacial	0.13	545	7.30	13	0.13				
GR8	Glacial	0.69	444	7.20	11	0.15	0.046	0.04	0.050	0.05
GR10	Fjord	0.43	162	6.96	2650	0.27				
GR11	Non-glacial	1.44	4	6.81	25	0.36	0.609	0.04	0.886	0.05
GR12	Non-glacial	12.70	14	8.3	198	1.74				
GR14	Non-glacial	0.25	2	8.1	120	0.56				
ILU-1	Glacial Fjord	0.03	1	6.13	2000	0.16				
ILU-2	Glacial Fjord	N.D	10	N.D.	14.6(mS)	N.D				
ILU-3	Non-glacial	0.01	1	6.73	96	0.15				
ILU-4	Non-glacial	0.01	9	6.53	24	0.08				
ILU-5	Non-glacial	0.04	4	6.13	57	0.14				
ILU-6	Glacial Fjord	N.D.	23	8.1	23.45(mS)	1.21				
EQI-1	Glacial	0.03	274	6.73	16	0.12				
EQI-2	Non-glacial	0.08	11	6.36	8	0.06				
EQI-3	Non-glacial	0.04	1	6.64	40	0.06				
Glacial Average**		0.18	506	7.42	13	0.12				
Non-glacial Average		1.82	6	6.95	71	0.39				

5.3.2 Bedrock iron composition.

The iron stable isotopic compositions and iron concentrations of bedrock samples from the Greenlandic mainland are presented in Table 5.2. The bedrock samples are within isotopic error of one another with an average value of δFe^{56}= 0.041±.08‰. This value is consistent with previously reported values of Greenlandic TTG (δFe^{56}= 0.074±.06‰, Dauphaus et al., 2004, 2009). The average total iron concentrations of our bedrock samples is also consistent with published iron concentration values of Greenlandic TTG (0.59±0.33 mol/kg; Kalsbeek and Skjernna 1998, Kalsbeek 2001)

Table 5.2 Greenlandic Bedrock Composition. *Iron isotope values reflect the average iron isotope composition of Greenlandic TTG as reported by Dauphas et al., (2004) and Dauphas et al., (2009). The iron concentration values reflect the average of measurement of Greenlandic TTG as reported by Kalsbeek and Skjernna (1998) and Kalsbeek (2001). Our average bedrock composition is within error of the published TTG values.

Rocks					
Sample	δ56Fe	σ	δ57Fe	σ	[Fe] (mol/kg)
GR1	0.091	0.09	0.136	0.13	0.83
GR2	-0.013	0.09	-0.055	0.08	0.40
GR3	0.035	0.04	0.056	0.08	1.24
GR5	0.014	0.02	0.031	0.04	1.03
GR6	0.035	0.03	0.053	0.04	0.21
GRKISS	0.081	0.06	0.106	0.12	1.53
Average	0.041	0.04	0.054	0.13	0.74
Published TTG*	0.074	0.06	0.109	0.08	0.59

5.3.3 Riverbed sediment (RBS) iron compositions

The iron stable isotope compositions and iron concentrations of RBS are reported in Table 5.3. Most of the samples have isotope compositions within the compositional range of bedrock samples, but a few samples are significantly enriched in the heavy isotope of iron. The isotopically heavy samples reflect a combination of glacial and non-glacial locations.

Table 5.3. River Bedload Sediment Compositions. *These samples were with measured utilizing a $Fe^{57/58}$ double spike and the reported $\delta^{57/54}Fe$ values are spike-corrected rather than raw values. A) The reported standard deviations are the 2 σ values of the measurements.

River Bedload Sediments						
Sample	Catchment Type	δ56Fe	σ	δ57Fe	σ	[Fe] (mol/kg)
GR1	Glacial	0.070	0.04	0.120	0.12	0.57
GR2	Glacial	0.051	0.03	0.069*	0.04	0.48
GR3	Glacial	0.060	0.07	0.077	0.10	0.77
GR4	Glacial	0.185	0.07	0.220	0.09	1.27
GR5	Glacial	0.064	0.05	0.130	0.15	0.69
GR7	Glacial	0.064	0.04	0.091	0.06	0.56
GR8	Glacial	0.069	0.04	0.121	0.05	0.39
GR9	Glacial	0.118	0.02	0.170	0.06	0.88
GR10	Fjord	0.090	0.04	0.097	0.15	0.65
GR11	Nonglacial	0.092	0.03	0.204	0.04	0.49
GR12	Nonglacial	0.054	0.03	0.135	0.10	0.97
GR13	Nonglacial	0.065	0.02	0.190	0.05	0.45
GR14	Nonglacial	0.081	0.04	0.135	0.07	0.60
GR15	Nonglacial	0.053	0.05	0.151	0.05	0.59
ILU-3 BL	Nonglacial	0.523	0.05	0.723*	0.06	0.14
ILU-4 BL	Nonglacial	0.326	0.06	0.441*	0.07	0.53
ILU-5 BL	Nonglacial	0.088	0.04	0.093*	0.04	0.41
EQI-1 BL	Glacial	0.361	0.06	0.523*	0.08	0.23

5.3.4 Suspended Particulate Material (SPM)

The iron stable isotope compositions and iron concentrations of the SPM samples are reported in Table 5.4 alongside the total carbon and total nitrogen concentrations. The nitrogen concentrations generally scale with the carbon concentrations consistent with an organic source for both elements. None of the measured glacial samples contain more than 1 wt. % total carbon while a single non-glacial sample contains at least 3 wt. % C. The highest total carbon sample also has the highest total iron concentration.

All the glacial SPM samples have iron isotope compositions $\delta^{56}Fe \geq 0.0‰$ with the most fractionated samples approaching an iron isotope composition of $\delta^{56}Fe = 0.20‰$. Three of the non-glacial samples have compositions around $\delta^{56}Fe = -0.30‰$. These highly negative samples are from locations with among the highest Fe_{SPM} concentrations of the samples.

Table 5.4. River Suspended Sediment Compositions. *These samples were with measured utilizing a $Fe^{57/58}$ double spike so the reported $\delta^{57/54}Fe$ values represent spike corrected rather than raw values. **The Glacial Averages reflect only river samples i.e. they exclude the ice and fjord samples.

Sample	Type	$[Fe_{SPM}]$ mol/kg	$\delta^{56}Fe_{SPM}$ ‰	σ ‰	$\delta^{57}Fe_{SPM}$	σ	TC_{SPM} wt %	TN_{SPM} wt%
GR2	Glacial	0.77	0.134	0.03	0.146	0.03	0.12	0.01
GR3	Supraglacial	0.80	0.154	0.06	0.227	0.12	0.61	0.04
GR4	Glacial	1.24	-0.043	0.05	0.037	0.07	0.20	0.01
GR5	Glacial	0.72	0.203	0.03	0.267	0.08	0.21	0.01
GR7	Glacial	0.91	0.058	0.04	0.107	0.08	0.21	0.02
GR8	Glacial	0.82	0.075	0.03	0.239	0.10	0.21	0.02
GR9	Glacial	1.16	0.033	0.05	0.080	0.04	0.54	0.05
GR10	Fjord	0.74	0.122	0.01	0.149	0.02	0.23	0.02
GR11	Non-glacial	1.29	-0.377	0.04	-0.605*	0.03		
GR12	Non-glacial	2.11	-0.378	0.01	-0.594	0.02	>3	0.60
ILU-1	Glacial Fjord	0.60	0.076	0.04	0.082*	0.05		
ILU-1 ice	Ice	0.78	0.164	0.04	0.197*	0.05		
ILU-2	Glacial Fjord	0.48	0.056	0.04	0.131	0.03		
ILU-3	Non-glacial	0.39	0.151	0.04	0.179*	0.04		
ILU-4	Non-glacial	0.79	0.189	0.05	0.248*	0.06		
ILU-5	Non-glacial	1.47	-0.273	0.04	-0.445*	0.06		
EQI-1	Glacial	0.55	0.122	0.04	0.146*	0.05		
EQI-2	Non-glacial	1.25	0.063	0.04	0.062*	0.04		
EQI-3	Non-glacial	0.53	0.078	0.03	0.083*	0.03		

5.4. Discussion

5.4.1 Iron Cycling in the Rivers

Figure 5.3 shows the iron isotope compositions of the Fe_F and SPM pools of the glacial and non-glacial sample locations relative to the TSS concentrations in the same samples. The three groups identified on the basis of bulk riverine chemistry in Section 5.3.1 correspond to different patterns in river iron cycling.

The iron stable isotope composition of glacial Fe_F is heavier than TTG but lighter than the co-occuring SPM samples by on average -0.07‰. This pattern is consistent with iron oxidation in the absence of organic matter (Skulkan et al., 2002, Wu et al., 2011). The isotope compositions of the SPM pools from the iron poor non-glacial rivers are also consistent with

inorganic iron cycling. The isotope composition of the Fe_F pools in the iron poor non-glacial samples were not measured due to the low absolute iron concentrations in the samples. As organic matter is expected to be positively correlated with Fe_F in Greenlandic samples e.g. Bhatia et al., (2013), the fact that these samples are iron poor also supports the assumption the systems are characterized by equilibrium iron cycling.

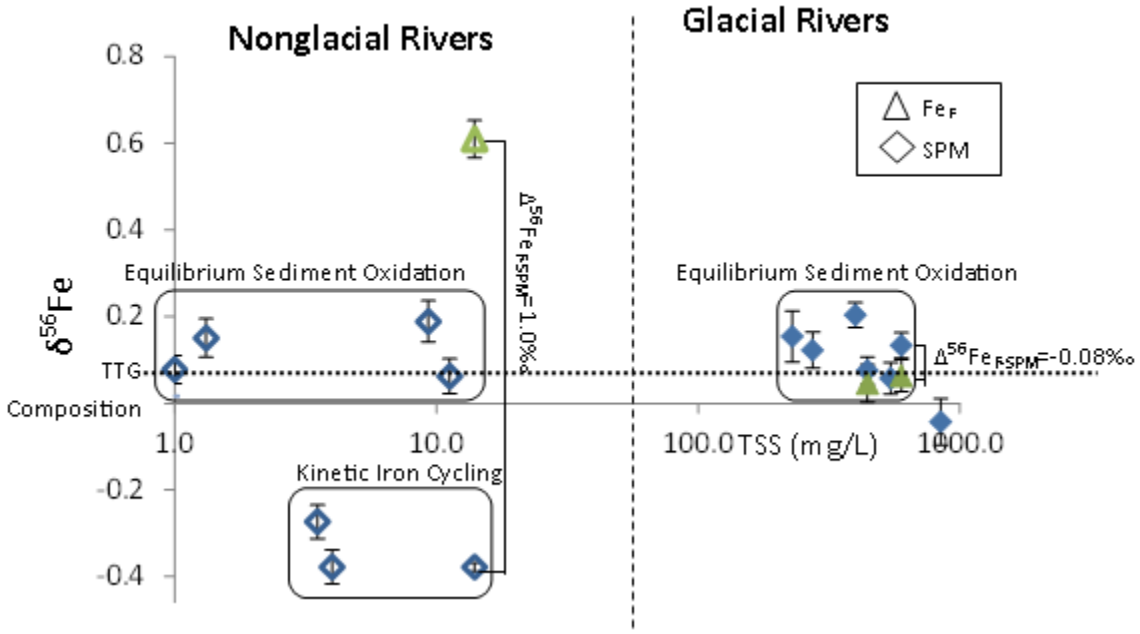

Figure 5.3 Sample Iron Stable isotope fractionations. The offset in the iron stable isotope composition of the Fe_F pools (shown as green triangles) and SPM pools (shown as blue diamonds) reflects $Fe_{aq\text{-}s}$ partitioning in the environments. The low absolute offset in the glacial samples is consistent with equilibrium Fe^{3+} cycling while the larger offset in the non-glacial sample could reflect with kinetic Fe^{3+} cycling or cycling between organic and inorganic iron species.

The iron isotope compositions of the Fe_F and SPM pools in the iron rich non-glacial samples are significantly fractionated relative to the glacial and iron poor non-glacial samples. The isotopic offset between the Fe_F and SPM pools in the iron rich samples is on the order of $\Delta^{56}Fe_{F\text{-}SPM}$= 1.00. This level of isotope fraction is consistent with iron cycling in mixed redox systems. More specifically, the fractionation factor is consistent with rapid kinetic oxidation of iron (Skulkan et al., 2002). In real-world environment, this type of kinetic oxidation is most frequently associated with organic rich stratified systems where anoxic sediment reduction provides a continuous source of iron to overlaying oxic water i.e. Canfield et al., (1993) Reidel et al., (2013). The anoxic portion of mixed-redox systems is expected to be characterized by a pattern of iron isotope fractionation around $\Delta^{56}Fe_{aq\text{-}S} \approx$ -1.50‰ (Croal et al., 2004, Wiederhold et

al., 2006, Beard et al., 2010, Frierdich et al., 2014). [See Chapter 3 for a detailed analysis of the relationship between iron isotope fractionation and environmental conditions]. The isotopically light aqueous iron then precipitates in the overlaying oxygenated waters leading to the formation of isotopically light suspended material. The same redox fractionation process leads to the formation of bedload sediments in anoxic systems which are significantly enriched in the heavy isotopes relative to the initial bedrock composition. Two of the non-glacial locations (ILU-3 and ILU-4) contained RBS with very heavy isotope compositions.

All of the significantly fractionated samples were collected either from pro-glacial lakes or small streams which drain the lakes. The lakes themselves are are known to be highly stratified, poorly ventilated and organic rich environments (e.g. Anderson et al., 1998, Palmtag 2015) providing a clear link between the proposed iron cycling patterns and physical descriptions of the environments. The difference in residence times between Fe_F, RBS and SPM with-in the lake systems is the most likely explanation for why mixed redox weathering does not necessarily appear in both the RBS and SPM samples from several the location. The SPM and Fe_F pools reflects the active iron cycling conditions occurring at any given location. The RBS pool preserves a longer-term record of chemical weathering which isn't rapidly altered as the sediment moves through the system.

5.4.3 Fe_{OOH} export Rates.

In addition to providing information on general iron cycling dynamics during chemical weathering, iron isotopes can be used to approximate sediment Fe_{OOH} concentrations. The estimated Fe_{OOH} concentrations of the SPM pools, based on their iron isotope composition and total iron concentration, are reported on Table 5.5. On average, non-glacial SPM is preferentially enriched in Fe_{OOH} relative to glacial SPM. This offset is entirely due to three non-glacial samples (GR11, GR12 and ILU-5) having substantially higher Fe_{OOH} concentrations than the rest of the samples. GR11 and GR12 also have very high Fe_F concentrations indicating the presence of high concentrations of organic matter in the samples, which is further supported by the high total carbon concentration measured in GR12.

Table 5.5. Fe_{OOH} concentration and export rates from glacial and non-glacial samples

Sample		[Fe_F] µmol/L	Particulate Fe_{OOH} mol/kg	TSS mg/L	Fe_{OOH} Flux µmol/L
GR2	Glacial	0.12	0.37	598	220.6
GR3	Supraglacial	0.06	0.50	229	114.0
GR4	Glacial	0.09	0.34	846	286.8
GR5	Glacial	0.10	0.52	399	206.4
GR7	Glacial	0.13	0.11	545	59.8
GR8	Glacial	0.69	0.02	444	9.5
EQI-1	Glacial	0.03	0.25	274	161.4
Glacial Average		0.17	0.30	476	151.2
GR11	Non-glacial	1.44	1.19	4	2.4
GR12	Non-glacial	12.70	1.91	14	29.4
ILU-4	Non-glacial	0.01	0.59	9	0.8
ILU-5	Non-glacial	0.04	1.17	4	0.7
EQI-2	Non-glacial	0.08	0.15	11	13.2
EQI-3	Non-glacial	0.04	0.03	1	0.3
ILU-3	Non-glacial	0.01	0.19	1	0.6
Non-glacial Average		2.05	0.75	6	6.8

Iron does not mix conservatively within the low salinity zone resulting in the near quantitative deposition of iron within coastal waters (Sholkovitz and Coopland 1981; Berquist and Boyle 2009). The sum of Fe_F and particulate Fe_{OOH} concentrations therefore provides a first order estimate of flux normalized Fe_{OOH} export rates from river systems. Table 5.5 contains such flux normalized Fe_{OOH} export rates for the glacial and non-glacial catchments in Greenland. On average glacial rivers export around 150 µmol Fe_{OOH} /L while non-glacial rivers export less than 10µmol Fe_{OOH}/L.

Our flux estimates are of the same magnitude as those published by Bhatia et al., (2013), the only other study which has published Fe_{OOH} discharge estimates from Greenland. Bhatia et al., (2013) sampled a catchment region about halfway between our Kangerlussuaq and Illussat field areas and measured filterable iron (<0.2 µm) as well as the extractable iron concentrations of sediments >0.7µm. The study found glacial rivers contained 40-320 µmol Fe_{OOH}/L. The same study also measured one location consistent with how we have described non-glacial weathering i.e. drainage from a proglacial lake and found it contained 278 µmol Fe_{OOH}/L. Due to the methodology used by Bhatia et al., (2013) it unclear if this high Fe_{OOH} concentration reflects high TSS concentrations or very high Fe_{OOH} concentrations within the

SPM pool. In either case, we cannot exclude the potential that some non-glacial systems export nearly as much Fe_{OOH} as glacial samples on a discharge normalized basis. Overall, we still expect glacial weathering to result in enhanced Fe_{OOH} export relative to non-glacial weathering across Greenland.

5.5. Summary and Conclusion

The iron stable isotope ratios of alluvial sediments indicate iron-cycling in non-glacial regions of Greenland can differ substantially from the iron-cycling pattern affiliated with glacial weathering. Specially, iron cycling during chemical weathering within proglacial redox stratified and organic rich lakes differs significantly from iron cycling during (sub)glacial weathering.

In the context of Fe_{OOH} discharge to the ocean the physical difference in sediment erosion between glacial and non-glacial catchments dominates the chemical differences between the environments. Glacial weathering enhances Fe_{OOH} discharge to nearshore marine environments, because glacial weathering promotes total sediment discharge to nearshore marine environments. This supports the hypothesis that glacial weathering enhances marine organic carbon burial which will act as a positive climate feedback mechanism.

5.6 References

Anderson N.J., Bennike O., Christoffersen K., Jeppesen E., Markager S., Miller G., Renber I. (1998) Limnolocal and palaeolimnological studies of lakes in south-western Greenland. *Geology of Greenland Survey Bulletin* **183**.

Bales R.C., Guo Q., Shen D., McConnell J.R. Du G., Burhhart J.F., Spikes V.B., Hanna E., Cappelen J. (2009) Annual accumulation for Greenland updated using ice core data developed during 2000-2006 and analysis of daily coastal meterological data. *Journ. Geophys Res*. **114**. D06116

Beard B.L., Handler R.M., Scherer M.M., Wu L., Czaja A.D., Heimann A., Johnson C.M. (2010) Iron isotope fractionation between aqueous ferrous iron and goethite. *Ear Plan Sci Lett*. **295**: 241-250.

Berner R.A. (1970) Sedimentary Pyrite Formation. *American Journal of Science* **268**: 1-23.

Bergquist B.A. and Boyle E.A. (2006) Iron isotopes in the Amazon River system: weathering and transport signatures. Ear Plan Sci Lett **248**: 54-68.

Bhatia M.P., Kujawinski E.B., Das S.B., Breier C.F., Henderson P.B., Charette M.A. (2013) Greenland meltwater as a significant and potentially bioavailable source of iron to the ocean. *Nat. Geosci*. **6**: 271-278.

Blair N.E. and Aller R.C. (2013) The fate of terrestrial organic carbon in the marine environment. *Annu. Rev. Marine Sci*. **4**: 401-423.

Burdige D.J. (2007) Preservation of organic matter in marine sediments: controls, mechanisms, and an imbalance in sediment organic carbon budgets? *Chem. Rev.* **107**: 467-485.

Canfield D.E., Thamdrup B, Hansem J.W. (1993) The anaerobic degradation of organic matter in Danish coastal sediments: Iron reduction, manganese reduction and sulfate reduction. *Gechem Cosmochem Act*, **57**:3867-3883.

Canfield D.E. (1994) Factors influencing organic carbon preservation in marine sediments. Chem. Geo. **114**: 315-329.

Craddock P.R. and Dauphas N. (2010) Iron isotopic composition of geological reference materials and chondrites. *Geostand. Geoanaly. Res*. **35**(1):101-123.

Croal L.R., Johnson C.M., Beard B.L., Kewman D.K. (2004) Iron isotope fractionation by Fe(II)-oxidizing photoautotrophic bacteria. Geoch. Cosmo. Act. 68(6):1227-1242.

Dauphas N., van Zuilen M., Wadhwa M., Davis A.M., Marty B., Janney P.E. (2004) Clues from Fe Isotope Variations on the Origin of Early Archean BIFs from Greenland. *Science* **306**: 2077-2080.

Dauphas N., Craddock P.R., Asimow P.D., Bennett V.C., Nutman A.P., Ohnestetter D. (2009). Iron isotopes may reveal redox conditions of mantle melting from Archean to Present. *Earth Plant. Sci. Lett.* **288**:255-267.

Frierdich A.J., Beard B.L., Scherer M.M., Johnson C.M. (2014) Determination of the Fe(II)aq-mangnetite equilibrium iron isotope fractionation factor using the three-isotope method and multi-direction approach to equilibrium. *Earth and Planetary Science Letters* **391**:77-86

Gool J.A.M. and Marker M. (2007) Explanatory notes to the Geological map of Greenland, 1:100000, Ussuit 67 V.2 Nord. *Geolgical Survey of Denmark and Greenland*. ISSN 1604-9780

Hilton R.G., Galy A, Hovius N, Horng M-J, Chen H. (2010) The isotopic composition of particulate organic carbon in mountain rivers of Taiwan. *Geochem Cosmochem Act*, **74**: 3164-3181.

Hedges J.I. and Keil R.G. (1995) Sedimentary organic matter preservation: an assessment and speculative synthesis. Mar. Chem. **49**: 81-115.

Johnson K.S., Gordon R.M., Coale K.H. (1997) What controls dissolve iron concentrations in the world ocean*? Mar. Chem*. **57**: 137-161.

Jorgensen A.S. and Andreasen F. (2007). Aping permafrost surface using ground-penetrating radar at Kangerlussuaq Airport, western Greenland. *Cold Regions Science and Technology.* **48**: 64-72

Kaiser K. and Guggenberget G. (2000) The role of DOM sorption to mineral surfaces in the preservation of organic matter in soils. *Organic Geochem.* **31**:711-725

Kalsbeek F. (2001) Geochemical comparison between Archean and Proterozoic orthogneisses from the Nagssugtoqidian orogeny, West Greenland. *Precambrian Research.* **105**:165-181.

Kalsbeek F., Skjernaa L. (1999) The Archean Ata intrusive complex (Ata tonalite), north-east Disko Bugt, West Greenland. *Geology of Greenland Survey Bulletin.* **181:** 103-112.

Keil R.G., Montlucon D.B., Prahl F.G., Hedges J.I. (1994) Sorptive preservation of labile organic matter in marine sediments*. Nature*. **370**: 549-552.

Kiem R., Kognel-Knbaner I. (2002) Refractory organic carbon in particle-size fractions of arable soils II: organic carbon in relation to mineral surface area and iron oxides fractions <6 µm. Organic Geochem. 33: 1699-1713.

Kögel-Knabner I., Guggenberger G, Kleber M., Kandeler E., Kalbitz K, Scheu S., Eusterhues K, Leinweber P. (2008) Organo-mineral associations in temperate soils: integrating biology, mineralogy and organic matter chemistry. *J. Plant Nutr. Soil Sci*. **171**: 61-82.

Lalonde K., Mucci A., Ouellet A., Gelinas Y. (2012) Preservation of organic matter in sediments promoted by iron. *Nature.* **483**: 198-200.

Liu X. and Millero F.J. (1999). The solubility of iron hydroxide in sodium chloride solutions. *Geochim Cosmochem. Act.* **63** (19/30):3487-3497.

Lutzow M., Kogel-Knabner I., Ludwig B., Matzner E., Flessa H., Ekschmitt K., Guggenberger G., Marschner B., Kalbitz K. (2008) Stabilization mechanisms of organic matter in four temperate soils: development and application of a conceptual model. *J. Plant Nutr. Soil Sci*. **171**: 111-124.

Lyven B., Hassellov M., Turner D.R., Halraldsson C., Andersson K. (2003) Competition between iron- and carbon-based colloidal carriers for trace metals in a freshwater assessed using flow filed-flow fractionation coupled to ICPMS. *Geochem Cosmo Act*. **67**(20):3791-3802.

Martin J.H. (1990) Glacial-interglacial CO2 change: the iron hypothesis. *Paleoceanogr.* **5**(1):1-13.

Mayer L.M. (1994) Surface area control of organic carbon accumulation in continental shelf sediements. *Geoch. Cosmoch. Act.* **58**(4):1271-1284.

McMillan M., Nienow P., Shepard A., Benham T., Sole A. (2007). Seasonal evolution of supra-glacial lakes on the Greenland Ice Sheet. *Earth Planet Sci Lett.* **262**:484-492.

Millero, FJ. (1998). Solubility of Fe(III) in seawater. *Earth Planet Sci Lett*. **154**: 323-329

Millet M-A. Baker J.A., Payne C.E. (2012) Ultra-precise stable Fe isotope measurments by high resolution multiple-collector inductively couple plasma mass spectrometry with a 57Fe-58Fe double spike. *Chem. Geol*. **304-305**:18-25.

Mikutta R., Kleber M., Torn M.S., Jahn R. (2006) Stabilization of soil organic matter: association with minerals or chemical recalcitrance? *Biogeochem*. **77**: 25-56.

Nesbitt H.W. and Wilson R.E. (1992) Recent chemical weathering of basalts. *Amer. Journ. Sci*. **292**: 740-777.

Palmtag J., Hugelius G., Lashchinskiy N., Tamstorf M.P., Richter A. Elberling B., Kuhry P. (2015). Storage, landscape distribution, and burial history of soil organic matter in constrasting areas of continuous permafrost. *Arctic, Antarctic, and Alpine Research.* **47**(1): 71-88.

Poulton S.W. and Raiswell R. (2005) Chemical and physical characteristics of iron oxides in riverine and glacial meltwater sediments. *Chem Geo.* **218**:203-221.

Raiswell R. and Canfield D.E. (2012) The iron biogeochemical cycle past and present. Geochemical Perspectives, European Association of Geochemistry, 1(1)

Riedel T., Zak D., Beister H., Dittmar T. (2013). Iron traps terrestrially derived dissolved organic matter at redox interfaces. *PNAS* **110**(25):10101-10105.

Sabadini-Santos E., Senez T.M., Silve, T.S., Moreira M.R., Mendoca-Filho J.G., Santelli R.E. Crapez M.A.C. (2014) Organic matter and pyritization relationship in recent sediments from a tropical and eutrophic bay. *Marine Pollution Bullet*. **89**: 220-228.

Schrumpf M., Kaiser K., Guggenberger G., Persson T., Kogel-Knabner I., Schulze E.-D. (2013) Storage and stability of organic carbon in soils as related to depth, occlusion within aggregates and attachment to minerals. *Biogeosci*. **10**: 1675-1691.

Sholkovitz E.R. and Copland D. (1981) The coagulation, solubility and adsorption properties of Fe, Mn, Cu, Ni, Cd, Co and humic acids in a river water. *Geochem Cosmochem Act*. **45**: 181-189.

Song Y., Li L., Zheng J., Pan G., Zhang X., heng J., Hussain Q., Han X., Yu X. (2012) Sequestration of maize crop straw C in different soils: Role of oxyhydrates in chemical binding and stabilization as recalcitrance. *Chemosphere*. **87** (6):649-654.

Skulkan J.L., Beard B.L., Johnson C.M. (2002). Kinetic and equilibrium Fe isotope fractionantion between aqueous Fe(III) and hematite. Geoch. Cosmo. Act. 66(17): 2995-3015.

Sheng, Y., Sun Q., Shi W., Bottrell S., Mortimer R. (2015). Geochemistry of reduced inorganic sulfur, reactive iron, and orgnanic carbon in fluvial and marine surface sediment in the Laizhou Bay region, China. *Environ. Earth Sci*. **74**: 1151-1160.

Stefansson A., Gislason S.R., Arnorsson S. (2001) Dissolution of primary minerals in natural waters II. mineral saturation state. *Chem. Geol*. 172: 251-276.

Syvitski J.P.M., Milliman J.D. (2007). Geology, geography and humans battle for dominance over the delivery of fluvial sediment to the coastal ocean. *Geology* **115**: 1-19.

Thompson A., Rancourt D.G., Chadwick O.A., Chorver J. (2011) Iron soild-phase differentiatone along a redox gradient in basaltic soils. *Geochem Cosmochem. Act.* **75**: 119-133.

Wiederhold J.G., Kraemer S.M., Teutsch N., Borer P.M., Halliday A.N., Kretzschmar R. (2006). Iron isotope fractionation during proton-promoted, ligand-controled, and reductive dissolution of Geothite. *Environ. Sci. Technol*. **40**: 3787-3793.

Williams H.M., McCammon C.A., Peslier A.H., Halliday A.N., Teutsch N., Leevasseur S., Burh J-P. (2004) Iron Isotope Fractionation and the Oxygen Fugacity of the Mantle. *Science*. **304**: 1656-1659.

Williams H.M, Wood, B.J., Wade J., Frost D.J., Tuff J. (2012) Isotopic evidence for internal oxidation of the Earth's mantle during accretion. *Earth Planet. Sci. Lett.* **321-322**:54-63.

Williams H.M. and Bizimis M. (2014). Iron isotope tracing of mantle heterogeneity with the source regions of oceanic basalts. *Earth Plant. Sci*. **404**: 396-407

Wimpenny J., James R.H., Burton K.W., Gannoun A., Mokadem F., Gislason S.R. (2010) Glacial effects on weathering processes: new insights from the elemental and lithium isotopic composition of West Greenland rivers. *Ear. Plan. Sci. Lett.* **290**: 427-437.

Wu L., Beard B.L., Roden E.E., Johnson C.M. (2011) Stable iron isotope fractionation between aqueous Fe(II) and hydrous ferric oxide. *Environmental Science and Technology*. **45**: 1847-1852

Xu-hui Z., Lian-qing L., Gen-xing P. (2007) Topsoil organic carbon mineralization and CO2 evolution of three paddy soils from South China and the temperature dependence. *Journ. Environ. Sciences.* **19**: 319-326.

Chapter 6
Translating Riverine Fluxes to Organic Carbon Burial

Abstract

Discussion in the preceding chapters has been limited to comparing the relative differences in continental weathering between glacial and non-glacial systems. The extent to which these relative differences reflect a geologically significant climate driver depends on the absolute magnitude of the feedback between continental weathering and carbon burial. This final chapter comprises a simple thought experiment: based on the data presented in the preceding chapters: How did the collapse of the Laurentide Ice Sheet alter carbon burial over the last 21000 years? The thought experiment provides a valuable means of considering the potential magnitude of the feedback between weathering and climate over glacial-interglacial cycles using a realistic set of parameters.

6.1 The Laurentide Ice Sheet.

The Laurentide Ice Sheet provides a reliable starting point for conducting a thought experiment which helps place the carbon burial changes highlighted in the previous chapters into a wider geologic context. During the Last Glacial Maximum (LGM) the Laurentide Ice Sheet covered all of Canada (~10 million km^2) (Dyke et al., 2002). A few glaciers still exist in Canada but their overall land surface coverage is minimal i.e. 10 million km^2 of land in Canada has switched from glacial to non-glacial weathering since the LGM. Canada is specifically relevant to the work in this thesis because much of the country is dominated by Precambrian bedrock known as the Canadian shield. Rocks in the Canadian shield are broadly equivalent to Greenlandic TTG providing a basis for using the weathering trends we measured in Greenland to think about the larger scale changes which have occurred in Canada since the LGM.

6.2 Sediment and Fe_{OOH} export from Greenland.

Net precipitation accumulation rates (precipitation-evapotranspiration) allow the conversion of river sediment concentration data to total sediment export rates. In terrains, such as Greenland where groundwater formation is extremely restricted (Jorgensen and Andreasen 2007)) net precipitation accumulation can be assumed to equal to net hydrologic flux. Bales et al., (2009) produced a net precipitation accumulation map of Greenland, and integrating the map results in a total precipitation accumulation estimate of 1.045×10^{15} L yr^{-1} for Greenland.

In the previous chapter the total sediment concentration of glacial discharge from Greenland was estimated to contain 506 mg sediment L^{-1} and 151 µmol Fe_{OOH} L^{-1}. These values equate to total yearly discharge rates of 528 Tg sed. yr^{-1} and 8.8 Tg of Fe_{OOH} yr^{-1} assuming 100% of the discharge from Greenland is associate with glacial rivers. Greenland has a total land surface area of 2.1 million km^2 (Cappelen and Vinther 2013) equating to area normalized sediment discharge rates of $2.4x10^8$ g sed km^{-2} yr^{-1} and 7.3×10^4 mol Fe_{OOH} km^{-2} yr^{-1}. If, as a result of climate change, 100% of the discharge was associated with non-glacial rivers the export rates would drop to $2.9x10^6$ g sed km^{-2} yr^{-1} and $3.3x10^3$ mol Fe_{OOH} km^{-2} yr^{-1}.

The preceding values for glacial systems assume sediment export occurs in affiliation with meltwater rivers. Glacial systems can also directly discharge ice into the ocean, and there is a significant difference between sediment discharge associated with ice-rafting and melt-water rivers. In the preceding chapters the Fe_{OOH} concentrations of sediment entrained in glacial ice from Iceland and Greenland were found to be in the same range as glacial sediment from melt-water rivers. We did not measure the ice meltwater volumes, but based on field observations the total sediment concentrations of ice appear significantly lower than the sediment concentrations of glacial rivers. This is consistent with Raiswell et al., (2006)'s estimate that on average glacial ice contains 0.5 kg sed m^{-3} or 0.5 mg sed L^{-1} or $1/1000^{th}$ of what we measured in glacial rivers, and equates to export rates around $2.4x10^5$ g sed km^{-2} yr^{-1} and $1.2x10^2$ mol Fe_{OOH} km^{-2} yr^{-1}.

The sediment and Fe_{OOH} flux rates in the proceeding paragraphs have been normalized on a km^2 basis for a specific reason. Spatially scaling down sediment discharge changes to the km^2 level allows the continental weathering changes to be compared without the need to account for the complex relationship between climate change and hydrologic discharge. This is encapsulated by the fact that over the last 100 years coastal regions of both Iceland and Greenland have transitioned from experiencing ice-calving to being ice-free/non-glacial terrains while local precipitation rates have remained relatively constant. (Hanna et al., 2004; Cappelen and Vinther 2013).

Over longer term periods net precipitation accumulation is expected to change as a function of climate change such that peak glacial hydrologic discharge is not expected to equal peak inter-glacial hydrologic discharge. Over the last 150 years Greenland has become both warmer and wetter on average, even while many areas in South-west Greenland have not become wetter in response to global climate change (Cappelen and Vinther 2013). More rainfall means higher riverine discharge rates such that total riverine discharge associated with annual precipitation is expected to increase as atmospheric CO_2 concentrations increases. The warmer

temperatures have also increased glacial retreat providing an additional source of hydrologic run-off from the ice sheet (Rignot et al., 2009). In all likelihood peak run-off rates from Greenland occur in the middle of a glacial-interglacial transition when glacial melting and precipitation rates are both high. Similarly, the lowest run-off rates are likely to occur during the onset of a glacial cycle as precipitation rates fall and precipitation is increasingly bound in terrestrial ice. However, limited data is available to quantify the magnitude of these patterns preventing their explicit incorporation into our sediment discharge estimates. As a result, our sediment discharge estimates become more speculative as they are scaled-up to longer glacial-interglacial timescales.

6.3 Marine sediment and OM accumulation

The global rate of marine organic carbon (OC) accumulation is estimated to be 309 Tg of organic carbon yr^{-1} (Burdige 2007). The global rate of marine sediment accumulation due to continental weathering is estimated at 126100 Tg sed yr^{-1} Syvitski et al., (2005). This equates to an OC accumulation rate=0.24% the total sediment accumulation rate. A complete different global data set, shown previously in Chapter 4 Figure 4.1, displays almost the same relationship between total sediment and OC accumulation (OM=0.23% total sediment).

Utilizing the Greenlandic sediment discharge rates derived in the previous section, carbon burial is therefore expected to decrease along the trend glacial rivers>>non-glacial rivers>>ice rafting on the order of 4.8 $x10^5$ g C km^{-2} yr^{-1}>> 5.8 x 10^3 g C km^{-2} yr^{-1}>> 4.8 $x10^2$ g C km^{-2} yr^{-1}.

Deriving the carbon burial rates from $Fe_{OOH,}$ rather than total sediment accumulation, results in a similar set of values. The molar ratio of Fe_{OOH} to OC in oxygenated marine sediments and mature soils is about 1:2 (See Chapter 5, Figure 5.1). Therefore, carbon burial in nearshore marine environments is predicted to decrease along the trends: 1.7$x10^6$ g C km^{-2} yr^{-1} for glacial rivers>> 8.0$x10^4$ g C km^{-2} yr^{-1} for non-glacial rivers>> 2.9$x10^3$ g C km^{-2} yr^{-1} for ice-rafted debris.

The offset between the iron based estimates and the total sediment based estimates most likely reflects the impact of sampling biases on the two data sets. The iron data all stems from nearshore environments while the total sediment data set contains a substantial number of open marine sample. Nearshore environments are known to accumulate OC at higher rates than open marine environments (Burdige 2007) which biases the iron based estimates towards higher values.

6.4 Changes in Carbon burial over glacial-interglacial cycles

The final step in the thought experiment is to integrate the carbon burial changes calculated in the previous sections across last glacial-interglacial transition for the Laurentide Ice Sheet. It is first useful to consider the steady state-end member systems. When the Laurentide ice sheet was at its peak, exporting sediment mainly via ice rafting, the associated carbon burial rates would be expected to be on the order of <0.05 Tg C yr^{-1}. Once the ice sheet retreated such that there was no longer directly calving this carbon burial rate would have shot up to around 4.8 Tg C yr^{-1}. Current, near ice-free conditions, are predicted to be associated with the burial of around 1 Tg C yr^{-1}. This means carbon burial would have been very low when the Laurentide Ice Sheet began to collapse due to the dominance of ice calving. As soon as the ice sheet transitioned onto the land carbon burial would have rapidly increased. Continued melting and the increase of ice-free conditions would have then caused a reduction in carbon burial. The overall picture is of non-linear response between climate change and carbon burial where the endmembers of the system vary by ~5 TG C yr^{-1}. If these estimates are of the correct order of magnitude they reflect a geologically significant climate feedback mechanism.

The most recent IPCC climate summary report, Ciasis et al., (2013), concluded that the 'Iron Hypothesis' has led to a net source of 10.5 Pg C over the last 21,000 years. This accounts for more than half of the total carbon impact estimated by the IPCC for all geologic processes since the LGM. Our estimates suggest the effects of the Iron Hypothesis could have been totally offset by the increase in carbon burial associated with the transition of ice-rafting to riverine melt-water discharge. It is also worth noting that carbon burial changes on this magnitude are significantly less than the uncertainty associated with the current best estimate of the modern marine carbon burial rate (Burdige 2007). If we can't measure carbon burial to this level of accuracy today detecting such changes in the sedimentary record will be all but impossible. In other words, climate feedbacks on this scale are difficult to isolate within the geologic record even when the cumulative impact of climate change is readily measured.

Comparing our carbon burial estimates to the Iron Hypothesis is also instructive when considering the speculative nature of our estimates. John Martin (1990) was the first to propose the link between continental weathering and primary production, and it was the speculative nature of the original proposal that forced the 'hypothesis' designation of the Iron Hypothesis. Martin's original idea held a lot of merit, but was based on extremely broad extrapolations and an equally limited amount of data. Martin (1990) did not have iron measurement from the

Southern Ocean and freely admits in the study to having no direct evidence that iron limited primary productivity in the Southern Ocean. Additionally, Martin (1990) makes a ballpark guess that iron deposition in the Southern Ocean was 50 times higher during the LGM than today and that carbon burial scales directly with this changes in iron inputs. Neither of these guesses are supported by any measurements. Given the lack of concrete evidence it is unsurprising that a number of Martin (1990)'s claims were immediately refuted due to significant evidence that the claims were highly improbable e.g. Peng and Broecker (1991). It is also now well understood that some of the original numbers used in the hypothesis were not very accurate e.g. iron deposition in the Southern Ocean was about only twice the modern rate during the LGM not 50 times higher (Martinez-Garcia et al., 2014). However, after several decades of intense investigation the scientific consensus is that despite limited data Martin (1990) correctly identified a global pattern (e.g. Coale et., 2004, Martinez-Garcia et al., 2014) which has subsequently helped re-defined the relationship between biotic and abiotic Earth System processes.

Throughout this thesis there has been an attempt to repeatedly identify patterns in climate change and continental weathering, continental weathering and sediment accumulation, sediment accumulation and organic carbon accumulation, and organic carbon burial and climate change. Definitively linking all these patterns in a robust scientific theory represents a monumental task and one which is beyond the scope of data presented in this thesis. But every theory must start with a hypothesis. Our elemental and isotopic data is consistent with glacial weathering enhancing total sediment and Fe_{OOH} accumulation rates in nearshore marine environments. The data is supported by a wealth of published information linking climate change to glacial-interglacial cycles, sediment and/or Fe_{OOH} accumulation of organic carbon preservation, and organic carbon preservation to climate change. This allow is the proposal of a hypothesis: continental weathering, organic carbon burial and Earth's climate are all coupled in a dynamic geochemical feedback cycle.

6.5 References

Bales R.C., Guo Q., Shen D., McConnell J.R. Du G., Burhhart J.F., Spikes V.B., Hanna E., Cappelen J. (2009) Annual accumulation for Greenland updated using ice core data developed during 2000-2006 and analysis of daily coastal meterological data. *Journ. Geophys Res*. **114**. D06116

Burdige D.J. (2007) Preservation of organic matter in marine sediments: controls, mechanisms, and an imbalance in sediment organic carbon budgets? Chem. Rev. 107: 467-485.

Ciasis P and Sabine C. (2013). *Carbon and Other Biogeochemical Cycles.* In: Climate Change 2013: The Physcial Sciences Basis. Contribution of Working Group 1 to the Fifth Assessment Report of the Intergovernmental Panel on Climate Change. Cambridge University Press, United Kingdom.

Coale K.H., Johnson K.S., Chavez F.P., Buesseler K.O., Barber R.T., Brzezinski M.A., Cochlan W.P., Millero F.J., Falkowski P.G., Bauer J.E., Wanninkhof R.H., Kudeka R.M., Altabet M.A., Hales, B.E., Takahashi T., Landry M.R. Bidigare R.R., Wnad X., chase Z., Strutton P.G., Friederich G.E., Gorbunov M.Y., Lance V.P., Hilting A.K., Hiscock M.R., Demarest M., Hiscock W.T., Sullivan K.F., Tanner S.J., Gordon R.M., Hunter C.N., Elrod V.A., Fitzwater S.E., Jones J.L., Tozzi S., Koblizek M., Roberts A.E., Herndon J., Brewster J., Ladizinsky N., Smith G., Cooper D., Timothy D., Brown S.L., Selph K.E., Sheridan C.C., Twining B.S., Johnson Z.I. (2004) Southern Ocean iron enrichments experiment: carbon cycling in high- and low-si waters. *Science*, **304**: 408-414.

Cappelen J., Vinther B.M. (2014). SW Greenland temperature data 1784-2013. Technical Report 14-06. Danish Ministry of Climate and Energy.

Dyke A.S., Andrews JT, Ckark PU, England JH, Miller GH, Shaw J, Veillette JJ (2002); The Laurentide and Innuitian ice sheets during the Last Glacial Maximum. *Quaternary Science Review*, **21**: 9-31.

Hanna E., Jonsson T. Box J.E. (2004) An analysis of Icelandic climate since the nineteenth Century. *Int. J. Climatol*. **24**: 1193-1210.

Jorgensen A.S. and Andreasen F. (2007). Aping permafrost surface using ground-penetrating radar at Kangerlussuaq Airport, western Greenland. *Cold Regions Science and Technology.* **48**: 64-72.

Martin J.H. (1990) Glacial-interglacial CO2 change: the iron hypothesis. Paleoceanogr. **5**(1):1-13.

Martinez-Garcia A., Sigman D.M., Ren H., Anderson R.F., Straub M., Hodell D.A., Jaccard S.L. Eglinton T.I. Haug G.H. (2014) Iron fertilization of the subantarctic ocean during the last ice age. *Science*. **334**: 1347-1350.

Peng T.H. and Broecker W.S. (1991) Factors limiting the reduction of atmospheric CO2 by iron fertilization. Limnol. Oceanogr. 36(8): 1919-1927

Raiswell R., Tranter M., Benning L.G. Siegert M., De'ath R., Huybrechts P., Payne T. (2006) Contributions from glacially derived sediment to the global iron (oxyhydr)oxide cycle: implication for iron delivery to the oceans. Geoch. Cosmo. Act. 70: 2764-2780.

Syvitski J.P.M., Vorosmarty C.J., Kettner A.J. Green P. (2005) Impact of humans of the flux of terrestrial sediment to the global coastal ocean*. Science*. **308**: 376-380.

Rignot E., Box J.E., Burgess E., Hanna E. (2008) Mass balance of the Greenland ice sheet from 1958 to 2007*. Geophys. Res. Lett*. **35**: L20502

Appendices

1.0 Data Tables

1.1 Icelandic river Compositions

Sample ID	Collection Year	Na	Ca	Al	Fe	Cl^-	TSS	pH	Catchment Type
		µmol/L	µmol/L	µmol/L	µmol/L	µmol/L	mg/L		
A1	2003	303	68.2	0.18	0.14	379	359	7.76	Ng
A2	2003	324	86.8	0.31	0.89	282	569	8.08	Ng
A3	2003	361	112.0	0.25	1.69	402	522	8.07	Ng
A3#2	2005	440	98.1	0.23	0.59	174		8.08	Ng
A4	2003	309	98.1	1.19	1.05	361	612	7.93	Ng+Gl
A4#2	2005	299	79.1	1.59	0.28	274		8.15	Ng+Gl
A6	2003	283	109.0	0.19	0.72	312	525	8.02	Ng
A6#2	2005	323	118.0	0.21	0.38	143		8.27	Ng
A6-13	2013	297	50.0	0.19	0.45	226	12	8.60	Ng
A7	2003	362	129.0	0.16	1.71	434	558	8.00	Ng
A7#2	2005	487	143.0	0.15	1.07	197		8.15	Ng
A7-13	2013	362	60.0	0.12	0.60	195	0	8.69	Ng
A8*	2003	270	74.3	2.14	0.41	236	635	8.56	Ng
A8#2*	2005	272	72.1	2.75	0.44	63		8.87	Ng
A8-12*	2012	264	23.3	1.43	0.31	93	145	7.56	Ng
A8-13*	2013	302	23.0	1.66	0.37	174	83	9.10	Ng
A9	2003	509	150.0	0.37	3.88	414	679	8.11	Gl+Hydro
A10	2003	282	85.6	0.62	0.97	325	427	7.83	Gl+Ng
A11	2003	306	120.0	0.12	0.99	140	362	7.95	Ng
A12	2003	267	69.8	2.69	0.44	62	675	9.30	Gl
A12-12	2012	55	51.9	1.95	0.39		1531	7.85	Gl
A13	2003	311	91.6	0.91	0.77	84	406	8.44	Gl
A14	2003	125	57.3	0.76	0.06	28		7.79	Gl
A14-12	2012	87	25.5	0.86	0.09	23	2047	6.35	Gl
A16	2003	255	68.0	1.25	0.11	100	364	9.54	Gl
G1	2003	280	62.4	1.84	0.03	60		9.89	Gw
G1-12	2012	386	27.8	1.12	0.09	82	95	9.11	Gw
G2	2003	367	78.6	1.73	1.38	76	517	9.13	Gl
G3	2003	187	57.2	1.31	0.09	41		8.07	Gl
G4	2012	701	28.3	1.50	0.10	169	56	9.58	Gw
E1	2003	205	106.0	3.54	1.60	163	1890	9.11	Gl
E3	2003	66	160.0	4.97	0.13	164	1380	9.63	Gl
E4	2003	117	27.9	0.22		166	1650	7.72	Gl
E5	2003	132	92.1	3.61	0.45	180	2790	9.69	Gl
E5-12	2012	112	28.3	1.63	0.28	24	780	9.31	Gl
E6	2003	136	60.9	0.79	0.05	112	1570	7.98	Gl
E8-12	2012	302	29.3	0.40	0.21	22	1294	9.52	Gl
E10-12	2012	113	56.0	1.01	0.18	30	768	9.36	Gl
E11-12	2012	202	35.5	0.77	0.13	50	910	8.66	Gl
E11-13 W	2013	217	21.8	0.65	0.16	62	45	7.40	Gl+Ng
E11-13 E	2013	127	26.5	0.38	0.31	27	434	7.52	Gl
Ice (langjokull)	2005	61	0.7	0.05	BDL	7			Ice
E9 (ICE)	2012	38	2.5	0.07	0.09	15			Ice
A 15 ice	2012	11	14.3		BDL	27			Ice
Nonglacial Average		330±63	85±36	0.67±0.87	0.72±0.48	229±111	342±241	8.25±0.43	
Glacial Average		178±85	60±35	1.55±1.31	0.38±0.45	78±57	1120±730	8.55±0.98	

1.2 Non-glacial PHREEQC (oxyhydr)oxide precipitation estimates

Nonglacial			
Location	FeOOH	AlOOH	Source
A1	34.7	29.2	Pogge von Strandmann et al 2006
A2	35.3	33.7	Pogge von Strandmann et al 2006
A3	39.1	44.9	Pogge von Strandmann et al 2006
A3-2	37.6	54.0	Pogge von Strandmann et al 2006
A4	65.4	46.0	Pogge von Strandmann et al 2006
A4-2	55.9	34.8	Pogge von Strandmann et al 2006
A6	53.5	40.8	Pogge von Strandmann et al 2006
A6-2	49.4	48.8	Pogge von Strandmann et al 2006
A6-13	25.9	27.8	This Study
A7	52.3	41.2	Pogge von Strandmann et al 2006
A7-2	47.7	60.0	Pogge von Strandmann et al 2006
A7-13	16.5	33.5	This Study
A11	39.5	47.1	Pogge von Strandmann et al 2006
Nordurra-Stekkur	30.1	40.6	Gislason et al 1993
Seydisa	39.0	46.4	Gislason et al 1993
Langidalur	53.7	68.7	Gislason et al 1993
Midhlutara	43.3	54.8	Gislason et al 1993
Skjalfandafljot	40.1	73.4	Gislason et al 1993
Sog	38.9	51.4	Gislason et al 1993
Fremmstrava	27.9	37.7	Gislason et al 1993
Thjorsa	38.6	60.3	Gislason et al 1993
vatnsfjodure	18.4	8.6	Gislason et al 1993
Olfusa	48.4	49.8	Gislason et al 1993
Bruara	47.0	29.6	Gislason et al 1993
Blonduhlid	49.8	69.6	Gislason et al 1993
Fossa	50.9	66.7	Gislason et al 1993
Tungufljot	37.4	37.5	Gislason et al 1993
Tungufljot	39.0	31.9	Gislason et al 1993
Fossa	58.0	48.5	Gislason et al 1996
Tungufjot	35.9	42.0	Gislason et al 1996
Bruara, Estidalur	32.6	39.3	Gislason et al 1996
Olfusa	41.6	49.9	Gislason et al 1996
Sog	35.4	47.9	Gislason et al 1996
Nordua, Stekkur	39.0	37.8	Gislason et al 1996
Hvita-w, Ferjukot	35.9	43.1	Gislason et al 1996
Nordura (96-53)	44.6	20.6	Arnorsson et al 2002
Nordura (97-53)	46.3	22.6	Arnorsson et al 2002
Nordurra (98-21)	61.4	32.6	Arnorsson et al 2002
Egilsa (96-54)	50.4	28.7	Arnorsson et al 2002
Egilsa (97-55)	42.9	24.1	Arnorsson et al 2002
Egilsa (98-20)	59.0	40.3	Arnorsson et al 2002
N-Foss (97-76)	62.3	28.9	Arnorsson et al 2002

Arnorsson S., Gunnarsson I., Stefansson A., Andresdottir A., Sveinbjornsdottir A.E. (2002). Major element chemistry of surface- and groundwaters in basaltic terrain, N-Iceland. I. Primary mineral saturation. *Geochem. Cosmochem. Act.***66**(23): 4015-4046.

Gislason S.R. and Arnorsson S. (1993) Dissolution of primary basaltic minerals in natural waters: saturation state and kinetics. *Chem. Geo.* **105**: 117-135.

Pogge von Strandmann P.A.E., Burton K.W., James R.H., van Calsteren P., Gislason S.R., Mokaden F. (2006) Riverine behaviour of uranium and lithium isotopes in an actively glaciated basaltic terrain. Ear. Plan. Sci. Lett. 251: 134-147.

1.3 Glacial PHREEQC (oxyhydr)oxide precipitation estimates

Glacial			
Sample Location	FeOOH	AlOOH	Source
A12	34.2	44.3	Pogge von Strandmann et al 2006
A12-12	11.4	11.4	This Study
A13	41.0	47.6	Pogge von Strandmann et al 2006
A14	19.6	27.3	Pogge von Strandmann et al 2006
A14-12	10.3	7.6	This Study
A16	33.1	25.6	Pogge von Strandmann et al 2006
G2	42.6	52.4	Pogge von Strandmann et al 2006
G3	30.7	31.3	Pogge von Strandmann et al 2006
E1	43.5	42.8	Pogge von Strandmann et al 2006
E5	91.2	41.4	Pogge von Strandmann et al 2006
E5-12	6.4	18.7	This Study
E6	29.7	27.0	Pogge von Strandmann et al 2006
E8-12	5.5	20.6	This Study
E10-12	12.1	26.8	This Study
E11-12	30.1	24.9	This Study
E11-13 G	9.8	16.5	This Study
Blondudalur	48.1	65.2	Gislason et al 1993
Vestari Jokulsa	44.8	53.1	Gislason et al 1993
Skagafjordur	49.3	93.5	Gislason et al 1993
Hvita-w	38.4	41.8	Gislason et al 1993
Hvita-w	35.7	39.5	Gislason et al 1993
Geldingsa	38.1	30.0	Gislason et al 1993
Eystri Jokula	38.2	45.7	Gislason et al 1993
Hvita-s, Gulfoss	39.3	51.9	Gislason et al 1996
Hvitarvatn	39.7	48.7	Gislason et al 1996
Hvitarvatn	37.2	44.2	Gislason et al 1996
Hivta-w, Kjafoaa	34.8	44.0	Gislason et al 1996
Bruara, Dynjandi	35.9	48.2	Gislason et al 1996
Bruara, Estidalur	40.2	50.6	Gislason et al 1996
Eystri Jokula (98-96)	38.5	46.0	Arnorsson et al 2002
Eystri-Jokul (96-59)	36.9	35.5	Arnorsson et al 2002
Eystru Jokulk (97-58)	31.9	30.9	Arnorsson et al 2002
Eystru Jokulk (97-62)	21.1	25.3	Arnorsson et al 2002
Vestri-Jokul (97-87)	8.8	8.6	Arnorsson et al 2002
Vestri-Jokul (98-27)	25.8	39.5	Arnorsson et al 2002
Vestri-Jokul (98-57)	34.0	38.2	Arnorsson et al 2002
Fossa (97-88)	9.4	8.1	Arnorsson et al 2002

Arnorsson S., Gunnarsson I., Stefansson A., Andresdottir A., Sveinbjornsdottir A.E. (2002). Major element chemistry of surface- and groundwaters in basaltic terrain, N-Iceland. I. Primary mineral saturation. *Geochem. Cosmochem. Act.* **66**(23): 4015-4046.

Gislason S.R. and Arnorsson S. (1993) Dissolution of primary basaltic minerals in natural waters: saturation state and kinetics. *Chem. Geo.* **105**: 117-135.

Gislason S.R., Arnorsson S., Armannsson H. (1996) Chemical weathering of basalt in southwest Iceland: effects of runoff, age or rocks and vegetative/glacial cover. *Amer. Journ. Sci.*, **296**: 837-907.

Pogge von Strandmann P.A.E., Burton K.W., James R.H., van Calsteren P., Gislason S.R., Mokaden F. (2006) Riverine behaviour of uranium and lithium isotopes in an actively glaciated basaltic terrain. Ear. Plan. Sci. Lett. 251: 134-147.

1.4 Additional Iron Isotope Data.

Two field areas were samples during the course of field work and the data has not been reported elsewhere in this thesis and are reported below. The locations of these samples are listed in Appendix 1.5.

	56Fe	σ	[Fe] wt. %
DK-1 BL	0.049	0.04	9.79
DK-2 BL	0.210	0.03	12.34
DK-2 SPM	0.033	0.03	9.21
SKA-1 BL	0.071	0.06	9.51
SKA-2 BL	0.094	0.03	9.58
SKA-3 BL	0.032	0.07	8.07
SKA-3 NG BL 2014	0.097	0.04	8.69
SKA-5 BL	0.018	0.06	9.55
SKA-4 BL	0.009	0.01	7.96
SKA1 SPM 2014	0.091	0.02	9.03
SKA-2 SPM	0.082	0.04	9.29
SKA-3 SPM	0.057	0.04	9.47
SKA-4 SPM	0.072	0.03	7.55
SKA4 SPM 2014	0.089	0.03	13.79
SKA5 SPM 2014	0.052	0.00	9.35

1.5 Illulissat Field Sample Location

Sample Type Code: F=Filterable, S=Suspended, I=Ice, IS= Ice Particulate material and BL=bedload

Sample	Latitude	Longitude	Origin	Sample Types
ILU-1	N 69°11'57.57"	W 50°3'55.11"	Ice Fjord	F ,S, I, IS
ILU-2	N 69°10'52.96"	W 51°2'38.65"	Ice Fjord	F, S
ILU-3	N 69°11'14.74"	W 51°1'47.54"	Non-glacial	F,S, BL
ILU-4	N 69°12'8.35"	W 51°2'14.42"	Non-glacial	F,S, BL
ILU-5	N 69°14'15.52"	W 51°3'49.07"	Non-glacial	F,S, BL
ILU-6	N 69°11'59.19"	W 51°7'31.50"	Ice Fjord	F ,S, I, IS

1.6 Eqi Field Sample Location

Sample	Latitude	Longitude	Origin	Sample Types
EQI-1	N 69°45'16.24"	W 50°17'20.39"	Glacial	F,S, BL
EQI-2	N 69°45'34.35"	W 50°12'26.57"	Non-glacial	F,S
EQI-3	N 69°44'58.47"	W 50°14'10.38"	Non-glacial	F,S, BL
EQI-SOIL	N 69°45'7.96"	W 50°14'0.40"	Non-glacial	F, Soil

1.7 Disko Field Sample Location

Sample	Latitude	Longitude	Origin	Sample Types
DK-1	N 69°15'50.58"	W 53°26'52.12"	Non-glacial	F, Rock
DK-2	N 69°15'10.84"	W 53°29'57.14"	Glacial	F, S, BL

1.8 Borgarfjordur Field Sample Locations

	Lattitue N	Longitude W	Principle Water Type	Year(s) Collected	Sample Type
A1	65°10'58.85"	19°41'45.60"	Rain	2003	F, S Bl
A2	64°32'24.42"	21°20'9.06"	Rain	2003	F, S, Bl
A3	64°35'32.00"	21°34'32.00"	Rain	2003, 2005	F, S, Bl
A4	64°36'11.60"	21°42'23.80"	Rain+Glacial+Groundwater	2003, 2005, 2012	F, S, Bl
A6	64°42'39.70"	21°36'6.00"	Rain	2003, 2005, 2013	F, S, Bl
A7	64°40'52.50"	21°31'8.30"	Rain	2003, 2005, 2013	F, S, Bl
A8	64°41'31.90"	21°24'40.50"	Glacial+Groundwater	2003, 2005, 2012, 2013	F, S, Bl
A9	64°39'45.71"	21°23'52.28"	Rain+Groundwater	2003	F, S, Bl
A10	64°40'48.78"	21°2'15.54"	Rain	2003	F, S, Bl
A11	64°45'56.40"	21°30'48.84"	Rain	2005	F
A12	64°42'21.54"	21°2'21.18"	Glacial+Groundwater	2005, 2012	F, S, Bl

A13	64°48'6.06"	20°41'18.36"	Glacial	2005	F
A14	64°39'18.84"	20°42'3.96"	Glacial	2005, 2012	F, S, Bl
A15	64°38'47.46"	20°34'0.18"	Glacial	2005, 2012	F, S, Bl
A16	64°28'58.85"	19°41'45.60"	Glacial	2005	F, S
G1	64°42'6.71"	20°58'21.17"	Groundwater	2005, 2012	F
G2	64°42'14.04"	20°59'34.26"	Glacial+Groundwater	2005	F
G3	64°42'54.60"	20°50'1.86"	Glacial	2005	F
G4	64°15'5.82"	20°39'34.14"	Groundwater	2012	F
A6-Fe	64°42'40.61"	21°36'10.23"	Groundwater	2013	F, S

1.9 Vatnajokull Field Sample Locations

	Lattitue N	Longitude W	Principle Water Source	Year(s) Collected	Sample Type
E1	63°58'35.10"	16°59'55.74"	Mix	2003	F, S Bl
E2	64°2'51.78"	16°10'54.54"	Esturine	2003, 2012	F, S
E3	64°0'45.36"	16°22'28.23"	Glacial	2003	F, S
E4	63°57'16.80"	16°51'6.00"	Glacial	2003, 2014	F, S, BL
E5	64°0'23.17"	16°56'2.53"	Glacial	2003, 2014	F, S, BL
E6	63°56'20.97"	17°21'52.13"	Glacial	2003, 2014	F, S, BL
E7	63°46'3.60"	18°7'43.50"	Mix	2003	F, S BL
E8	64°1'36.72"	16°56'8.04"	Glacial	2012	F, S BL
E9	64°0'19.19"	16°52'59.98"	Glacial	2012	F, S, BL
E10	63°59'30.61"	16°52'18.56"	Glacial	2012	F, S, BL
E11	63°57'22.13"	17°28'10.41"	Mix	2012, 2013	F, S, BL
E12	64°14'47.16"	15°40'28.44"	Glacial	2012	F, S, BL
E13	63°56'15.76"	16°26'1.96"	Glacial	2012	F, S, BL

1.10 Skafta Field Sample Locations

	Lattitue N	Longitude W	Principle Water Source	Year(s) Collected	Sample Type
SKA-1	63°47'32.40"	18°2'14.16"	Mix	2013, 2014	F, S, BL
SKA-2	63°47'33.96"	18°29'43.98"	Mix	2013, 2014	F, S, BL
SKA-3	63°54'36.18"	18°35'54.84"	Mix	2013, 2014	F, S, BL
SKA-4	64°4'46.16"	18°24'25.15"	Glacial	2013, 2014	F, S, BL
SKA-5	64°14'2327"	18°08'26.54"	Glacial	2014	F, S, BL

2.0 Greenland Field Area Descriptions

2.1 Geology

The geology of south-west Greenland have been extensively studied by the Geolgic Survey of Denmark (GEUS) and summarized in a series of reports by Higgins and Watt (1999), Henriksen et al (2000) and Gool and Marker (2007). Most of the region is composed of Proterozoic tonalite- trondhjemite-granodiorite (TTG) orthogenesis and associated metasediments which formed during early craton stabilization. Three geologic super-groups, the Northern (NNO), Central (CNO) and Southern Nagssuqtogidian Orogenic (SNO) Zones, are recognized for the area although Kalsbeek (2001) found limited compositional variability across the TTGs bodies in the region facilitating a level of regional geochemical homogeneity.

The SNO is a thrust bounded region frequently described as a transition zone between the North Atlantic Craton and the core of the CNO. The distinguishing feature of the SNO is the presents of the pre-orogenic Kangâmuit ultramafic kimberlite/lamproite dykes swarm (Jensen et al 2001; Mayborn and Lesher 2006). Kangâmuit dykes have high MgO contents (>30 wt. %) and enriched trace element patterns not found elsewhere in South-west Greenland (Mayborn and Lesher 2006; Tappe et al 2011).

The CNO and NNO were extensively mapped as part of the Disko Bugt Project summarized in Garde and Steengelt (1999). Deformation and metamorphism progressively increase from the north to the south across the units leaving no definitive CNO-NNO boundary. The NNO and CNO contain geologic relics of the continental arc accretion process including shallow water meta-sediment and failed/discontinuous ophiolite deposits The CNO is distinguished by the presents of Calc-Alkaline intrusive rock suites interpreted to be the remnants of ocean arc accretion (Kalsbeek and Mantaschak 1999).

South-west Greenland also hosts the Tertiary West Greenland Continental Flood Basalt Province. The basalts erupted about 63 Ma into a sedimentary basin during a period of rifting between Greenland and Canada, and geochemically fall into distinct picritic and tholeiitic lavas (Lightfoot et al., 1997). The Picrites are geochemically similar to recent Icelandic picrites (Lightfoot et al., 1997) indicating little to no crustal contamination occurred during emplacement. This is in stark contrast to the Qeqertarsuaq tholeiitic lavas which are heavily contaminated with (supra)crustal material. The crustal material was likely rich in carbon and sulphide minerals which lead to the development of extremely reducing conditions during lava emplacement. The

tholeiitic lavas contain a number of ultra-reduced native iron and iron-carbon minerals which will only form on Earth under very specific and unusual conditions (Lightfoot et al., 1997).

2.2 Climatology and Glaciology of South West Greenland

The Greenland Ice Sheet covers about 80% of Greenland's 216000km^2 land surface. The ice sheet formed during Pliocene (~3.2 Ma), and has subsequently waxed and waned in phase with global climate cycles (Letreguilly et al., 1991). The ice sheets combined persistence through yet reactivity too climate change makes Greenland an ideal location to study the effect of ice fluctuations over recent geologic history.

Annual temperature and precipitation records from stations on the east and west coast of the island over the past 100 years indicate precipitation and temperature respond in phase to global climate change patterns. In both locations average annual temperatures are below zero but temperatures from May-September are significantly above zero, creating a pronounced summer melt season. The balance of ice lost during summer melting and ice formed during winter snow accumulation determines the size/extent of the ice sheet such that winter precipitation accumulation rates help define the limits of the icesheet. Precipitation rates across Greenland are positively correlated with mean annual temperature, and differences in precipitation patterns across the country explain why different areas of the country respond differently to global climate change. In the east of the country yearly precipitation is dominated by winter snowfall so increases in net precipitation increase winter ice growth (Cappelen and Vinther 2013). Over the last few Ma central and eastern portions of the country have always hosted glacial ice formation as ice formation keeps pace with ice loss in these areas even when temperatures are substantially warmer than present day (Letreguilly et al 1991). Along the west coast of Greenland the majority of precipitation falls as rain during the summer, which does not form glacial ice, so increased precipitation rates do not buffer the icesheet against increasing ice loses. Presently ice and ice melt drainage in Western Greenland exceeds winter ice accumulation rates by 30% accounting for a significant percentage of the ice sheets net losses (Rignot et al 2008). This study focuses on catchments in the South-west of the country where the icesheet is highly sensitive to temperature change.

2.3 Hydrology of South-West Greenland

Permafrost coverage inhibits the formation and flow of groundwater forcing a surface flow dominated hydrologic cycle (Jorgensen and Andreasen 2007). Greenland's proglacial landscapes are characterized by limited vegetation cover and/or soil formation increasing the

influence of surface topography on catchment morphology. These factors create significant differences between drainage catchments fed by glacial melt and those fed by direct precipitation.

Direct precipitation accounts for about 1/2 of the freshwater discharged from South-west Greenland annually, 10-30 g cm^2 a^{-1} of precipitation (Bales et al 2009) compared to 21.6 g cm^2 a^{-1} total marine discharge (Rignot et al 2008). Rain and snow melt collects in topographic lows driving the formation of small lakes in proglacial areas. Following periods of peak snow melt and/or rainfall these lakes feed into streams which ultimately drain into the ocean. Drainage from the lakes is often restricted by high local evaporation rates (Anderson et al 1998). In some areas yearly evaporation exceeds precipitation causing local lakes to become (semi)saline and highly stratified (Anderson et al 1998). The very fine nature of sediments within these lakes indicates that the lakes act as settling pools reducing inorganic limiting physical exports and increasing the relative influence of chemical versus physical wreathing in non-glacial riverine exports.

Glacial meltwater provide the other main source of water to Greenlandic rivers. Most glacial meltwaters originate from melting in the interior of the icesheet and flow via complex subglacial networks before entering proglacial river systems. The nature of the subglacial drainage networks makes glacial rivers prone to large periodic floods with total drainage rates typically peaking in the late summer (McMillian et al 2007). Greenland's proglacial landscape offers few natural barriers to the concentrated high volume flows created by the glacial melting processes allowing the formation of large rapidly draining rivers. These glacial rivers generally flow uninterrupted to the sea giving them substantially more power to physically transport inorganic sediments than their non-glacial analogues.

2.4 Field Areas

Four catchment areas were sampled along the west coast of the Greenland over the course of two field season. Samples of glacial melt streams and streams draining semi-saline lakes were collected by during the summer of 2009 by Wimpenny et al (2010) near the town of Kangerlussuaq to investigate the effects of glacial weathering in Greenland. Samples from three additional catchments were collected during the summer of 2013 to increase the diversity of weathering localities in Greenland.

2.4.1 Kangerlussuaq and Field Areas .

The Kangerlussuaq field areaencompasses a 600km^2 catchment between the Greenland Ice Sheet and the Søndre Strømfjord within the Southern Nagssuqtoqidian Orogen. Image J was used to estimate that the 106 pro-glacial lakes in the field area covered 6.7% of the total land surface area. The catchment drains ancient TTG, typical for the region, and is topographically elevated from the fjord preventing any tidal influence within the catchment area. Kangerlussauq has a precipitation accumulation rate of 5-15 g H_2O cm^{-2} year^{-1} (Ohmura 1991; Bales 2009).

Samples of glacial river water, precipitation fed lake water, suspended particulate material and riverine bed load samples were collected according to table x.y. Samples GR1, GR2, GR4, GR5, GR7, GR8 and GR9 were taken along the main forks of the glacial river that flows from the ice sheet to Søndre 7Strømfjord via Kangerlussauq. GR6, GR11, GR13 and GR15 sampled streams draining precipitation fed lakes. GR3 was collected from a supraglacial pool. Significant particulate material, originating from either wet or dry deposition, was widely present on the ice and within the sample such that particulate dissolution cannot be excluded from the sample. GR12 sampled a small strongly coloured flow assumed to be overflow from the nearby and topographically elevated lake. The actual source of the flow could not be directly determined however and similar flows have previously been attributed to snow melt which rapidly becomes saline due to a combination of high evaporation rates and the dissolution on surface salt deposits. GR10 was collected from near the Kangerlussuaq harbour to characterize the balance of fresh and marine waters in the fjord. An additional river, GR14, 100km west of Kangerlussuaq, near the town of Sisimuit in the Central Nagssuqtoqidian Orogen, was sampled during the same trip. Major element, trace element, and physical data along with lithium isotope compositions for all the sample localities are published in Wimpenny et al (2010) and magnesium isotope compositions are published in Wimpenny et al (2011).

2.4.2 ILU-Sample

The Ilulissat field area covered about 30km^2 of nonglacial lakes and streams on the north side of the Jakobshaven ice fjord 50km west of the Jakobshavn glacial. Image J was used to estimate that the 35 pro-glacial lakes in the field area covered 5.4% of the total land surface area. The catchment is composted TTG type orthgneisis from the Proterozoic Northern Nagassugtoqidian Orogen. Yearly precipitation accumulation rates in Ilulissat are 25-30 g/cm^2 (Bales et al 2009; Ohmura 1991) sustaining numerous freshwater lakes in the area. While no

glacial rivers drain through the area the Jakobshavn icefjord is the most concentrated area of glacial retreat in Greenland. The icefjord covers less than 0.45% of Greenland's total land surface but carries about 50 km^3 of ice per year to the ocean, equivalent to 7% of icesheet's total volume (Holland et al 2008). The mouth of the fjord shallows rapidly from 700m to less than 300m near its outlet creating a bathymetric barrier which traps large icebergs (Holland et al 2008) causing the whole fjord to fill with ice.

Post-glacial lake water, glacial fjord water, ice, suspended particulate matter and river bedload samples were collected from near the town of Ilulissat In August 2013. Samples ILU-3 and ILU-4 were taken from steep streams which drained freshwater lakes. ILU-5 was collected from a small meandering stream after it drained across a large area of low laying bog. No glacial rivers directly drained through the field area but ice and water from within the icefjord were sampled at ILU-1, ILU-2 and ILU-6 to characterize glacial outflow.

2.4.3 EQI Samples

Eqi is about 60km north-east of Ilulissat and less than 3km from edge of the ice sheet. The 15km^2 field area was bounded by the icesheet to the north, east and south and by a large glacial outflow river to the west. Image J was used to estimate that the 20 pro-glacial lakes in the field area covered 3.8% of the total land surface area. The field area is on the boundary between Rinkian fold belt and the Nagssuqtoqidian orogen which contain metamorphosed Archean and Proterozoic terrains. The nearest meteorological station, Qutdligssat (alternative spelling Qullissat), reports average precipitation accumulation rates of 20-30 gH_2O (Ohmura 1991; Bales et al 2009).

Glacial river water, post-glacial lake water, bog water, suspended particulate material and river bedload samples were collectednear the Eqi glacial ice camp in August 2013. A large braided river directly drains the glacier within the field area which was near the outlet of the river at Eqi-1. Eqi-2 sampled a steep rapidly flowing stream draining a large fresh water lake. Eqi-3 drained the an adjacent lake but across a across a much shallower slope that included areas of significant vegetation. A bog/soil and associated water sample were also collected from a shallow water-logged area between Eqi-1 and Eqi-3.

2.4.4 Disko Island

Qeqertarsuaq (formerly Disko Island) is an 8500 km^2 island west of Ilulissat separated from the mainland by the 50km Disko Bugt. The main city on the island shares its names with

island (formerly known as Godhavn) is on the southern tip of island. The field area extended east about 4km along the coast from the city of Qeqertarsuaq. The city has a precipitation accumulation rate in excess of 40g/cm^2/year, double the rate of the other field areas in Greenland. Qeqertarsuaq marks the southernmost exposure the of the West Greenland Flood Basalt Province. As discussed in section 3.4 the basalts on the island have are geochemically distinct due to extensive crustal contamination during emplacement. The area has discontinuous permafrost coverage (Jorgensen and Andreasen 2007) and host far fewer lakes than the mainland.

Two localities were sampled east of the city of Qeuertarsuaq in August 2013. DK-1 sampled a groundwater flow as the water emerged along the boundary of two lava flows from the base of a 30+m cliff. The groundwater contained no appreciable amount of suspended material so a bulk rock samples was taken from the lava-water contact. The main glacial river in the area, the Rode Elv, was sampled from a footbridge at DK-2. Rode Elv means red river named because it has a distinct reddish hue and contains bright red suspended material due to the oxidation of the unusual iron bearing minerals phases hosted in the islands basalts

Anderson N.J., Bennike O., Christoffersen K., Jeppesen E., Markager S., Miller G., Renber I. (1998) Limnolocal and palaeolimnological studies of lakes in south-western Greenland. *Geology of Greenland Survey Bulletin* **183**.

Bales R.C., Guo Q., Shen D., McConnell J.R. Du G., Burhhart J.F., Spikes V.B., Hanna E., Cappelen J. (2009) Annual accumulation for Greenland updated using ice core data developed during 2000-2006 and analysis of daily coastal meterological data. *Journ. Geophys Res*. **114**. D06116

Cappelen J., Vinther B.M. (2014). SW Greenland temperature data 1784-2013. Technical Report 14-06. Danish Ministry of Climate and Energy.

Garde A.A., Steenfelt A. (1999). Precambrian geology of Nuussuaq and the area noth-east of Disko Bugt, West Greenland. *Geology of Greebland Survey Bulletin*. **181:** 6-40.

Gool J.A.M. and Marker M. (2007) Explanatory notes to the Geological map of Greenland, 1:100000, Ussuit 67 V.2 Nord. *Geolgical Survey of Denmark and Greenland*. ISSN 1604-9780

Henriksen N., Higgins A.K. Kalsbeek F., Pulvertaft C.R. (2000) Greenland from Archean to Quaternary Descripitive text to the Geological map of Greenland 1:2500000. *Geology of Greenland Survey Bulletin*. **185**. ISSN 1397-1905

Higgins A.K., Watt W.S. (1999) Review of Greenland Activities 1998. *Geology of Greenland Survey Bulletin* **183**. ISSN 1397-1905

Holland D.M. Thomas R.H. Young B.S. Ribergaard M.H. Lyberth B. (2008). Acceleration of Jakobshavn Isbrae triggered by want subsurface ocean water. *Nature Geoscience*. **1**: 659-664.

Jorgensen A.S. and Andreasen F. (2007). Aping permafrost surface using ground-penetrating radar at Kangerlussuaq Airport, western Greenland. *Cold Regions Science and Technology.* **48**: 64-72.

Kalsbeek F., Manatschal G. (1999). Geochemisty and tectonic significance of peridotitic and metakomatiitic rocks from the Ussuit area, Nagssugtoqidian orogeny, West Greenland. *Precambrian Research*. **94**: 101-120.

Kalsbeek F. (2001) Geochemical comparison between Archean and Proterozoic orthogneisses from the Nagssugtoqidian orogeny, West Greenland. *Precambrian Research.* **105**:165-181.

Lightfoot P.C, Hawkesworth C.J., Olshefsky K., Green T., Doberty W., Keays R.R. (1997) Geochemistry of Tertiary tholeiites and picrites form Qeqertarssuaq (Disko Island) and Nuunssuaq, West

Greenland with implication for the mineral potential of comagmatic intrusions. *Contrib, Mineral. Petrol.* **128**:139-163.
Letreguilly A., Reeh N., Huybrechts P. (1991) The Greenland ice sheet through the last glacial-interglacial cycle. *Palaeogeogr. Palaeoclim. Palaeoeco*. **90:** 385-394.
Mayborn K.R. and Lesher C.E. (2006) Origin and evolution of the Kangamiut mafic dyke swarm, West Greenland. *Geological Survey of Denmark and Greenland Bulletin.* **11**: 61-86.
McMillan M., Nienow P., Shepard A., Benham T., Sole A. (2007). Seasonal evolution of supra-glacial lakes on the Greenland Ice Sheet. *Earth Planet Sci Lett.* **262**:484-492.
Ohmura A. Reeh N. (1991) New Precipitation and accumulation maps for Greenland. *Journal of Glaciology.* **37** (125): 140-148
Rignot E., Box J.E., Burgess E., Hanna E. (2008) Mass balance of the Greenland ice sheet from 1958 to 2007. *Geophys. Res. Lett*. **35**: L20502
Tappe S., Pearson D.G., Nowell G., Nielsen T., Milstead P. Muehlenbachs. (2011) A fresh isotopic look at Greenland Kimberlites: Cratonic mantle lithosphere imprint on a deep source signal. *Earth Planet. Sci. Lett*. **305**: 235-248.
Wimpenny J., James R.H., Burton K.W., Gannoun A., Mokadem F., Gislason S.R. (2010) Glacial effects on weathering processes: new insights from the elemental and lithium isotopic composition of West Greenland rivers. Ear. Plan. Sci. Lett. 290: 427-437.
Wimpenny J., Burton K.W., James R.H., Gannoun A., Mokadem F., Gislason S.R. (2011). The behaviour of magnesium and its isotopes during glacial weathering in an ancient shield terrain in West Greenland. Ear. Plan. Sci. Lett. 307:260-269

3.0 Iceland Field Area Descriptions

3.1 Geology and Hydrology

Iceland is a geologically young and active island formed primarily, >80%, of lavas with a mixed mid-ocean ridges-ocean island basalt melt source composition (Jakobsson 1972). The remainder of the island is comprised of andesitic-rhyolitic lavas clustered near the largest volcanic centres (Schuesler et al., 2009). For weathering purposes Icelandic basalts are used to broadly split into two age defined regions, younger and older than 0.8Ma, based on the effect of age of elevation, eruptive style, porosity and soil formation.

The topography of Iceland is negatively correlated with age due to the thermal buoyancy of the mid-Atlantic Ridge raising the youngest and most active central regions of the island. Iceland's climate is also heavily dependent on topography leading to the formation of two distinct microclimates on the island: the Central Highlands and Coastal Lowlands. The Central Highlands are defined by a 500+m plateau which forms the core of the island. The highlands host an arid boreal to subartic climate characterized by dust and ash deserts with sparse vegetation between large volcanic peaks (Hanna et al 2004). The highlands are comprised largely of youngest basalts (<0.8 Ma) many of which were erupted subglacially forming hyaloclastitic ridges parallel to the mid-Atlantic ridge axis. Hyalocalstites have inherently higher permeability's than sub-aerial lavas and their young age has limited porosity reduction due to

weathering. As a result precipitation and melt waters are able to penetrate into the bedrock and flow as groundwater often intersecting the water table in the valleys between the ridges. The increased permeability in the younger lavas also concentrates groundwater formation near active volcanic centres where they are prone to geothermal alteration increasing geothermal groundwater formation in the centre of the island (Kaasalainen and Stefanson 2012). The combination of young rocks, limited total precipitation and significant groundwater formation has greatly limited soil formation within the highlands. While Iceland as a whole is sparsely vegetated (<25%) and characterized by limited soil formation in most areas (Gislason et al 1996) vegetation and soil formation processes have a significant impact on the chemical and physical evolution of the landscape (review by Arnalds and Gretarrson 2001; Pogge von Strandmann et al 2012; Opgerfelt et al 2013; Opgerfelt et al 2014). The Central Highlands are dominated by Vitrisols, Figure (), which differ from fresh basalts due to the presence of ferrihydrite, up to 3%, but are very immature containing less than 1% organic carbon (Arnalds and Gretarrson 2001).

Away from the centre of the island Iceland's Costal Lowlands have a temperate and wet climate buffered against large intra-annual variability by the Atlantic Ocean (Gislason et al 1996). Precipitation rates increase from west to east across the lowlands and is greater along the south coast than the north (Hanna et al 2004). The coastal lowland are composed primarily of the older (>0.8Ma) basalt which were erupted mainly subaerially creating layered lava flows. Subsequent aerial exposure and weathering has reduced any of the original permeability of these older lavas restricting the formation and flow of groundwater. The permeability difference between older and younger basalts forces groundwater flow to the surface wherever the two groups meet creating large springs in areas such as Hraunfossar. The geologic and climatologic differences between the Lowlands and Highlands have facilitated much more extensive soil formation across the Lowlands. The Lowland region is dominated by the Brown, Glyeic and Histic Andosols as well as Histosols. Brown and Glyeic Andosols represent the continued weathering products of Vitrisols containing up to 10% of both ferrihydrite and organic carbon. Histic Andosols and Histosols contain up to and greater than 20% organic carbon respectively (Arnarlds and Gretarrson 2001).

Climatic between the Central Highlands and Coastal Lowlands have been a major factor in determining how glacial retreat has occurred across the island. Iceland was completely glaciated 9.6ka but rapidly (in less than 2ka) collapsed to near its modern state in the early Holocene (Gislason 1996; Norddahl and Petursson 2005). Within the last 100 years Iceland's

glaciers have begun another period of rapid retreat, leaving large terminal moraines, which is set to continue in response to Anthropogenic warming. This makes Iceland an ideal location to study both the effects of rapid climate change on weathering and investigate the slightly longer term effects of deglaciation on river catchments.

3.2 Field Areas

Rivers and streams in Borgarfjordur, Vatnajokull and Skafta catchment areas, were sampled during the summers of 2003, 2005, 2009, 2010, 2012, 2013 and 2014. Sampling locations were selected to isolated differences between weathering and sediment transport in glacial and non-glacial catchements. A soil sampling was conducted in 2009 targeting the main Icelandic soil types.

3.2.1 Borgarfjordur Area (A+G Samples)

The Borgarfjordur area, shown in figure 2.3, encompasses a 1685 km^2 drainage basin east of the town of Borgarnes between the Langjokull icecap and the Borgarfjordur estuary. The area includes two major sub-catchments, the Nordura and Hvita, as well as a number of smaller tributaries which in total discharge 9km^3/a into the Borgarfjordur estuary (Gannoun 2006). The eastern most part of catchment, sampled at A13, A14, A15 and G3, is a dominantly fed by glacial meltwater from the Langjokull icecap. A significant portion of water in the upper reaches of the catchments penetrates into the young hyaloclastites and flows as groundwater until the water table intersect older lava flows. A series of springs, sampled at G1 and G4, form along the boundary between the older and younger basalts and significantly increasing flow in the lower areas of the catchment. The waters sampled G1 and G4 are similar to rainwaters and ice melt from the region suggesting they have not experienced hydrothermal alteration. Sulphidic hydrothermal groundwaters are present in the region, sampled directly at B4, but their elemental concentrations is inconstant with hydrothermal alteration of surface waters (Kaasalainen and Stefansson 2012) indicative of an isolated deeper aquifer disconnected from the normal hydrologic cycle. The river sample collected at A9, adjacent to B4, does show signs of mixing between typical surface waters for the region and the sulphur rich hydrothermal waters. Rainwater and snowmelt provide the sources of water for the north-west and southern portions of the catchments samples at A1, A2, A3, A6, A7 and A11. The rest of the sample localities reflect a mixture of glacial melt, groundwater and precipitation sources.

3.2.2 Vatnajokull and Skafta

Vatnajokull is Iceland's largest icecap and is located in the wettest region of the iceland where currents from the southern Atlantic intersect the Icelandic coast. Most of the drainage from the icesheet is directly across the Coastal Lowlands along the south and east boundaries of the icecap. Glacial retreat during the Anthropocene has resulted in the formation of significant glacial moraines hundreds of meters to over a kilometre beyond the current edge of the glacial tongues. These moraines now defined the boundaries of proglacial lakes which have 1 or 2 overflow outlets which drain into sea. Samples of glacial meltwater were collected from these overflow outlets at E1, E3, E4, E5, E6, E11, E12, E13 from road bridges where the road crossed the rivers. E1 differs from the other samples in that are drains an area of acidic bedrock. Two visually distinct streams join just upstream of the E11 bridge and remain unmixed at the sampling location so samples of both streams were taken. Samples E8, E9 and E10 were collected along the glacial fronts allowing ice to be directly sampled as well as melt streams within meters of the glacial front. Sample E2 is an estuarine sample taken during tidal outflow from Jokulsarlon glacial lagoon. Precipitation rates across the field area are among the highest in Iceland so all the samples may reflect some degree of supra-glacial/rainwater runoff as well as subglacial drainage.

The south-west corner of the Vatnajokull icecap drains into the Skafta river which is significantly different from other rivers in the area. The Skafta river is near the centre of the Mid-Atlantic Ridge in the most geothermally active area of the country making it prone to large inputs of sulphur rich groundwaters and jökulhlaup floods (Old et al 2004). Significant subglacial hydrothermal activity was occurring during the 2012 sampling season with the resulting jökulhlaup eventually occurring in a catchment just to the west of the Skafta. Samples were collected from five main locations along the river from its source to where it interests the main road near Kirkjubaejarklaustur. Several lake fed streams also drain into the catchment with the largest entering the main catchment just downstream of Skafta-3 so both the main flow and the side stream were collected in 2014 at the locality.

Arnalds O. and Gretarsson E. (2001) Soil Map of Iceland, second editions. Agricultural Research Institute, Reykjavik. Available from: <ww.rala.is/desert>

Arnalds O. and Kimble J. (2001) Andisols of Deserts in Iceland. *Soil Sci. Am. J.* **65**: 1778-1786.

Gannoun A., Burton K.W., Vigier N., Gislason S.R., Rogers N., Mokadem F., Sigfusson B. (2006) The influence of weathering process on riverine osmium isotopes in a basaltic terrain. *EPSL*. **243**: 732-748.

Gislason S.R., Arnorsson S., Armannsson H. (1996) Chemical weathering of basalt in southwest Iceland: effects of runoff, age or rocks and vegetative/glacial cover. *Amer. Journ. Sci*., **296**: 837-907.

Hanna E., Jonsson T. Box J.E. (2004) An analysis of Icelandic climate since the nineteenth Century. *Int. J. Climatol*. **24**: 1193-1210.

Jakobsson S.P. (1972) Chemistry and distribution pattern of Recent basaltic rocks in Iceland. *Lithos*. **5**: 365-386.

Kaasalainen H. and Stefansson A. (2012) The chemistry of trace elements in surface geothermal waters and steam, Iceland. *Chem. Geo*. **330-331**: 60-85.

Nordðahl H. and Petursson H.G. (2005) Relatice seal-level changes in Iceland: new aspects of the Weichselian deglaciation of Iceland. *Iceland-Modern processes and past environments*. Elsevier. 25-78.

Old G.H., Lawler D.M., Snorrason A., (2005) Discharge and suspended sediment dynamics during two jokulhlaups in the Skafta river, Iceland*. Earth Surf. Process. Landforms.* **30**: 1441-1460.

Opfergelt S., Burton K.W., Pogge von Strandmann P.A.E., Gislason S.R., Halliday A.N. (2013) Riverine silicon isotope variations in glaciated basaltic terrains: implications for the Si delivery to the ocean over glacial-interglacial intervals. *EPSL.* **369-370**: 211-219.

Opfergelt S., Burton K.W., Georg R.B., West A.J. Guicharnaud R.A., Sigfusson B., Siebert C., Gislason S.R., Halliday, A.N. (2014). Magnesium retention on the soil exchange complex controlling Mg isotope variations in soils, soil solutions and vegetation in volcanic soils, Iceland. *Geochem Cosmo. Acta*. **125**: 110-130.

Pogge von Strandmann P.A.E., Opfergelt S., Lai Y.-J., Sigfusson B., Gislason S.R., Burton K. (2012) Lithium, magnesium and silicon isotope behaviour accompanying weathering in a basaltic soil and pore water profile in Iceland. *EPSL* **339-340**:11-23

Schuessler J.A., Schoenber R, Sigmarsson O. (2009) Iron and lithium isotope systematics of the Hekla volcanoe, Iceland- Evidence for iron isotope fractionation during magma differentiation. *Chemical Geology*. **258**: 78-91